

THE IMPACT OF NANOCCLAY ADDITION ON PVC PRESSURE-SENSITIVE DIGITAL PRINTED
FILMS

A Thesis

Presented to

The Graduate Faculty of The University of Akron

In Partial Fulfillment

Of the Requirements for the Degree

Master of Science

Jason Schaner

December, 2018

THE IMPACT OF NANOCCLAY ADDITION ON PVC PRESSURE-SENSITIVE DIGITAL PRINTED
FILMS

Jason Schaner

Thesis

Approved:

Accepted:

Advisor
Dr. Sadhan C. Jana

Dean of the College
Dr. Ali Dhinojwala

Committee Member
Dr. Erol Sancaktar

Dean of the Graduate School
Dr. Chand Midha

Committee Member
Dr. Younjin Min

Date

Department Chair
Dr. Sadhan C. Jana

ABSTRACT

Polyvinyl chloride (PVC) is an important polymer used to produce digital printable flexible films. It is often chosen due to its favorable cost to performance ratio. In order to produce films that meet a wide range of applications, several additives are typically incorporated into the formulation. These additives are often migratory, most notably plasticizers, which are added to PVC to improve its flexibility. Pressure-sensitive adhesives (PSA) are coated onto the backside of the PVC film so that the film can be applied to various substrates. The goal was to improve the stability of the PVC films by addition of nanoclay which acts to form a barrier layer. This included consistent print surface, mechanical properties, and adhesive properties.

Two different approaches were investigated to incorporate nanoclay into the PVC film products. The first was to disperse nanoclay directly into the PVC film. The film was made by preparing an organosol formulation and casting onto a rigid film web. The second approach was to disperse nanoclay into a thin polymer coating which was applied to the backside of the PVC film. The nanocomposite structures were characterized by microscopy techniques including AFM, SEM and TEM. The mechanical and adhesive properties were evaluated as a function of thermal aging. The thermal stability, durability, barrier, and surface properties were also evaluated.

ACKNOWLEDGEMENTS

I would like to express my gratitude and appreciation to my advisor Dr. Sadhan C. Jana. He has provided me with a great deal of guidance and support on my research and aided in developing my personal career. I would also like to thank my colleagues who supported in analytical testing. Thank you to Dr. Erol Sancaktar and Dr. Younjin Min for reviewing my thesis as committee members.

TABLE OF CONTENTS

	Page
LIST OF TABLES.....	ix
LIST OF FIGURES.....	xi
CHAPTER	
I. INTRODUCTION.....	1
II. BACKGROUND	
2.1 Polymer-clay nanocomposites.....	3
2.1.1 Polyvinyl chloride (PVC) overview.....	4
2.1.2 Plasticizer migration in flexible PVC.....	5
2.2 Introduction of nanoclay.....	7
2.2.1 Montmorillonite (MMT).....	7
2.2.2 Organically modified montmorillonite (OMMT).....	8
2.2.3 Other types of nanoclay studied in conjunction with PVC.....	9
2.2.4 Other types of nanoparticles studied in PVC.....	10
2.3 PVC-clay processing techniques.....	13
2.3.1 Melt compounding.....	14
2.3.2 Solution blending.....	15

2.3.3	In-situ polymerization	18
2.4	Nanocomposite structure characterization	19
2.4.1	Wide angle x-ray diffraction (WAXD)	19
2.4.2	Microscopy	22
2.5	Nanocomposite properties	23
2.5.1	Plasticizer migration resistance	23
2.5.2	Barrier properties.....	24
2.5.3	Mechanical properties	26
2.5.4	Thermal stability.....	27
2.5.5	Fire retardancy	31
III.	MATERIALS AND METHODS.....	32
3.1	Approaches and film constructions	32
3.2	PVC –nanoclay cast film	35
3.2.1	Materials	36
3.2.2	Sample preparation.....	37
3.3	Coating on calendered PVC film.....	43
3.3.1	Materials	43
3.3.2	Sample preparation.....	44
3.4	Characterization	47

3.4.1	Wide-angle x-ray diffraction (WAXD).....	47
3.4.2	Thermal stability.....	47
3.4.3	DSC	48
3.4.4	Appearance and optical properties	48
3.4.5	Plasticizer migration.....	49
3.4.6	Microscopy: AFM, SEM, TEM	50
3.4.7	Mechanical testing.....	51
3.4.8	Accelerated weathering	51
3.4.9	Adhesive testing.....	53
3.4.10	Barrier testing.....	55
3.4.11	Printing and surface analysis.....	57
IV. RESULTS AND DISCUSSION		61
4.1	PVC-nanoclay cast film	61
4.1.1	Structure characterization	61
4.1.2	Thermal stability.....	71
4.1.3	Appearance and optical properties	77
4.1.4	Mechanical properties	81
4.1.5	Durability and barrier properties	85
4.1.6	Printing and surface analysis.....	98

4.2	Coating on calendered PVC film.....	106
4.2.1	Thermal stability.....	106
4.2.2	Appearance and optical properties	107
4.2.3	Mechanical properties	108
4.2.4	Durability and barrier properties	113
4.2.5	Adhesive properties	116
4.2.6	Surface analysis.....	119
V.	CONCLUSIONS.....	121
	REFERENCES.....	123

LIST OF TABLES

Table	Page
3.1 List of nanoclays.....	37
3.2 White PVC film formulations	37
3.3 White PVC film formulations mixed using 2 step method	38
3.4 Clear PVC film formulations.....	38
3.5 Clear PVC film formulations mixed using 2 step method	39
3.6 Polyamide-nanoclay coating formulations	44
3.7 Brookfield viscosity of coatings	46
3.8 Accelerated weathering test method details	52
4.1 Tg results measured by DSC for white and clear films	75
4.2 L*, a*, b* color values and ΔE color difference for white and clear films.....	77
4.3 Gloss values for white and clear films	78
4.4 Surface roughness measurements for print film with different nanoclay types and loadings.....	79
4.5 White and clear film transmission results (a) WVTR and (b) OTR	97
4.6 White and clear film transmission results for samples mixed with high speed homogenizer (a) WVTR and (b) OTR.....	98
4.7 Initial contact angle measurements of white films	99
4.8 Dot size measurements for PVC films printed with (a) latex ink (b) eco-solvent Ink.....	101

4.9 Bleed measurements for PVC films printed with (a) latex inks (b) eco solvent inks	103
4.10 Dot size measurements for PVC films printed with eco-solvent ink	106
4.11 Bleed measurements for PVC films printed with eco solvent inks.....	106
4.12 Transmission results for nanoclay coating on PVC film (a) WVTR and (b) OTR.....	115
4.13 Weight loss measurements of calendered PVC without nanoclay coating.....	116
4.14 Contact angle measurements comparing initial versus aged results.....	120

LIST OF FIGURES

Figure	Page
1.1 PVC chemical structure.....	5
3.1 Schematic of approaches.....	32
3.2 Schematic of cast PVC structure.....	33
3.3 Schematic of cast PVC lamination process.....	34
3.4 Schematic of clear film and print film laminated together.....	34
3.5 Schematic of calendered PVC film with nanoclay coating.....	35
3.6 Photographs showing mixing setup (a) dispersion mixer (b) high speed homogenizer c) close up of dispersion impeller.....	40
3.7 Photograph comparing Cloisite® 10A mixing procedures (a) mixed with dispersion blade only (b) mixed with dispersion blade and high speed homogenizer.....	41
3.8 Photograph showing separation of liquid nanoclay coating over time (a) immediately after mixing (b) 2 weeks after mixing- stored at room temperature.....	45
3.9 Schematic of peel adhesion, loop tack and static shear tests.....	54
3.10 Photograph of wide format printer with samples laminated to print roll.....	60
4.1 WAXD spectra of (a) Cloisite® 20 powder and (b) Cloisite® 20 powder and white PVC film with 3 PHR Cloisite® 20.....	62
4.2 SEM top view images taken at 2000x and 5000x (a)(d) Cloisite® 10A (b)(e) Cloisite® Na+ (c)(f) Cloisite® 20.....	63
4.3 SEM cross-section images of (a) white PVC film with 5 phr Cloisite® 10A (b) clear film with 5 phr Cloisite® 10A.....	64
4.4 SEM top view image of TiO ₂ particles at 15,000x.....	64

4.5 AFM images of white films (a) 0 phr 10 μm (b) 0 phr 2 μm (c) 5 phr 10 μm (d) 5 phr 2 μm	65
4.6 AFM images of clear films (a) 0 phr 10 μm (b) 0 phr 2 μm (c) 5 phr 10 μm (d) 5 phr 2 μm	66
4.7 AFM images of clear films (a) 0 phr 10 μm (b) 0.5 phr 10 μm (c) 1 phr 10 μm (d) 5 phr 10 μm	66
4.8 TEM images of print film (a) 0.5 phr bright field mode (b,c) 0.5 phr dark field mode	67
4.9 EDS Spectra of 0.5 phr white film confirming that the white particles in Figure 4.7b,c are TiO_2	68
4.10 EDS spectra of 0.5 phr white film confirming that the white layers in Figure 4.7b,c are nanoclay.....	69
4.11 TEM images of print films (a,b,c) 5 phr bright field mode (d,e) 5 phr dark field mode	70
4.12 TEM images of clear films (a,b,c) 0.5 PHR dark field mode (d,e,) 5 phr dark field mode	71
4.13 Photographs of the films after heating in Metrastat (a) white print films, film only on left, film/adhesive/liner on right (b) clear films, film only left, film/adhesive/liner on right.....	72
4.14 Photographs of the white films after heating in Metrastat	73
4.15 Photographs of nanoclay disks after thermal aging for 30 minutes at 180°C.....	74
4.16 Color change of nanoclay disks after thermal aging for 2 minutes and 30 minutes at 180°C.....	74
4.17 DSC thermogram for white PVC-clay nanocomposites with Cloisite® 10A, 0-5 phr loading.....	75
4.18 DSC thermogram for clear PVC-clay nanocomposites with Cloisite® 10A, 0-5 phr loading.....	76
4.19 Impact of nanoclay loading on (a) Haze (b) Clarity (c) transmission of clear films ..	80
4.20 Impact of mixing procedure on haze of clear films	80

4.21 Young's modulus versus nanoclay loading for (a) white film (c) clear film and elongation at break versus nanoclay loading for (b) white film (d) clear film	82
4.22 Young's modulus versus nanoclay loading for (a) white film (c) clear film and elongation at break versus nanoclay loading for (b) white film (d) clear film	83
4.23 Stress-strain curves for (a) print films and (b) clear films mixed with high speed homogenizer	84
4.24 Effect of mixing method on elongation (b) white film (d) clear film and modulus (a) white film (c) clear film	85
4.25 Color shifts of white films after Super UV test (a) white films with Cloisite® 20, (b) white films with Cloisite® 10A, and (c) white films with Cloisite® Na+	87
4.26 Color shifts of white films after Super UV test (a) white films with Cloisite® 10A and (b) white films with Cloisite® 10A plus clear PVC layer on top.....	88
4.27 White film ΔE results (a) Xenon D4956, (b) QUV, (c) Xenon D7869	89
4.28 Gloss changes of white films (a) Xenon D4956, (b) QUV, (c) Xenon D7869.....	90
4.29 Color shift of clear films after Super UV test (a) clear films with Cloisite® 20 (b) clear films with Cloisite® 10A (c) clear films with Cloisite® Na+.....	91
4.30 Color shift of clear films after Super UV test (a) clear films with Cloisite® 10A (b) clear films with Cloisite® 10A plus white PVC layer underneath.....	91
4.31 Color shift of clear films after accelerated weathering (a) Xenon D4956, (b) QUV, (c) Xenon D7869.....	92
4.32 Gloss change of clear films after accelerated weathering (a) Xenon D4956 (b) QUV (c) Xenon D7869.....	93
4.33 Photograph of clear films after 1250 hrs D7869 test (a) clear films with Cloisite 20 (b) top is clear film with Cloisite 20 bottom 2 films are clear films with Cloisite 20 plus white PVC layer underneath (c) clear films with Cloisite 20 plus white PVC layer underneath	94
4.34 Photograph of clear films after 1250 hrs D7869 test (a) clear films with Cloisite Na+ (b) clear films with Cloisite Na+ plus white PVC layer underneath	94
4.35 Photograph of clear films after 1250 hrs D7869 test (a) clear films with Cloisite 10A (b) clear films with Cloisite 10A plus white PVC layer underneath	95

4.36 Photograph of clear films after 1000 hrs QUV test (a) clear films with Cloisite 10A (b) clear films with Cloisite 10A plus white PVC film underneath (c) clear films with Cloisite 20 (d) clear films with Cloisite 20 plus white PVC film underneath (e) clear films with Cloisite Na+ (f) clear films with Cloisite Na+ plus white PVC film underneath	95
4.37 Effect of PVC film thickness and addition of PSA to (a) WVTR and (b) OTR	97
4.38 Nanocontact angle of water drop over time (a) initial and (b) films aged 1 wk at 80°C.....	100
4.39 Images of ink dots printed with eco-solvent ink onto PVC film with different loadings of Cloisite® 10A (a) 0 phr (b) 0.5 phr (c) 1 phr (d) 3 phr (e) 5 phr	102
4.40 Images of ink dots printed with latex ink onto PVC film with different loadings of Cloisite® 10A (a) 0 phr (b) 0.5 phr (c) 1 phr (d) 3 phr (e) 5 phr.....	102
4.41 Images of black ink for bleed measurement with eco-solvent ink onto PVC film with different loadings of Cloisite® 10A (a) 0 phr (b) 0.5 phr (c) 1 phr (d) 3 phr (e) 5 phr	104
4.42 Images of black ink for bleed measurement with latex ink onto PVC film with different loadings of Cloisite® 10A (a) 0 PHR (b) 0.5 phr (c) 1 phr (d) 3 phr (e) 5 phr....	104
4.43 Images of ink dots printed with eco-solvent ink onto PVC film with different loadings of Cloisite® 10A after aging for 1 wk 80°C (a) 0 phr (b) 0.5 phr (c) 1 phr (d) 3 phr (e) 5 phr.....	105
4.44 Photographs of films after Metrastat thermal aging at 180°C (a) shows full construction film, coating, adhesive, and liner, (b) coating on PET.	107
4.45 Effect of nanoclay level on haze, clarity and transmission.....	108
4.46 Stress-strain curve for calendered PVC film after aging (a) film with PSA and (b) film only.....	110
4.47 Effect of aging on (a) elongation at break, (b) tensile strength, and (c) Young's modulus	111
4.48 Effect of aging on (a) elongation at break, (b) tensile strength, and (c) Young's modulus	112
4.49 Effect of eco-solvent printing on (a) Young's modulus, (b) elongation at break, and (c) tensile strength	113

4.50 Super UV results for PVC films with nanoclay coating	114
4.51 Effect of aging at (a) 60°C and (b) 80°C on peel adhesion and tack of PSA	117
4.52 Effect of thermal aging on peel adhesion of nanoclay coated films at (a) 60°C and (b) 80°C on peel adhesion.....	118
4.53 Effect of thermal aging on tack of nanoclay coated films at (a) 60°C and (b) 80°C.....	119

CHAPTER I

INTRODUCTION

Pressure sensitive graphic films are used in a wide variety of applications across the globe. The market for these films in the digital print segment has shown high growth in recent years. They are constructed with a face film, pressure sensitive adhesive (PSA), and a release liner. The face film may be multilayered and may contain coatings on the adhesive or top side for certain applications. The film is applied by removing the release liner to expose the adhesive, then using hand pressure or roll lamination to mount the film onto a substrate. The converting processes used for these films include printing or plotter cutting letters to create designs. The films are printed via digital and screen printing processes. The majority of the graphics industry has shifted to digital printing over screen printing due to its superior image quality, ink durability, and quick changeover for customized short run projects. The digital print inks typically used in the wide format graphics industry are classified as hard solvent, mild/eco-solvent, latex, or UV. Printer and ink manufacturers are moving away from the solvent inks in favor of latex and UV inks due to the negative health impacts related to the volatile components found in solvent inks.

The films produced for the wide format graphics industry are typically polyvinyl chloride (PVC) based materials due to their favorable cost to performance ratio versus

other polymer films such as acrylic, polyurethane, etc. The PVC films are produced by either calendaring or casting processes. Cast PVC films are made using liquid formulations termed organosols. The organosol is cast onto a rigid film web to hold it in place during drying and fusing processes. Calendered PVC films are made by dry blending the PVC formulations and using a series of rolls to heat the materials and to convert them into sheet form. Cast PVC is known to have better performance characteristics than calendered PVC. Calendered PVC shows higher shrinkage due to the inherent stresses induced into the film during the calendaring process. Calendered PVC also tends to be less durable and less stable over time, and typically is of higher thickness compared to cast PVC due to process limitations. The higher thickness does not allow calendered films to be used in some applications where a high degree of conformability or flexibility is required.

The focus of this research was on the study of cast and calendered PVC film and the influence of adding inorganic nanoparticles to mitigate the effects of plasticizer and additive migration. The nanoparticles chosen for the study were montmorillonite (MMT) nanoclays. The nanoclay was expected to provide a barrier layer that would reduce permeation of plasticizer and other small molecular weight additives to improve the stability of the PVC film products over time. The goal was to produce films that had consistent print quality, mechanical properties, durability, and adhesive performance.

CHAPTER II

BACKGROUND

2.1 Polymer-clay nanocomposites

Polymer-clay nanocomposites have been studied extensively in the past three decades. They are classified based on their structure and degree of nanoclay dispersion within the polymer matrix. Alexandre and Dubois [1] classified the different types of materials as phase separated microcomposites, intercalated nanocomposites, or exfoliated nanocomposites. The ultimate goal was to produce exfoliated nanocomposites which revealed new properties that could not be achieved by the unfilled polymer or by the microcomposites or the intercalated nanocomposites. The structure of microcomposites was observed to have large domains of nanoclay sheets and polymer chains which did not show break-up of original nanoclay layers or diffusion of polymer chains within the clay galleries. Consequently, the microcomposites show properties similar to those of unfilled polymers. The intercalated nanocomposites show well-defined structures of polymer chains and nanoclay layers where single polymer chains are intercalated between each layer. The exfoliated nanocomposites show the highest degree of uniformity and dispersion of nanoclay layers within the polymer, where the polymer chains fully expand the layers from the original gallery spacing.

A wide range of polymer-clay nanocomposites have been studied by previous researchers. Leszczynska et al. [2], [3] studied the effect of MMT nanoclay addition to several different thermoplastic and thermoset polymers including polyolefins, polyamides, polyesters, epoxies, PMMA, and PVC. In general, the author reported that the type of nanoclay must be carefully selected for each polymer, as they will interact differently. They also stated that the degree of enhancement to performance is highly influenced by the degree of nanoclay dispersion. Ray and Okamoto [4] reviewed the different classes of polymers that were used to prepare polymer-clay nanocomposites.

2.1.1 Polyvinyl chloride (PVC) overview

Flexible PVC film formulations are typically produced with several different components. These components vary depending on the mixing process, melt compounding or solution blending, and performance requirements dictated by the end use applications. Solution blended formulations include plastisol and organosol types. These components include PVC resin, plasticizer or plasticizer blends, polymer modifiers, solvents, UV stabilizers, heat stabilizers, dispersing additives, colorants, fillers, etc. Plasticizers are added to PVC to improve its flexibility and low temperature performance. There was a long history of studying plasticizer use in PVC. [5]

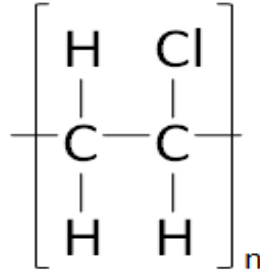


Figure 1.1 PVC chemical structure

The plasticization process was described in literature using three theories: lubrication theory, gel theory, and free volume theory. [6] Lubrication theory viewed the plasticizer as disrupting the van der Waals' forces between the polymer molecules and lowering the glass transition temperature (T_g) where the polymer chains became more mobile. Gel theory described that the plasticizer and PVC are held together by weak secondary bonding which can be easily altered by external forces. Lastly, free volume theory described the plasticizer's ability to lower the PVC T_g by increasing free volume, thus allowing the polymer chains to move.

2.1.2 Plasticizer migration in flexible PVC

It has been well documented that plasticizers tend to migrate in flexible PVC materials. Wilkes et al. [6] described the interactions between PVC and plasticizer. They explained that plasticizer and PVC are compatible but the plasticizer will not undergo chemical bonding to the PVC molecule. Plasticizer loss from PVC materials can be driven by diffusion or extraction mechanisms. Stark et al. [7] showed that the rate of plasticizer loss by diffusion was a function of initial plasticizer loading in the material. The loss rate was higher at higher plasticizer loading because the polymer matrix was

more susceptible to volatile losses at the surface. The diffusion rate decreased as the volatile loss increased, where a tortuous path was created to slow down the diffusion rate. The authors also determined that plasticizer loss from diffusion was time dependent. For the plasticized PVC materials they studied, it was found that the plasticizer loss amount was a linear function with the square root of time.

Earlier researchers proposed methods for studying plasticizer migration into solid and liquid materials. Messadi et al. [8] used Fick's law to study plasticizer migration into solid materials and proposed that plasticizer migration into liquids was controlled by two mechanisms of boundary layer interactions and internal diffusion. They calculated diffusion coefficients for different PVC plasticizer materials.

Plasticizer loss from PVC by extraction was shown to occur when bringing the PVC materials in contact with an external medium. The external medium was a liquid solvent or another solid polymer material. The authors [7] determined that extraction was driven by the compatibility of plasticizer and external medium. The other factor was the molecular weight of the external medium which determined the extent to which it could enter and diffuse through the material's structure.

In addition to PVC-plasticizer compatibility, the plasticizer molecular weight and structure played a key role in plasticizer migration. Two classes of plasticizer, termed monomeric and polymeric, were used regularly in industry. Monomeric plasticizers were low molecular weight and low cost. Typical industrial monomeric plasticizers have molecular weights in the range of 300-500. [5] Phthalate plasticizers diisooheptyl phthalate (DIHP), diisononyl phthalate (DINP), and dioctyl phthalate (DOP) are some of

the most commonly used. Polymeric plasticizers had molecular weights in the range of ~1,000- 8,000 which provided lower plasticizer migration. [5] The author also showed that plasticizers with more complex branched structures had better permanence than those with linear structures.

2.2 Introduction of nanoclay

Polymer-clay nanocomposites have been studied for a wide range of end-use applications. The goal of nanocomposite materials was to provide enhanced properties that could not be achieved by the individual polymer alone. Nanoclays are classified as mineral silicates that include montmorillonite, bentonite, kaolinite, hectorite, and halloysite. One of the most studied types of nanoclay was MMT. The MMT was either natural or chemically modified to add organic functionality. Previous authors have classified the chemically treated nanoclay as organically modified montmorillonite (OMMT). [9]

2.2.1 Montmorillonite (MMT)

The majority of past research efforts were focused on MMT nanoclay due to its high surface area and high aspect ratio, low cost, and ease of incorporation in polymers. [9], [10] It is a naturally occurring material that is mined across the world. One author reported that the surface area was $800 \text{ m}^2/\text{g}$. [9] MMT was classified as a smectite type clay with 2:1 layer structure, with each layer having dimensions of 200 nm by 1 nm. MMT was supplied with each layer in a stacked form ~10 μm in size, which must undergo a process termed exfoliation, where the layers are un-stacked. The layers must

be fully un-stacked in order to realize the full potential of the nanomaterial. The general chemical structure of MMT was given as $M_x(\text{Al}_{4-x}\text{Mg}_x)\text{Si}_8\text{O}_{20}(\text{OH})_4$, where “M” is the monovalent cation and “x” is the degree of substitution. [10]

Previous researchers [9] indicated that natural MMT could not be properly dispersed into hydrophobic polymers due to the hydrophilic nature of MMT. [9] In order to solve this issue, OMMT clays were produced, where the MMT was modified with alkyl quaternary ammonium or other organic cations. [11] The modification was completed utilizing an ion exchange process where the metal ions on the nanoclay sheets were replaced with quaternary ammonium ions. The quaternary ammonium ions were hydrophobic which allowed the nanoclay to be compatible with organic solvents and hydrophobic polymers. [12]

2.2.2 Organically modified montmorillonite (OMMT)

Several researchers studied different types of MMT and OMMT and their effect on thermal stability of polymers. [9] Thermal stability is critical to the manufacture of PVC formulations. [13] The processing conditions must be taken into effect when selecting appropriate nanoclay to maintain thermal stability. [14] Certain mixing processes can experience high temperatures and high levels of shear forces which can lead to pre-mature degradation of the PVC.

Stoeffler et al [15] studied the thermal stability of organoclays with phosphonium, pyridinium, and imidazolium salts and compared with an organoclay modified with ammonium salt. They used thermogravimetric analysis (TGA) to conclude that the ammonium salt had a lower degradation temperature versus the other three

organoclays which had good stability at greater than 290°C. Pagacz and Pielichowski [9] outlined the chemical structure of typical OMMT nanoclays that have been used in research. They outlined the different onium salts that were used for clay modification and describe their preparation.

Petersen et al. [16] proposed that Hansen solubility parameters were a critical tool in proper selection of the organic modifier used for MMT. They found that alkyl citrates could be used as the organic modifier on MMT nanoclay prepared with PVC. This is due to the higher thermal stability of this material versus traditional organic modifiers.

2.2.3 Other types of nanoclay studied in conjunction with PVC

Benderly et al. [12] studied hectorite and bentonite clays in melt compounded PVC materials. For processing, they studied the effect of pre-mixing clay in plasticizer on the ultimate dispersion in the nanocomposite. They also studied mechanical properties, thermal stability, barrier properties, and flame retardancy. The plasticizer was diisodecyl phthalate (DIDP) and the bentonite and hectorite clays were organically modified with tallow triethanol ammonium. They claimed that this new organic modifier provided better thermal stability in PVC versus other modifiers that were studied previously. For their experiments, they compared the tallow triethanol ammonium modifier versus a standard dihydrogenated tallow ammonium modifier. They concluded that pre-dispersion of the nanoclay in plasticizer provided a higher degree of dispersion in the PVC matrix which led to superior performance of the final material. Hectorite clay was shown to have better performance for thermal stability

over bentonite clay. Both types of clay showed improvement to fire retardancy, mechanical strength, and barrier properties.

Another type of nanoclay studied by past researchers was halloysite. Halloysite was termed aluminosilicate with a 1:1 layered structure. One author described it as a hollow tubular structure similar to that of carbon nanotubes. [10] The researchers evaluated halloysite as a performance enhancement agent in PVC. [17]–[19] They added the material at low loading levels and investigated similar properties that were mentioned previously including mechanical, barrier, flame retardancy, and thermal stability.

One group of researchers prepared PVC-halloysite nanocomposites by a melt compounding method with DOP plasticizer. [17] They showed that the thermal stability of PVC was improved with the inclusion of halloysite. They also determined that the flame retardancy was greatly improved. They suggested that the tubular structure altered the degradation mechanism in PVC by delaying the chain re-arrangement. They also used transmission electron microscopy (TEM) to show that intercalated structures could be prepared with these materials.

2.2.4 Other types of nanoparticles studied in PVC

In addition to nanoclay, researchers have studied other types of nanoparticles in PVC materials to enhance its properties. [20]–[26] Two commonly studied nanoparticles were graphene and carbon nanotubes. Breuer and Sundararaj [27] reviewed prior research on polymers filled with carbon nanotubes. They explained that these materials were heavily studied due to their unique structure and ability to enhance polymer

properties at low levels. The focus was typically on enhancement of mechanical, electrical, thermal, and optical properties.

Gholami et al. [28] investigated different types of nanoparticles and their influence on the properties of PVC. Their primary focus was on plasticizer migration resistance. They prepared PVC nanocomposites with DOP plasticizer using a melt compounding procedure. They compared 4 different nanoparticles which were carbon nanotubes, nanoclay, titanium dioxide, and zinc oxide. They characterized plasticizer migration by direct measurement of weight loss over time, and also by measuring the change in T_g using DSC. It was expected that the T_g would increase after plasticizer migration had occurred. The authors found that carbon nanotubes provided the greatest performance for plasticizer migration resistance. Their results indicated a 36% improvement in plasticizer migration. They suggested that plasticizer migration was highly driven by the degree of nanoparticle dispersion in the polymer matrix. This explained the difference in performance of titanium dioxide versus zinc oxide. Using scanning electron microscopy (SEM) and X-ray diffraction (XRD), they found that titanium dioxide particles had better dispersion in PVC, thus providing better plasticizer migration resistance. They also attributed the difference in dispersion to particle size. They found that smaller particle size had better dispersion. The particle size of the zinc oxide and titanium dioxide were measured using XRD with values of $\sim 255\text{\AA}$ and $\sim 75\text{\AA}$ respectively.

Broza et al. [21] studied PVC materials filled with carbon nanotubes. The films were made from a solution PVC method using THF as the solvent. The authors used

SEM to show that carbon nanotubes were uniformly dispersed in the PVC. They observed an improvement in mechanical properties and electrical conductivity with the addition of carbon nanotubes. They concluded that the solution PVC method could properly disperse the carbon nanotubes. They proposed that electrical conductivity was highly influenced by the carbon nanotube loading, and highlighted that previous work was done to show that carbon nanotube size and structure were also a key driver for enhanced properties of these nanocomposites.

Hasan and Lee [20] studied the addition of carbon nanotubes and graphene to PVC cast films. The films were made by a solution method with THF as the solvent. The PVC-carbon nanotube materials did not function properly due to poor dispersion. The PVC-graphene films showed improvement to modulus, tensile strength, and thermal stability. The authors reported a shift in T_g to higher temperature with the addition of graphene. They suggested that these materials could be used for high temperature applications that could not be serviced by virgin PVC.

Another research group [23] studied polymer-graphene coatings used in combination with several industrial polymers including PVC. The coatings were prepared from solution formulations and deposited onto the polymer films. Some of the coatings contained graphene which was pre-exfoliated using an electrochemical process. This allowed for very thin coatings at the nanoscale level for application to the polymer film. The focus of the research was on enhancement to gas barrier properties. The coatings on PLA, Nylon 6,6, polypropylene and PVC all showed improved barrier properties. The greatest performance observed was a reduction of 90% of oxygen gas transmission.

Deshmukh et al. [25] prepared PVC-graphene oxide films by a solution casting method. The authors used ultrasonic mixing to enhance graphene oxide dispersion in the PVC matrix. They reported efficient dispersion of graphene oxide with minimal agglomeration using SEM and TEM to characterize the nanocomposite structures. These authors also considered contact angle measurements in the analysis. They determined that surface energy was a function of the level of graphene oxide in the materials. They observed that higher content of graphene oxide produced materials also with higher surface energy. They proposed that contact angle could be a useful tool for future research on nanocomposite surfaces. In another paper, Joshi and Deshmukh [25] studied the surface and electrical properties of graphene oxide dispersed in PVC by solution blending. They concluded that well dispersed nanocomposites were formed using the solution blending technique, and that these materials could be used for electrical applications.

2.3 PVC-clay processing techniques

There are many different grades of PVC resin that are used in industry based on the processing techniques and the end-user applications. The grades include dispersion, mass, and suspension resins which vary in particle size. PVC-clay nanocomposites have been prepared using melt compounding, solution blending, or in-situ polymerization techniques.[29] The majority of studies have focused on melt blending formulations, but some researchers have evaluated the merits of solution blending and in-situ polymerization methods.

2.3.1 Melt compounding

The majority of past research has focused on melt compounding methods due to their simplicity and effectiveness. Multiple authors [30], [31] studied different melt compounding procedures and the effect on nanocomposite structures. Kalendova et al. [30] used suspension PVC resin in conjunction with Cloisite® Na+, and Cloisite® 30B. They also evaluated the effect of plasticizer molecular weight on nanoclay dispersion. They determined that the molecular weight was a significant factor into the degree of intercalation of the polymer into the clay galleries. Samples with lower molecular weight plasticizer showed better nanoclay dispersion. They also found that lower screw speed on the extruder produced better dispersion of nanoclay.

Other researchers [32] evaluated the effect of mixing techniques on the dispersion of nanoclay in plasticizer when producing PVC nanocomposites. They also studied the effect of different plasticizers on nanoclay dispersion. The two mixing techniques were ultra sonic mixing and standard mechanical mixing. They found that pre-dispersing the nanoclay in plasticizer allowed for better performance of the final products. The pre-dispersion allowed for intercalation of the plasticizer into the nanoclay. Previous work by Wang et al. [14] was in line with these results. Using XRD and TEM, they showed that DOP plasticizer alone could intercalate in the nanoclay. They also obtained evidence that the intercalation process with DOP was reversible.

Shimpi and Mishra [33] studied melt compounded PVC materials at higher loading of nanoclay up to 12%. In addition to material property enhancement, they also proposed that nanoclay improved the melt processing procedure by acting as a lubricant

at high loadings. This allowed for better rheological control in the extruder. In another study on melt compounding of nanocomposites, Romero-Guzman et al. [34] concluded that the additives used in formulations had a significant impact on clay dispersion and could be used to improve the intercalation and exfoliation of nanoclay in PVC-clay nanocomposites.

Yalcin and Cakmak [35] completed similar research to investigate the influence of pre-blending nanoclay in plasticizer on the performance of the nanocomposite. They prepared their materials by melt compounding Cloisite 30B OMMT with DOP plasticizer. The DOP was added at levels of 30, 50 and 70 phr. They found that the layer spacing reduced as the level of nanoclay was increased. They attributed this to the need for higher energy required to disperse the larger quantities of nanoclay in plasticizer. Based on XRD results, they determined that the layer spacing increased as the level of plasticizer was increased. However the extent of nanoclay dispersion decreased, as observed from AFM imaging. They also noticed a change in the XRD peak from being narrow to being broad. They proposed that an optimal level of plasticizer was required to provide the best layer spacing and dispersion for each system under evaluation.

2.3.2 Solution blending

A disadvantage of the melt compounding method comes in the form of high processing temperatures and high shear rates, which in certain cases initiate degradation of the polymer-clay nanocomposites. One author prepared melt compounded nylon-6 nanocomposites at 240°C and observed degradation of the organic modifier of the nanoclay. [36] They noted that the degradation was dually

impacted by the high temperature and shear rates used. Davis et al. [37] reported similar results of degradation during melt compounding of polyethylene terephthalate (PET)-OMMT nanocomposite preparation caused by high temperature. Another author studied degradation of alkyl quaternary ammonium and quaternary phosphonium organic modifiers used in modification of MMT by melt compounding. [38], [39] Using TGA, the above studies found that degradation was initiated at temperatures of 180°-200°C. Solution blending typically requires much lower shear during the mixing process and lower temperatures during the fusion process for PVC materials.

Wang and Wilkie [29] were early researchers who studied PVC-clay nanocomposites prepared by solution blending. They used Cloisite® Na+ MMT and Cloisite® 30B OMMT with DOP plasticizer. The ingredients were mixed and dissolved in tetrahydrofuran (THF). THF was known to be a very compatible solvent that would completely dissolve the PVC resin. They used XRD and TEM for characterization of the material's structure. They determined that the nanocomposites made by solution blending had an intercalated structure. They also found that post heating the material at 90°C or 104°C improved intercalation of nanoclay.

Another author [40] studied the effect of nanoclays, specifically Cloisite® 30B OMMT, on the plasticizer migration of PVC nanocomposites prepared from plastisol formulations. The plastisol was cast onto PET film to form a 500 µm flexible PVC film. Using XRD and TEM, they explained that intercalated nanocomposites could be produced. They noted that the plastisol process sustained less shear and lower temperatures compared to the melt compounding process for producing PVC

nanocomposites. This indicates that the plastisol process would have lower susceptibility to thermal degradation. They showed that plasticizer migration resistance decreased with increasing loadings of Cloisite 30B from 1-5 wt %. In addition, the level of plasticizer migration resistance was more significant at higher levels of plasticizer, from 50 to 100 phr plasticizer levels. It was found that as the loading of nanoclay in the plastisol was increased, there was a reduction in tensile strength and elongation at break.

Zheng and Gilbert [41] compared melt compounding with solution blending of PVC-clay nanocomposites. They used Cloisite® Na+ MMT and Cloisite® 30B OMMT and DIDP plasticizer. The melt compounded material showed an intercalated structure. They noted that if they pre-blended with plasticizer, the nanoclay was not as well dispersed as the direct addition to the PVC method. The solution blending was carried out in THF solvent. Using XRD data, they found that the THF alone could intercalate the Cloisite® 30B clay galleries. The structure of the solution blended materials was highly exfoliated. They concluded that the THF solution blending technique allowed for more efficient dispersion of nanoclay than the melt compounding method.

Another group of researchers [42] studied rigid PVC nanocomposite materials produced from solution blending. They used Cloisite® Na+ MMT and Cloisite® 20A OMMT and studied two different processing techniques. The first was solution blending and the second was solution blending in combination with melt compounding. The nanoclay was dispersed in THF first using a high speed mixer then an ultrasonic mixer. The melt compounded samples were mixed in injection molding equipment at

175°C. The final materials were characterized using XRD and SEM. They concluded that the solution blending and solution blending in conjunction with melt compounding methods both produced exfoliated nanocomposites. The softening temperature of the materials decreased with increased contents of nanoclay. This was attributed to MMT acting as a plasticizer as the layer spacing of MMT was increased. The one benefit that the solution blending plus melt compounding method showed was an improvement in thermal stability.

2.3.3 In-situ polymerization

In addition to melt compounding and solution blending, researchers have also investigated the preparation of PVC-clay nanocomposites by in-situ polymerization. Haiyan et al. [43] produced PVC resin using suspension polymerization in the presence of different OMMT nanoclays. The author explained that intercalation of monomer proceeded more effectively than when polymerized materials are used due to much larger molecular size that impeded molecular diffusions. The nanoclays evaluated were Cloisite® 6A, Cloisite® 10A and Cloisite® 30B. After PVC was polymerized, it was melt compounded with plasticizer and stabilizers. The above authors compared the in-situ polymerized materials with the fully melt compounded materials. They observed that in-situ prepared nanocomposites had significantly higher extent of dispersion than the same materials prepared by melt compounding. This study did not observe any differences due to use of different types of OMMT when materials were prepared by in-situ method.

Another group of researchers used an in-situ method to produce PVC-clay nanocomposites. [44], [45] They compared formulations with MMT and OMMT at levels of 1, 3 and 5 wt%. The resultant composite particle size reduced at higher loadings of MMT and OMMT. The nanostructure provided enhanced tensile strength, modulus, and toughness. The thermal stability improved due to char formation which formed a barrier at the material's interface. The materials produced with OMMT showed increased degradation which was attributed to the quaternary ammonium used to modify MMT. These authors used XRD and TEM to show that fully exfoliated structures were produced with this method.

Chen et al. [46] found that they could produce a PMMA-clay nanocomposite using in-situ polymerization method. The process was completed using an OMMT nanoclay. Similar to the PVC-clay nanocomposites described earlier, they found that this method provided materials with excellent barrier properties and improve plasticizer migration resistance.

2.4 Nanocomposite structure characterization

2.4.1 Wide angle x-ray diffraction (WAXD)

X-ray diffraction was the most commonly used tool to characterize the structure of PVC-clay nanocomposites. Giannini [47] explained why the XRD techniques were critical for studying materials with nanofillers. XRD uses X-rays to penetrate sample materials and interact with the electron clouds of the individual atoms. The penetration depth for soft X-rays is on the order of hundreds of nanometers. XRD is commonly used

to study the crystalline nature of polymeric materials. The wide-angle X-ray diffraction (WAXD) technique was used to determine the gallery spacing or d-spacing of the clay sheets. The shift in the 2θ peaks on the X-ray diffraction pattern was related to the d-spacing of the clay in the Bragg equation.[9] In WAXD, the incident beam enters a sample at 2θ values $>10^\circ$. One author explained that PVC-clay samples are typically scanned for 2θ values from $1-10^\circ$ because PVC will not show any peaks in this range due to its amorphous nature, which allowed for the clay peaks to be easily identified. [1] They indicated that when exfoliated nanocomposite structures were studied using XRD, the diffraction peaks disappeared due to d-spacing which was greater than 8 nm or due to lack of order in the structure. Bragg's equation is given in equation (1), where λ is the wavelength of the incident beam, d is the spacing between adjacent parallel layers, and θ is the scattering angle.

$$\lambda = 2d \sin\theta \tag{1}$$

Zheng and Gilbert [40] used WAXD to study the structure of PVC-clay nanocomposite films produced using plastisol formulations. Cloisite[®] 30B OMMT nanoclay was blended with PVC at different loadings, with DOP plasticizer. They first scanned the Cloisite[®] 30B powder and located a peak at a 2θ value of 4.9° and calculated the d-spacing at 1.80 nm. They then scanned the nanocomposite and identified a shift in the clay peak to a 2θ value of 2.1° which was calculated to be a d-spacing of 4.20 nm. The authors concluded that the shift in the clay peak and the increase in d-spacing of the clay layers due to diffusion of PVC chains indicated that an

intercalated structure had been achieved. They also used XRD to determine that the DOP plasticizer alone was not capable of increasing the spacing between the clay layers. The above was confirmed done by scanning samples of Cloisite® 30B and Cloisite® 30B blended with the plasticizer and comparing the diffraction peaks to that of the Cloisite® 30B alone.

Pagacz et al. [48] prepared melt compounded PVC-MMT and PVC-OMMT nanocomposites. They studied the effects of nanoclay on thermal aging as well as accelerated aging in a weather-o-meter which exposed the materials to UV radiation, humidity, and high temperature. It was found during thermally aging of the PVC-OMMT samples at 180°C that the samples experienced pre-mature degradation as observed by color change and the loss of plasticizer. They believed that thermal degradation of PVC-OMMT samples was due to break down of the organic treatment on the clay. The samples made with MMT did not show the same color change and degradation observed as with the OMMT samples. They explained that the degradation mechanism was different for thermal aging than was for the materials experienced inside the weather-o-meter during aging. The weather-o-meter aging caused loss of inorganic components and loss of plasticizer which also caused “micropore” defects to appear on the surface which in turn accelerated degradation. The PVC nanocomposites with MMT showed improved weathering performance and similar thermal stability performance when compared with PVC without nanoclay. Wang et al. [29] used WAXD to study the structure of PVC loaded with sodium MMT and OMMT prepared from solution blending.

Research work by Ishida et al. [49] used X-ray diffraction extensively to study the structure of several polymer-clay nanocomposites. First, they scanned the nanoclay powder and generated the diffraction patterns. Each nanoclay showed a distinct intensity peak. Next, they scanned the nanocomposite materials to look for changes in the intensity peak. They indicated that a shift in the initial nanoclay peak found from powder diffraction indicated that the structure was intercalated. If the nanocomposite peak either vanished or decreased in intensity and shifted to a lower level, they concluded that an exfoliated structure was produced.

2.4.2 Microscopy

Transmission electron microscopy (TEM) is most widely used in the study of nanocomposites. For TEM analysis, the materials are cut into a thin sheet, ~100 nm in thickness, using a microtoming process. Then a beam of electrons, typically with energy of 60-300 keV, are transmitted through the sample and the scattering patterns are collected by a detector and converted into an image. Other microscopy techniques often used are atomic force microscopy (AFM) and scanning electron microscopy (SEM). AFM is used to study the surface topography, while SEM is used to study the surface or cross section of the nanocomposite materials.

Yalcin and Cakmak [35] used AFM imaging to study the morphology of PVC-clay nanocomposites. They used a melt compounding process for preparing their materials. In this work, they were able to focus on the geometry of the individual clay platelets. They observed that some of the platelets were arranged in a fashion similar to a deck of

cards sliding past each other. They also noted that some of the platelets were fractured during the dispersive mixing.

Chen et al. [50] used SEM to study the structure at the surface of rigid PVC-clay nanocomposites prepared by melt compounding. They prepared samples with MMT and OMMT at levels of 0-5 phr. The SEM images showed a change in the surface roughness and porosity as the OMMT nanoclay loading was increased. The surface of the MMT samples did not change, however. The authors attributed the change in the OMMT nanocomposite surface to the internal lubricity effect of the OMMT which caused an increase of crater formation as the clay level was increased.

2.5 Nanocomposite properties

2.5.1 Plasticizer migration resistance

Several authors demonstrated the improvement of plasticizer migration resistance in PVC formulations with the addition of nanoclay. They attributed the improvement to the high aspect ratio of the nanoclay sheets which when intercalated or fully exfoliated in the polymer matrix created a tortuous path and reduced the diffusion of plasticizer or small molecules through the nanocomposite.[51]

Zheng and Gilbert [40] studied the effect of OMMT nanoclay on the plasticizer migration resistance of PVC nanocomposite films prepared from plastisol formulations. They used Cloisite® 30B nanoclay, which is MMT modified with “methyl tallow bis-2-hydroxyethyl quaternary ammonium chloride” and DIDP plasticizer. They found that DIDP migration decreased with an increased loading of Cloisite® 30B from 1-5 wt%. The

level of DIDP migration resistance was more significant at higher levels of plasticizer, from 50 to 100 phr loading. They attributed this to the increased mobility of DIDP molecules at higher loadings in the formulation.

Chen et al. [46] reported the gas barrier properties of organoclay added into a polymethyl methacrylate (PMMA) - PVC blend materials. They prepared the material by dry blending: Cloisite® Na+ nanoclay, PVC, PMMA and dibutyl phthalate (DBP) plasticizer. They quantified the barrier properties by measuring the weight change of the nanocomposites when immersed in a solution of DBP and ethanol. The PVC-PMMA blend with nanoclay showed a lower change in weight compared to the materials without the nanoclay.

2.5.2 Barrier properties

Various authors showed that the addition of nanoclay into different polymer matrices provided improved gas and water barrier properties. Hong et al [52] showed that nanoclay improved the water vapor transmission rate in the biocomposite films. The nanoclay was dispersed into a material called agar and then cast to form a film. They compared two OMMT type nanoclays and 1 MMT type nanoclay. The OMMTs' were Cloisite® 30B and Cloisite® 20A and the MMT was Cloisite® Na+. The water vapor transmission rate was determined from gravimetric analysis. They concluded that the nanocomposites made with Cloisite® Na+ showed significant improvement in water vapor transmission, while the Cloisite® 30B and Cloisite® 20A materials did not. They attributed the difference in results to the hydrophilic nature of the Cloisite® Na+ clay

versus the hydrophobic nature of Cloisite® 30B and Cloisite® 20A which were not as effectively dispersed in the water based system.

Kalendova et al. [53] investigated the barrier properties of linear low-density polyethylene (LLDPE) and PVC modified with nanoclay. They studied four types of OMMT and one type of MMT. The OMMT's were Cloisite® 30B, Cloisite® 25A and Cloisite® 93A. The MMT was Cloisite® Na+. The materials were prepared by melt compounding and then tested for levels of water vapor, O₂, and CO₂ transmission. The nanoclay dispersion was characterized by XRD and microscopy techniques. Cloisite® 25A showed the highest performance in compounds with LLDPE, with a 52% reduction in water vapor transmission rate after the 30 day test. Cloisite® 30B showed the highest performance in PVC with a 76% reduction of water vapor transmission. The O₂ and CO₂ transmission tests showed improvements for all four LLDPE-nanoclay specimens. The reduction in transmission was ~40% for these materials. This same test showed even greater improvement for the PVC-nanoclay materials which showed an improvement of ~60%. The authors suggested that the most significant improvement to gas barrier properties was observed for the samples that showed the highest degree of nanoclay dispersion, especially when exfoliation occurred. This allowed for the nanoclay layers to align and form the most efficient tortuous path.

Benderly et al. [12] studied the effects of nanoclay in PVC films on their oxygen barrier properties. The nanocomposites were prepared using organically modified hectorite and bentonite clays. The gas permeation for the PVC nanocomposite with hectorite was 4.9 cc-mm/m²-day compared to a value of 8.1 cc-mm/m²-day for PVC

without nanoclay. The authors suggested that gas permeation data could be used as a secondary tool to measure the degree of dispersion of the nanoclay within the matrix.

Another group [54] studied gas barrier properties of PVC-clay nanocomposites prepared with DINP plasticizer and Cloisite® Na⁺ MMT. They used tributyl citrate as the organic modifier of the MMT. In prior work, the Petersen research group [16] cited alkyl citrate type modifiers, mainly tributyl citrate, as new organic modifiers that could be used in PVC. This was attributed to their superior thermal stability compared with typical organic modifiers used in past research. They also determined that alkyl citrate type modifiers showed sufficient compatibility and intercalation with PVC. The samples for the gas barrier study were prepared by melt compounding. It was shown that the oxygen transmission increased when the DINP plasticizer was used. They attributed this surprising result to the strong compatibility of tributyl citrate and DINP. When they repeated the experiment without DINP, they saw reduction in oxygen transmission, indicating that the OMMT was well dispersed in the PVC matrix. They claimed that the tributyl citrate alone provided some plasticization to the PVC materials.

2.5.3 Mechanical properties

In general, researchers have identified an improvement to mechanical properties with the addition of nanoclay into PVC materials. The property enhancement was highly influenced by the type and loading of MMT or OMMT, the type and loading of plasticizer, and the dispersion efficiency in the PVC matrix driven by the processing technique applied. Typically, modulus and elongation at break increase with the addition of low levels of MMT. [9]

Wan et al. [55] found that the stiffness, impact strength, and storage modulus increase with the addition of sodium nanoclay at 0.5-5 wt% in the formulation. They indicated that the loading should be kept below 5 wt% to achieve the target mechanical properties. Zheng and Gilbert [40] found that tensile strength and elongation at break decreased with higher loading of nanoclay, in the range of 1-5 wt%. They attributed the decrease to the difficulty in dispersing the clay properly at higher loadings which could cause stress concentrations in the films that were tested. They also suggested that the clay may alter the fusion process by slowing down inter-diffusion of PVC into clay galleries.

Ren et al. [11] reported similar results as reported by Zheng and Gilbert. [41] They found that tensile strength decreased with an increased loading of MMT. They also studied the melt compounded nanocomposites with OMMT loadings from 1-5 wt%.

2.5.4 Thermal stability

Thermal stability is an important performance attribute for PVC materials. PVC must be formulated with thermal stabilizers due to their inherent imperfections in the polymer chain that arise during the polymerization process. [13] These imperfections which include double bond, branching, and alternate end groups force the use of thermal stabilizers and limit the typical PVC processing temperature to <220°C. [6]

Past researchers have evaluated the degradation of OMMT and MMT. [9] It was shown that the organic modifiers used to produce OMMT often contributed to the degradation process of PVC. The degradation intensity and onset temperature were unique for each type of nanoclay. In a study by Dharaiya and Jana [56], the authors

suggested that contact angle could be used to study the progress of degradation of organic modifiers instead of X-ray diffraction due to its higher sensitivity. The contact angle measurements also provided useful information on surface polarity which directly impacted the degree of nanoclay dispersion in the polymer matrix.

Several researchers have studied the impact of nanoclay on the thermal stability of PVC. [9] It is evident that the type of nanoclay, type of organic modifier, loading %, and processing technique each affect the thermal stability. This was evident from the work by Esmizadeh et al. [57] who used a structured mixture design to study mechanical and thermal properties of PVC-clay nanocomposites. Wang et al. [14] used thermogravimetric analysis (TGA) to study the degradation of PVC-clay nanocomposites prepared with Cloisite® 30B OMMT nanoclay. They found that the thermal stability was improved at a nanoclay loading of 2%. In another paper, they studied sodium clay, Cloisite® Na+, and did not observe an improvement in thermal stability. [58] Wang and Wilkie [29] found that when they prepared PVC-clay nanocomposites from solution blending with THF, they observed improved thermal stability. They attributed this to the intercalated structures that were formed due to solution blending technique which changed the degradation mechanism.

Peprnicek et al. [59] studied thermal degradation of different nanoclays by heating the nanocomposites at 175°C for periods of 10-60 minutes and evaluating the change in color, which indicated the onset of degradation. They evaluated sodium clay, Cloisite® Na+, and two OMMT clays, Cloisite® 93A and Cloisite® 30B. They reported that the sodium clay had the highest thermal stability, followed by the Cloisite® 93A and

subsequently Cloisite® 30B. They attributed this to the difference in organic modification, as the Cloisite® 93A had less stable ternary ammonium salt versus the Cloisite® 30B which had quaternary ammonium salt. Zheng and Gilbert [60] also reported better stability of the organic modifier type on Cloisite® 30B clay.

Wan et al. [61] studied thermal degradation of sodium MMT compared with OMMT modified with alkyl quaternary ammonium using TGA to measure thermal decomposition and UV-visible spectroscopy to track color change. The nanocomposites were processed by melt compounding at 170°C. They determined that the nanocomposites made with MMT did not show a color change, while the OMMT samples did tend to discolor. They proposed that the alkyl quaternary ammonium generated acidic components during degradation which initiated the dehydrochlorination reaction of PVC. The TGA results showed an improvement in onset of degradation temperature of 20°C at 5 phr loading of OMMT. The MMT did not show an improvement based on the results from TGA. The author attributed this improvement to efficient dispersion of OMMT which created a barrier to volatile components in the material and also a barrier to heat transfer.

Ren et al. [62] achieved similar results to the previously described authors. They prepared PVC-clay nanocomposites with OMMT by melt compounding. The thermal stability was rated based on color change after exposing the materials to 170°C for various periods of time. They found that the OMMT samples showed higher amounts of color change versus the virgin PVC. Gong et al. [44] described the Hofmann degradation process for the ammonium salts used as the organic modifiers for nanoclay.

The hydrochloric acid (HCL) degradation product leads to acceleration of dehydrochlorination of PVC.

Du et al. [63] used XPS as a primary tool to study degradation of PVC-clay nanocomposites. The samples were solution blended in THF using OMMT and DOP plasticizer. Using XPS, they tracked the chloride spectra versus temperature. The nanocomposites showed improved thermal stability as observed by the reduction of chloride spectra at high temperature. The authors noted that the surface of PVC after thermal aging showed different behavior to other polymers of study including PMMA and PS. Instead of clay at the surface, the PVC material exhibited a char at the surface at higher temperatures.

In addition to thermal stability, Pagacz et al. [48] completed further research to understand the durability of PVC-nanoclay materials. They studied PVC-clay nanocomposites prepared by melt blending. They compared MMT and OMMT with DOP plasticizer. They compared thermal stability to accelerated weathering conditions including the impact of UV radiation and moisture. They found that under accelerated aging conditions, the materials made with OMMT showed more discoloration and degradation compared to the MMT materials. They attributed this to the degradation of the organic modifier on the OMMT. The discoloration was caused by formation of polyene sequences on the PVC chains. Plasticizer and additive loss were also reported over time under aging conditions.

2.5.5 Fire retardancy

The addition of nanoclay has been shown to improve the fire retardancy in PVC materials. Levchik and Weil [64] reviewed flame retardancy in PVC materials. They reported that PVC is generally a low flammability material due to its decomposition process where HCL is generated which causes charring. They explained that new inorganic fillers were used to enhance flame retardancy by increasing char formation. Gilman [65] summarized the results of fire retardancy studies of different polymers in the presence of nanoclay. He used a cone calorimeter to measure heat release rate and other parameters related to flammability. The improvement in fire retardancy was attributed to the barrier layer that is formed from the nanoclay layers which held the volatile decomposition products into the clay structures.

CHAPTER III

MATERIALS AND METHODS

3.1 Approaches and film constructions

The overall goal of the research was to study the impact of nanoclay in PVC products to maintain performance over time. To maintain performance over time, the objective was to provide a stable print surface for consistent digital printing, maintain adhesive performance, and maintain film integrity and mechanical properties. Two different approaches were taken to study the effects of nanoclay on migration resistance and barrier properties in PVC film products. These approaches are illustrated in Figure 3.1.

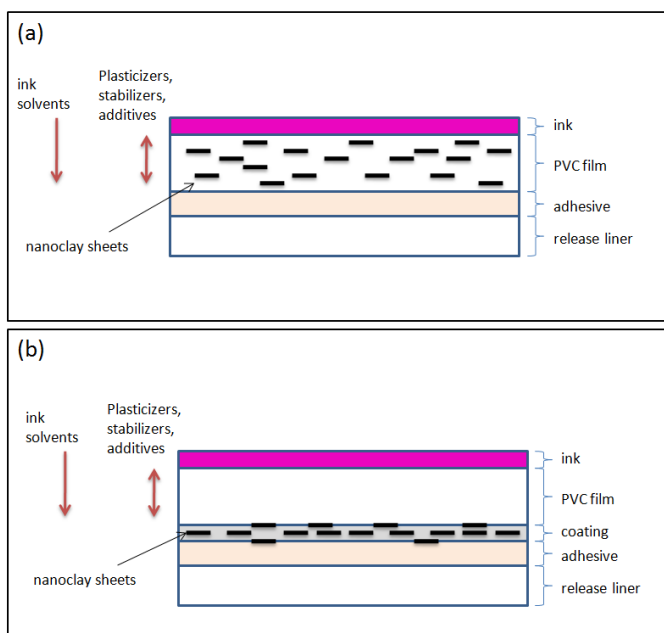


Figure 3.1 Schematic of approaches

The first approach was to disperse the nanoclay directly in the cast PVC film layer. The PVC film had a thickness of 50 μm , and was cast onto a 30 μm clear PET film. This structure is shown in Figure 3.2. The purpose of the PET film was to support the liquid PVC layer during the casting, drying, and fusing processes. PET was chosen due to its high modulus and dimensional stability at high temperatures. It was also beneficial because the PVC did not chemically bond to the PET film which allowed it to be removed at the end of the lamination process. After the PVC was fused into a film, the PET film was stripped and discarded. Both white pigmented and clear PVC films were evaluated. The white pigmented film was used for print applications, while the clear film was used as a protective overlay layer to shield the printed image from damage during its service life.

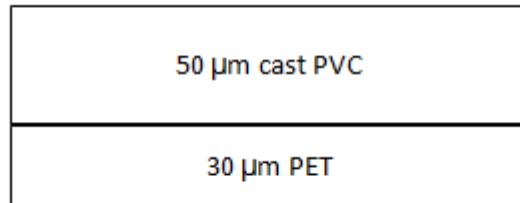


Figure 3.2 Schematic of cast PVC structure

After the casting process, the second step was to directly coat PSA onto a paper release liner. For these applications, the PSA is often made using solvent based or water based acrylic chemistries. For both approaches, a solvent based acrylic adhesive was used. The PSA was then laminated to the PVC film. The release liner was supplied with a silicone release layer so that the PSA could be removed from the liner. The PSA layer

had a thickness of $\sim 25 \mu\text{m}$ and the silicone coating had a thickness of $\sim 1 \mu\text{m}$. This structure is shown in Figure 3.3.

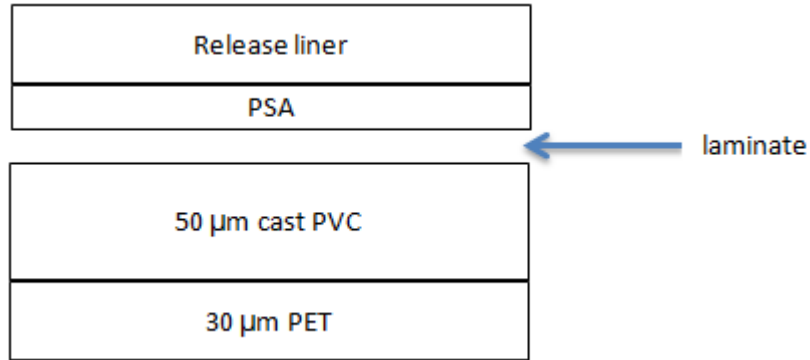


Figure 3.3 Schematic of cast PVC lamination process

Lastly, the PET film was removed by hand to expose the top side of the PVC film. The final print and overlay film constructions are shown in Figure 3.4.

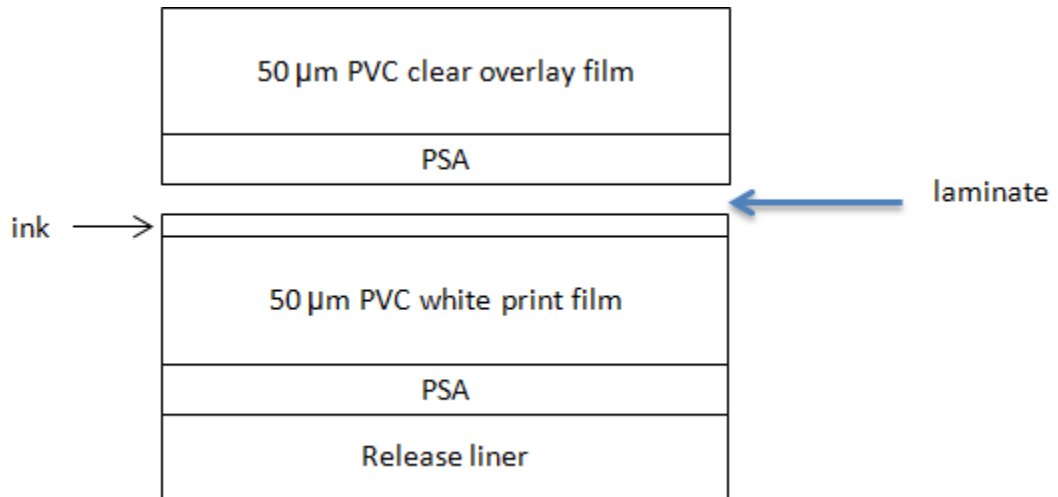


Figure 3.4 Schematic of clear film and print film laminated together

The second approach was to disperse the nanoclay into a thin coating formulation instead of directly into the cast PVC formulation. The coating was evaluated on calendered PVC film and applied between the PSA and PVC layers. The

PVC calendaring process did not use a PET film support layer like the casting process. The thickness of the PVC was 75 μm . The thickness of the coating was $\sim 7 \mu\text{m}$. The PSA was directly coated to release liner and laminated to the PVC using the same method described for the cast PVC process. The PSA layer had a thickness of $\sim 25 \mu\text{m}$ and the silicone coating had a thickness of $\sim 1 \mu\text{m}$. The layer construction is shown in Figure 3.5.

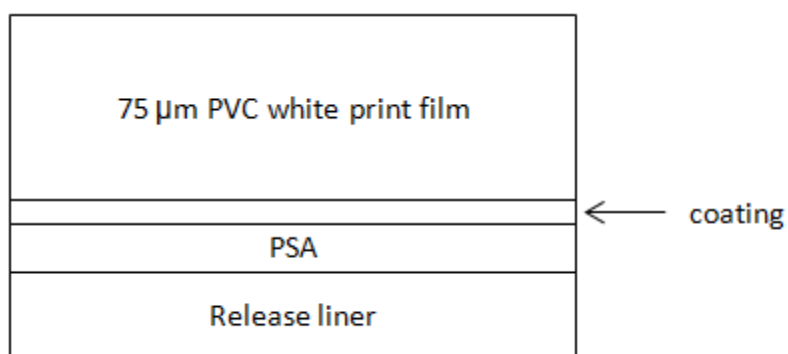


Figure 3.5 Schematic of calendared PVC film with nanoclay coating

3.2 PVC –nanoclay cast film

Plastisol and organsol are terms given to liquid cast PVC formulations. Plastisols are typically 100% or close to 100% solids formulations, while organsols contain volatile solvents, typically up to 25% by weight. They are viscous liquids that are cast onto a support film, then dried to remove the solvent and fused into a continuous flexible film. The work completed for this research project was done with organsol PVC formulations.

3.2.1 Materials

The white pigmented PVC film was made using a homopolymer dispersion resin with a K-value of 75. The K-value is a viscosity measurement which is related to molecular weight. [66] A higher K-value indicates a higher molecular weight. PVC manufacturers produce dispersion grade resins using an emulsion polymerization process which produces PVC at very fine particle sizes. Dispersion resins are typically used for thin film applications because of their relatively small particle size, which ranges from 0.4-2 μm . [6] The plasticizer was a polymeric type based on adipic acid chemistry, with a molecular weight of ~ 8500 g/mol. Two stabilizers were added to provide UV protection and thermal stability. The UV stabilizer was a benzophenone type and the heat stabilizer was based on calcium-zinc chemistry. Titanium dioxide pigment was added to provide color and opacity. The titanium dioxide was supplied as a liquid paste pre-dispersed in plasticizer and solvent. An aromatic hydrocarbon solvent composed of C8-C10 molecules and boiling point of 150°C was used to disperse the PVC and lower the viscosity so that the film could be cast properly.

The MMT type nanoclays were supplied by BYK Additives and listed in Table 3.1. Three different grades were evaluated: Cloisite[®] 10A, Cloisite[®] Na⁺ and Cloisite[®] 20. The Cloisite[®] 10A and Cloisite[®] 20 were organically modified with quaternary ammonium compounds. Cloisite[®] 10A was modified with benzyl(hydrogenated tallow alkyl) dimethyl salt, and Cloisite[®] 20 was modified with bis(hydrogenated tallow alkyl) dimethyl salt. Cloisite[®] Na⁺ was unmodified sodium nanoclay.

Name	Supplier	d50 dry particle size	Chemical composition
Cloisite 10A	BYK	< 10 μm	benzyl(hydrogenated tallow alkyl)dimethyl salt with bentonite
Cloisite 20	BYK	< 10 μm	bis(hydrogenated tallow alkyl)dimethyl salt with bentonite
Cloisite Na+	BYK	< 25 m	natural bentonite

*provided from BYK data sheet

Table 3.1 List of nanoclays

3.2.2 Sample preparation

The first set of white film formulations are listed in Table 3.2 below. They were mixed using a dispersion mixer with a Cowles type impeller. The nanoclay was loaded at 0, 1, 3, and 5 phr for each of the 3 nanoclays.

PHR	Cloisite 10A			Cloisite Na+			Cloisite 20		
PVC resin	100	100	100	100	100	100	100	100	100
plasticizer	20	20	20	20	20	20	20	20	20
solvent	75	75	75	75	75	75	75	75	75
TiO ₂ dispersion	85	85	85	85	85	85	85	85	85
UV stabilizer	1	1	1	1	1	1	1	1	1
heat stabilizer	1	1	1	1	1	1	1	1	1
Cloisite 10A	1	3	5						
Cloisite Na+				1	3	5			
Cloisite 20							1	3	5

Table 3.2 White PVC film formulations

The second set of formulations were prepared using a 2-step mixing process which added a high speed homogenization step. They are listed in Table 3.3. For these formulations, Cloisite[®] 10A was loaded at levels of 0.5, 1, 3 and 5 phr.

White print film formulations					
PHR	Cloisite 10A				
PVC resin	100	100	100	100	100
plasticizer	20	20	20	20	20
solvent	75	75	75	75	75
TiO ₂ dispersion	85	85	85	85	85
UV stabilizer	1	1	1	1	1
heat stabilizer	1	1	1	1	1
Cloisite 10A		0.5	1	3	5

Table 3.3 White PVC film formulations mixed using 2 step method

The PVC resin, plasticizer, and solvent used for the clear formulations were the same as detailed above in Table 3.2 for the white formulations. Higher levels of stabilizer were required for the clear formulations due to the absence of titanium dioxide which acted to scatter light. The UV stabilization included a cyanoacrylate based UV absorber and a hindered amine light stabilizer (HALS). For thermal stabilization, mixed metal stabilizers are commonly used in flexible PVC applications. They scavenge HCL and are used in combination with other stabilizers to improve the overall stability of the system. The clear formulation used a barium-zinc stabilizer in combination with epoxy ester, and phosphite stabilizers. The clear film formulations are listed in Tables 3.4 and 3.5.

Clear film formulations													
	100	Cloisite 20				Cloisite Na+				Cloisite 10A			
		100	100	100	100	100	100	100	100	100	100	100	
PVC resin	100	100	100	100	100	100	100	100	100	100	100	100	100
plasticizer	25	25	25	25	25	25	25	25	25	25	25	25	25
solvent	50	50	50	50	50	50	50	50	50	50	50	50	50
cyanoacrylate UV stabilizer	7	7	7	7	7	7	7	7	7	7	7	7	7
phosphite stabilizer	2	2	2	2	2	2	2	2	2	2	2	2	2
epoxide stabilizer	2	2	2	2	2	2	2	2	2	2	2	2	2
Ba - Zn stabilizer	5	5	5	5	5	5	5	5	5	5	5	5	5
HALS stabilizer	1.5	1.5	1.5	1.5	1.5	1.5	1.5	1.5	1.5	1.5	1.5	1.5	1.5
Cloisite 20		0.5	1	3	5								
Cloisite Na+						0.5	1	3	5				
Cloisite 10A										0.5	1	3	5

Table 3.4 Clear PVC film formulations

Clear film formulations					
		Cloisite 10A			
PVC resin	100	100	100	100	100
plasticizer	25	25	25	25	25
solvent	50	50	50	50	50
cyanoacrylate UV stabilizer	7	7	7	7	7
phosphite stabilizer	2	2	2	2	2
epoxide stabilizer	2	2	2	2	2
Ba - Zn stabilizer	5	5	5	5	5
HALS stabilizer	1.5	1.5	1.5	1.5	1.5
Cloisite 10A		0.5	1	3	5

Table 3.5 Clear PVC film formulations mixed using 2 step method

The initial mixing was done using a Caframo model BDC6015 stirrer. The impeller was a 1.5 inch diameter Cowles type dispersion blade. The batch size was 300 grams mixed in a 16 oz glass jar. The mixer was set to a speed of 350 rpm. The speed was verified using a handheld tachometer. Some agglomerates of nanoclay were observed during initial mixing experiments. This indicated that the nanoclay was not properly dispersed with the materials. An ultrasonic mixer and high speed homogenizer were both evaluated as options to improve nanoclay dispersion after the initial experiments. The homogenizer was chosen because of its better efficiency in dispersion over a shorter period of time. The ultrasonic mixer was not capable of breaking down the clay agglomerates in a reasonable amount of time, possibly due to the relatively high viscosity of the mixture. The process was switched to a two-step mixing which added the high speed homogenizer. The homogenizer was a rotor-stator type “Biohomogenizer” made by BioSpec products. It had two speed modes of 7,000 and 10,000 rpm. The diameter of the homogenizer shaft was 1 inch. The photos below

show the Cowles dispersion blade, Caframo mixer, and high speed homogenizer. The mixing setup is given in Figure 3.6.

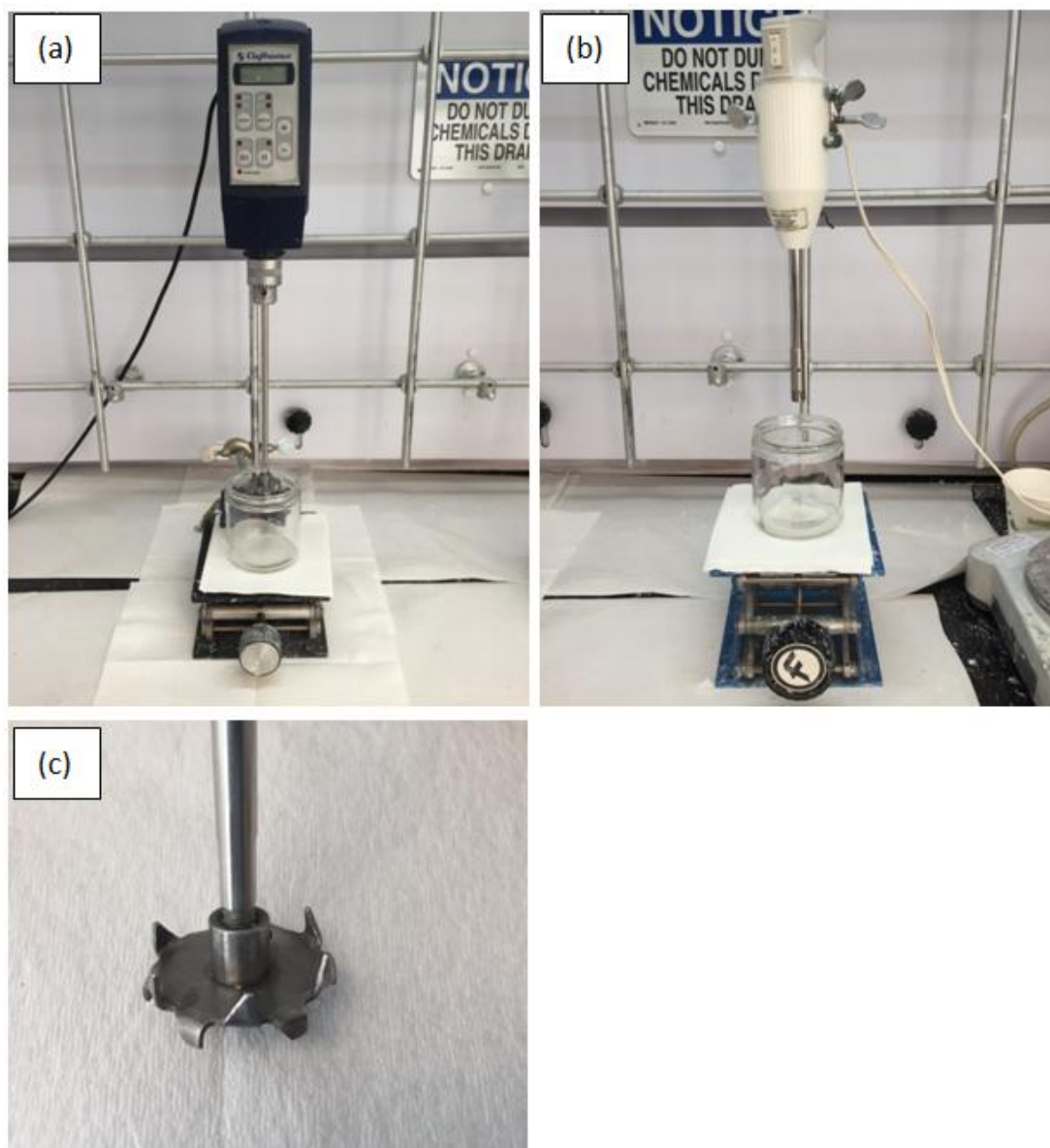


Figure 3.6 Photographs showing mixing setup (a) dispersion mixer (b) high speed homogenizer (c) close up of dispersion impeller

The photo in Figure 3.7 shows the comparison of the mixtures obtained by two different mixing methods. The mixture contained plasticizer, solvent, and nanoclay.

The sample shown in Figure 3.7b was mixed with the dispersion blade alone, while the sample shown in Figure 3.7a was mixed with the dispersion blade and homogenizer. The sample that was mixed using the homogenizer (Figure 3.7a) showed less separation over time.

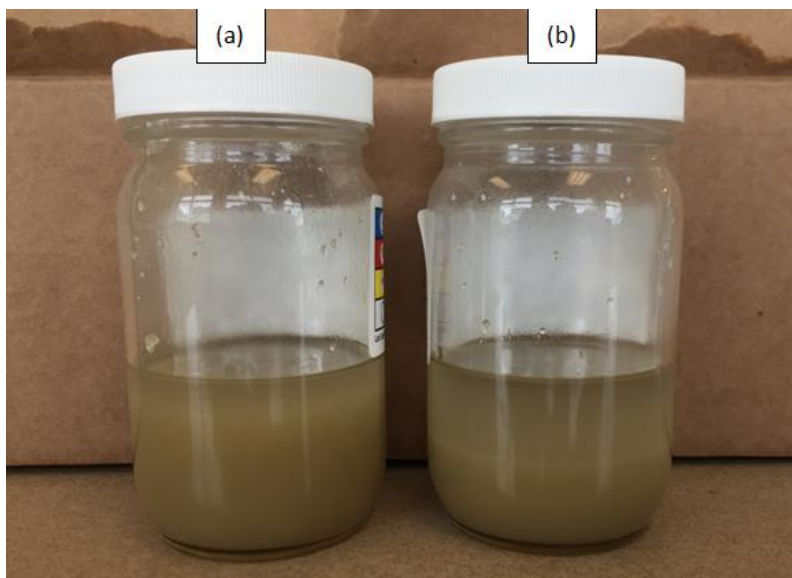


Figure 3.7 Photograph comparing Cloisite® 10A mixing procedures (a) mixed with dispersion blade only (b) mixed with dispersion blade and high speed homogenizer

The nanoclay was dried for 2 hours at 45°C to remove any moisture prior to mixing. The plasticizer was pre-blended with solvents to reduce the viscosity. It was anticipated that lower viscosity would allow for more efficient nanoclay dispersion. The plasticizer-solvent batch size was 600 grams. It was mixed with the dispersion blade in a 32 oz glass jar for 10 minutes at 350 rpm. At this point, a clear solution was obtained. Next, 90 grams of the plasticizer-solvent blend was poured off into an 8 oz glass jar. The nanoclay was slowly added to the plasticizer-solvent mixture, while mixing with the dispersion blade at 350 rpm. After all of the nanoclay was added, the samples were

mixed for another 5 minutes at 350 rpm. Then the samples were moved to the high speed homogenizer where they were mixed for 5 minutes at the 7,000 rpm setting. The homogenizer was operated for the 5 minute duration due to heat generation at the mixer head. This was also noted as the operating limit in the homogenizer manual.

After mixing with the homogenizer, the samples were poured into a 16 oz glass jar and the rest of the components were added. For the white formulation, the solid UV stabilizer and the liquid heat stabilizer were added while mixing with the dispersion blade for 5 minutes at 350 rpm. Next, the PVC resin was added over a period of 5 minutes, mixing at 350 rpm. Lastly, the titanium dioxide pigment dispersion was added. After all additions, the sample was mixed for another 10 minutes at 350 rpm to ensure that no agglomerates were left.

For the clear formulation, the stabilizers were all supplied in liquid form and added after the nanoclay dispersion step. Then the PVC was added in the same way as the white formulation. After mixing was completed, all samples were filtered through a medium mesh cone filter into a clean glass jar. The filter was used to screen out any large clumps of PVC that were caught on the sides of the jar and not broken apart. The final solids of the white and clear formulations were ~70% and ~75% respectively. It was noted that minimal heat was generated using these mixing procedures. All sample preparation was done at room temperature.

The samples were de-aerated in a vacuum bell jar to remove any air bubbles that could cause defects in casting. The casting process was completed within 24 hours after mixing. The samples were cast onto the PET sheet using a doctor blade coating setup.

The gap on the coater was set using a micrometer at either end to target a dry film thickness of 50 μm . The coated samples were approximately 300 mm width by 250 mm length.

The sample sheets were cut and fixed to cardboard and dried in a Blue M forced air oven at 180°C for 2 minutes. This temperature was chosen because it was high enough to remove the solvent and also fuse the PVC. After fusing, the film was allowed to cool at room temperature. The samples dwelled at room temperature for 24 hours before laminating to adhesive, or before any tests were started. Some tests required adhesive while other tests were done with film only. The PET cast sheet was removed for all tests.

3.3 Coating on calendered PVC film

3.3.1 Materials

The base polymer for the coating was a thermoplastic copolyamide. Polyamide was chosen for the coating because it was known to have good adhesion to the PVC and PSA. The polyamide was supplied as a liquid solution at 12% solids in a toluene and IPA solvent blend. The nanoclay used was Cloisite® 20. Nanoclay loadings of 0.5, 1 and 5 wt% based on solids were evaluated. The formulations are shown in Table 3.6.

Clear coating formulations				
	Cloisite 20			
	(0%)	(0.5%)	(1%)	(5%)
12% polyamide in solvent	100	100	100	100
Cloisite® 20		0.06	0.12	0.6

Table 3.6 Polyamide-nanoclay coating formulations

3.3.2 Sample preparation

The polyamide in solvent was observed to be a clear, low viscosity solution. The nanoclay was dried at 45°C for 2 hrs prior to mixing. First, the nanoclay was slowly added while mixing with the dispersion blade. The nanoclay was mixed for 5 minutes at 350 rpm. Next, the samples were transferred to the high speed homogenizer, and mixed for 3.5 minutes on the high speed, 10,000 rpm setting. After mixing, the samples were filtered through a medium mesh cone filter into a clean glass jar. The samples did not require de-aeration prior to coating due to their low viscosity. The samples were coated onto the backside of the white calendered PVC. The PVC film thickness was 75 µm. The samples were coated onto the PVC within 24 hours after mixing. The photos in Figure 3.8a shows the coatings immediately after mixing, then Figure 3.8b shows the coatings two weeks after mixing. The coatings with nanoclay appeared slightly hazy, and some separation was observed after two weeks at room temperature.

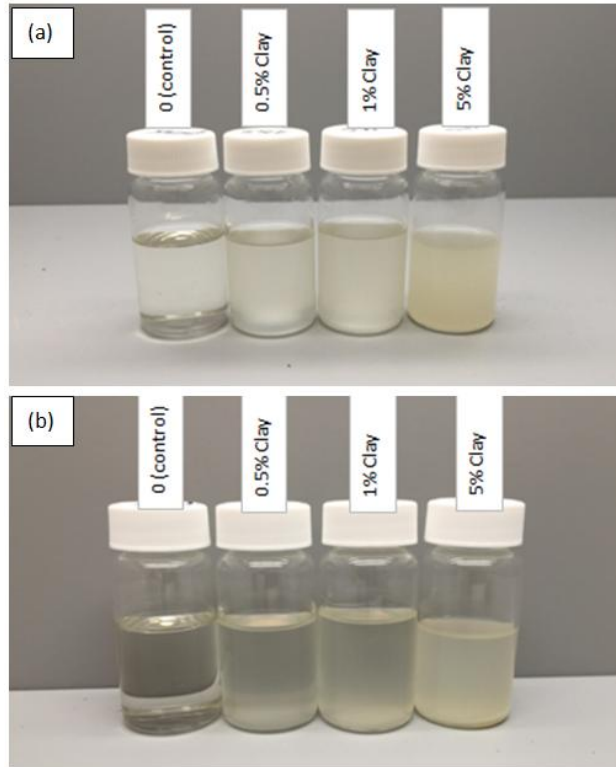


Figure 3.8 Photograph showing separation of liquid nanoclay coating over time (a) immediately after mixing (b) 2 weeks after mixing- stored at room temperature

The viscosities of the samples were measured prior to coating to ensure that the nanoclay did not significantly cause an increase. The results are reported in Table 3.7. Increased viscosity may have resulted in issues achieving a good quality coating. The viscosity was measured using a Brookfield DV-III viscometer with a #3 spindle at 50 rpm. The addition of nanoclay did not impact the viscosity in the low shear range measured by the Brookfield viscometer. The viscosity as a function of shear rate was not measured but it may be of interest for other coating applications.

<u>% nanoclay</u>	<u>viscosity (cps)</u>
0 (control)	154
0.5	130
1	132
5	138

Table 3.7 Brookfield viscosity of coatings

The samples were coated onto 75 μ m white calendered PVC using a #34G Mayer rod supplied by RDS Specialites. The dry thickness of the coating was \sim 7 μ m. The Mayer rod coating method is common in industry and often finds application for sample preparation in the lab. They are made of a thin metal wire wrapped around a solid metal rod. The wet film thickness is defined by the wire size and the spacing of the wire on the rod.

The samples were dried in a Blue M forced air oven at 82 $^{\circ}$ C for 2 minutes. This temperature was selected in order to minimize wrinkling of the calendered PVC film, while still removing the solvent. The PVC film was observed to soften and wrinkle at elevated temperatures greater than \sim 110 $^{\circ}$ C. The T_g of the calendered PVC sheet was 42 $^{\circ}$ C. The calendered PVC film was plasticized with a monomeric phthalate type plasticizer. The samples were laminated to PSA and allowed to dwell for 24 hours at room temperature before any testing was completed.

3.4 Characterization

3.4.1 Wide-angle x-ray diffraction (WAXD)

X-ray diffraction measurements were taken using a Rigaku SmartLab X-ray Diffractometer. The radiation source was Copper K alpha, with wavelength of 1.54 Angstroms. The data was collected over a range of 2θ in $0-10^\circ$ and $0-30^\circ$. The step size was 1° and the scan speed was 1 minute per step.

3.4.2 Thermal stability

Thermal stability was evaluated using a Metrastat PLC touch oven. The film samples were cut into 12.5 mm x 250 mm strips and placed into the Metrastat trays. The oven was programmed to a run cycle of 4 hours at 180°C . Over the 4 hour period, the sample tray was gradually moved out of the oven. After finishing the test, the strips were removed from the tray and photographed. The heat stability of the samples was compared based on the visual difference in color. As the exposure time increased, the samples turned from white to yellow to eventually dark brown and black. The samples were tested with free film alone and full construction with film, liner, and adhesive to determine the individual contribution of the PVC film and adhesive on thermal stability.

A second heat stability test was done to evaluate the stability of the nanoclay alone. The nanoclay powders were poured into a circular mold and placed into a Carver press. The nanoclays were pressed into 25 mm diameter disks then covered with a piece of clear PET film. The nanoclays disks were placed into an oven at 180°C at 2

minute and 30 minute periods. The color of the nanoclay was measured before and after heating to evaluate color shift using an X-Rite eXact spectrophotometer.

3.4.3 DSC

Modulated Differential Scanning Calorimetry (MDSC) tests were carried out using a TA Instruments Q2000 machine. The modulation amplitude was 0.53°C and the modulation period was 40 seconds to ensure that no cooling occurred during the experiments. The sample weight was ~3 mg. Each sample was heated from -90°C to 200°C at a rate of 5°C/min.

3.4.4 Appearance and optical properties

Color measurements were taken using an X-Rite eXact spectrophotometer. The test method measured color in the CIE L*a*b* color space using a D65 light source at 2° viewing angle. Three measurements were taken per sample and the mean and standard deviation were calculated and reported. Color difference was calculated using the CIE (1976) formulation given in Equation (2).

$$\Delta E = \sqrt{(L_2^* - L_1^*)^2 + (a_2^* - a_1^*)^2 + (b_2^* - b_1^*)^2} \quad (2)$$

Gloss measurements were taken using a BYK micro-TRI-gloss meter. Measurements were taken at 20°, 60°, and 85° illumination angles. Three measurements were taken per sample then the mean and standard deviation were calculated and reported. For improved resolution, low gloss films should be reported at

85°, and high gloss films at 20°. The 60° gloss was reported in the results section of this thesis.

The optical properties of the clear films and coatings were evaluated using a BYK Haze-Gard plus instrument. The instrument measured haze, transmittance, and clarity. Three measurements were taken per sample. Transmittance is the ratio of transmitted light to incident light. The amount of incident light reflected and absorbed will affect the value for transmitted light. Haze is perceived as the amount of cloudiness in a material. It is calculated by the amount of transmitted light that deviates from the incident beam by more than 2.5°. Clarity is perceived as the resolution of fine details. A material with low clarity will look distorted and less distinct. It is calculated from the amount of scattered light at narrow angles, less than 2.5°.

3.4.5 Plasticizer migration

Plasticizer migration from the PVC samples was evaluated using pressure tests. The method was a modified version of the ISO 177:2016 standard. Three film samples were cut into 76 mm x 76 mm squares and stacked in between Kimwipes® and sheets of paper. The stack was subjected to 2 different aging conditions. The first aging condition was with heat and pressure. The stack was placed under a 40 lb weight and put into an oven at 80°C. Each sample was weighed initially, then at different intervals to measure weight difference from plasticizer loss.

3.4.6 Microscopy: AFM, SEM, TEM

Tapping mode AFM was performed with a Digital Instruments Nanoscope III multimode scanning probe microscope. Topographic and phase images were recorded simultaneously in air at ambient conditions. The commercial single crystal silicon cantilever probe NSG10 from NTMDT was oscillated at its characteristic frequency, which was about 240 kHz. The cantilever was 95 μm long, 30 μm wide and 2 μm thick with a typical tip of radius 6 nm and force constant of 11.8 N/m.

The samples were prepared for SEM analysis by cutting the film and mounting it onto sample holders and then polishing them at -30°C using a RMC MT990 ultramicrotome. A thin layer of conductive gold coating was applied on the sample surface using a Denton vacuum desk IV with a sputter set point of 38% and time of 120 seconds. After coating, SEM images were captured using a JEOL JSM-6490LV instrument with a backscattered electron detector at an accelerating voltage of 10keV.

The samples were prepared for TEM analysis by first embedding the films into epoxy resin cured at 60°C followed by cryo-microtoming at -170°C . A thin section of around 100 nm thickness was cut along the z-direction or cross-section of the film. The section was mounted onto a full carbon coated TEM Cu grid. TEM measurements were carried out using a Tecnai instrument using a thermionic electron gun at 200 kV and a Gatan imaging filter (GIF) for zero loss imaging. A charge coupled detector (CCD) was used for bright-field imaging mode and a high angle annular dark field (HAADF) detector was used in scanning transmission electron microscopy (STEM) mode. Energy-dispersive

x-ray spectroscopy (EDS) was also performed at certain locations of the TEM image in order to study the elemental composition of the nanocomposite structure.

3.4.7 Mechanical testing

Mechanical property testing was conducted using a Sintech MTS model with a 500 N load cell. The tests were run at a rate of 12 inches per minute. The samples were cut into 1 inch x 6 inch strips using a rotary die slitter and loaded with a 2 inch gap between the lower and upper clamps in the machine. Before starting the test, the caliper of each sample was measured using a snap gauge. The caliper was entered into the Sintech software and used for calculations. All samples were tested in machine direction. Cast PVC films typically have similar mechanical properties in both machine direction (MD) and cross direction (CD). Calendered PVC films do have differences based on the test direction due to the stresses induced in the MD during the calendering process.

Five replicates were tested per sample and the mean and standard deviations were reported. The peak tensile stress, Young's modulus, break tensile stress, and elongation at break were obtained.

3.4.8 Accelerated weathering

The durability of the films was evaluated using four different accelerated weathering test methods that are outlined in Table 3.8.

	1- WOM	2- WOM	3- QUV	4- Super UV
Industry Standard	ISO 4892-2	ASTM D7869	ASTM G154, Cycle 4	Toyota TSH1583G
Light Exposure Spectrum (nm)	295 - 800	295 - 800	295 - 370	295 - 450
Irradiance 300-400 nm (W/m ²)	60	46 - 93	Not applicable	1500
Irradiance 340 nm (W/m ²)	0.51	0.4 - 0.8	1.55	Not applicable
Air Temperature (°C)	50	40 - 50	50	50
Black Panel Temperature (°C)	70	50 - 70	70	70
Humidity (%)	50	50 - 95	100 (during dark cycle)	50
Light Cycle (hours / day)	Constant light	14.82 light / 9.17 dark	16 light / 8 dark	Constant light
Water Spray Cycle	18 minutes every 2 hours	8.5 hours per day	None	None

Table 3.8 Accelerated weathering test method details

Accelerated weathering tests were performed using Xenon-arc, QUV and Super UV Weather-o-meters (WOM). These tests simulated outdoor weathering using light, moisture, and heat. Test method “1-WOM” was carried out in Atlas Ci5000 chambers following a modified ISO-4892-2 standard, which is a standard test used in the automotive industry. Test “2- WOM” was carried out in Q-lab Qsun units and used to simulate environments with high moisture such as south Florida. It was also used to evaluate the effect of cyclical light and dark versus the “1-WOM” which ran with constant light. This cycling often highlights failures in materials due to the stresses caused by thermal expansion and contraction.

The QUV was used to supplement the data from the Xenon-arc tests in order to accelerate the results. The QUV had a higher irradiance than the Xenon-arc tests but did not output light in the visible range of the spectrum. The QUV spectrum is 295-370 nm versus the Xenon-arc which covers a wider spectrum from 295-800. The SuperUV test had an irradiance 25 times higher than the standard Xenon-arc test and is typically

used as a fast screening tool for clear or white films. The irradiance for the SuperUV was 1500 W/m².

The film samples were prepared for the WOM tests by first applying adhesive to the non-cast side of the film. Next, a 1 inch strip of the sample was cut and laminated to a white painted aluminum panel. The samples were allowed to dwell for 24 hours on the panel before putting into the WOM chamber so that they could build to a suitable adhesion level. Color and gloss measurements were taken before starting the test. Measurements were taken at 250 hour intervals after they were put in the chamber. At each interval, the samples were also inspected for signs of degradation including cracks, brown spots, powdering/chalking surface, shrinkage, etc. Images were taken at certain intervals when these defects occurred.

3.4.9 Adhesive testing

It has been previously established that PSA in contact with flexible PVC films experiences a reduction in peel strength, tack, and cohesive strength over time due to plasticizer migration into the PSA. [67] The extent of this reduction is governed by the molecular weight of the plasticizer, chemical structure of the plasticizer and plasticizer compatibility with the PSA. If the plasticizer migrates and stays at the PSA-film interface, anchorage issues may occur and the film may separate from the PSA at relatively low forces. If the PSA-plasticizer compatibility is poor, the plasticizer may migrate through the PSA and form a layer at the PSA-substrate interface, reducing peel strength and tack. The use of solubility parameters is beneficial in establishing the

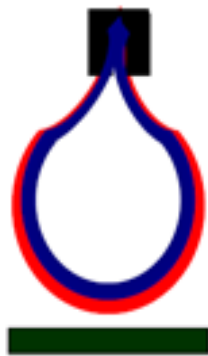
plasticizer compatibility with PSA. A reduction of plasticizer compatibility with the PSA may also be reduced by forming a tighter network structure through cross-linking.

The adhesive performance of the nanoclay coated film samples was studied. Three fundamental PSA tests were completed: peel adhesion, loop tack, and static shear. The adhesion tests are illustrated in Figure 3.9. Peel adhesion measures the force required to remove the PSA from a substrate. The test was carried out using 180° geometry. The substrate was applied to a stainless steel panel using a 4.2 lb hand roller and allowed to dwell for 15 minutes. Next, the sample was mounted into the Sintech machine and test initiated. The peel rate was 12 inches per minute and the test was conducted at room temperature. Three measurements were taken per sample. The average peel force over a 3 inch length was reported.

180° peel adhesion



Loop tack



Static shear

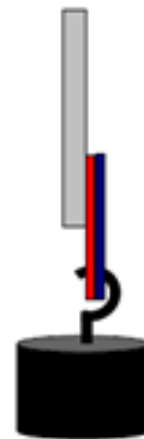


Figure 3.9 Schematic of peel adhesion, loop tack and static shear tests

Tack is a measure of the ability of the PSA to wet out a surface. It provides quantitative data for the perception of thumb tack. Loop tack was done using a 1 inch width sample. The test was done in the Sintech machine with a 6 inch gap between the jaws. The sample loop was lowered to the substrate at a rate of 12 inches / minute. The substrate was stainless steel and the test was done at room temperature. Three measurements were taken per sample. The peak force was reported and averaged between the three sample repeats.

Shear is a measure of the cohesive strength of the PSA. The sample size in contact with the stainless steel substrate was $1/4 \text{ in}^2$. The adhesive was applied to the substrate using a 4.2 lb hand roller and allowed to dwell for 15 minutes before hanging with a weight. The weight was 1 kg. The time in minutes for the sample to be removed from the panel was reported. Three measurements were taken per sample. The failure mode for each sample was also reported. Typical PSA failure modes include adhesive transfer, cohesive failure, or adhesive failure. Adhesive transfer occurs when the PSA is removed from the film substrate and left on the stainless steel panel, which indicates the PSA had poor anchorage to the face film. Cohesive failure occurs when the residual adhesive is observed on the face film and on the stainless steel substrate. This indicates that the PSA had poor internal strength. Lastly, adhesive failure occurs when the adhesive remains on the face film and not on the stainless steel substrate.

3.4.10 Barrier testing

The barrier properties of the film samples were studied by measuring water vapor transmission (WVTR) and oxygen transmission (OTR). The transmission was

measured at different temperature and relative humidity (RH). The oxygen transmission was tested at two conditions: 23°C / 0% RH and 38°C / 90% RH. The water vapor transmission was tested at two conditions: 23°C / 100% RH and 38°C / 100% RH.

WVTR was measured using a Mocon PermaTran-W 3/34G instrument following ASTM F 1249-13. The surface area of the sample was 5.00 cm². The instrument was operated at 23°C with both permeant and carrier humidified to 100% RH with wet sponges. The permeant was water vapor and the flow rate was 100 sccm of nitrogen gas. The sample underwent a half hour conditioning period. The exam time for each cycle was 30 minutes. Equilibrium was reached when the transmission rate varied between examinations by less than 1%. The steady-state after introduction of the water vapor into the test-gas side of the diffusion cell took approximately 15 hours but the test was sometimes allowed to continue for many more hours. The reported unit of measure was g/(m²-day). The minimum rate achievable was 0.005 g/(m²-day) with a 50.00 cm² sample size. The bias for this test method was determined at 15% and was derived from comparisons with known-value reference films. The precision was better than 10% relative to when samples were analyzed in duplicate.

OTR was measured using a Mocon Ox-Tran 2/22L instrument following ASTM D3985-17. The surface area of the samples tested was 5.00 cm². The instrument was operated at 23°C with both the permeant and carrier gases dried to a 0% RH environment. After completion of each pair of tests at 23.0°C, the instrument's temperature was increased to 37.8°C and both the permeant and carrier gases were humidified to 90% RH and the samples were re-tested. The permeant was oxygen and

the flow rate was 20 sccm of oxygen gas. The sample underwent a half hour conditioning period. The exam time for each cycle was 30 minutes. Equilibrium was reached when the transmission rate varied between examinations by less than 1%. The steady-state after introduction of the oxygen into the test-gas side of the diffusion cell took approximately 15 hours but the test was sometimes allowed to continue for many more hours. The reported unit of measure was $\text{cc}/(\text{m}^2\text{-day})$. The minimum rate achievable was $0.005 \text{ cc}/(\text{m}^2\text{-day})$ with a 50.00 cm^2 sample size. The bias for this test method was determined at 15% and was derived from comparisons with known-value reference films. The precision was better than 10% relative when samples were analyzed in duplicate.

3.4.11 Printing and surface analysis

Contact angle measurements were done using a Kruss 25E drop shape analyzer equipped with Kruss Advance software. Samples were prepared by cutting a strip of material in the cross direction in an area that appeared to have very little handling or wrinkling. Dry air was used to blow off any dust or debris on the surface. Four measurements were taken per sample.

Contact angle was determined using software that uses elliptical geometric fitting. When using this software, the user manually sets a baseline that operates as the bottom of the contact angle reading. It also assumes that the surface being analyzed is flat and smooth. Surface energy was calculated from contact angle using the OWRK method, which requires an equilibrium contact angle from both a polar and a dispersed fluid. The Young's and OWRK equations are shown in Equation (3) and (4) respectively.

$$\sigma_s = \sigma_{sl} + \sigma_l * \cos \theta \quad (3)$$

$$\sigma_{sl} = \sigma_s + \sigma_l - 2 \left(\sqrt{\sigma_s^D * \sigma_l^D} + \sqrt{\sigma_s^P * \sigma_l^P} \right) \quad (4)$$

σ_l = surface tension of the liquid

σ_s = surface free energy of the solid

σ_{sl} = interfacial tension between liquid and solid

σ_s^D = disperse component of surface free energy of the solid

σ_s^P = polar component of the surface free energy of the solid

σ_l^D = disperse component of surface free energy of the liquid

σ_l^P = polar component of the surface free energy of the liquid

For this experiment, water (polar) and diiodomethane (dispersed) fluids were used. The drop size for both fluids was 1 μL . There are several key assumptions that come with using this method. The OWRK equation is derived using the assumption that the surface is non-absorptive and flat. For films, this is typically a valid assumption. It also assumes that the drop formed is perfectly circular.

Another tool used to characterize the film surface was the nanocontact angle instrument. The difference between nanocontact angle and standard contact angle described above is that the nanocontact angle dispenses a smaller droplet, on the picoliter scale, whereas the standard contact angle dispenses a 1 μL droplet. The picoliter droplet size is important for studying materials that are digitally printed

because the digital printers dispense inks at this scale. The nanocontact angle also has the ability to measure dynamic contact angle over longer time scales. The nanocontact angle instrument has the ability to dispense water, inks, or many other fluids onto the surface. Nanocontact angle measurements were done using a Kyowa Interface Science MCA-3 Automatic Microscope contact angle meter. The droplets were dispensed using a DMC-M100 controller from Kyowa Interface Science. For each sample, 10 measurements were taken.

Digital printing was carried out on two wide format printers. The first was a Roland XF-640 printer using Eco-sol MAX 2® inks generally termed “eco-solvent” inks, and the second was an HP Latex 360 printer with HP 831A inks generally termed “latex inks”. The samples were fixed to a 1.5 meter roll and then printed. A photograph of the latex printer is shown in Figure 3.10. The image file was a print template set up to allow measurements of ink dot size and ink bleed. Another image file was used to study the impact of ink on the adhesive and film properties. This file was setup to print at a heavy ink load of the four combined CMYK (Cyan, Magenta, Yellow, and Black) inks at an excess of 250%. It was predicted that when printing at heaving ink loads, using either eco-solvent or latex inks, the film would become softer and the adhesive peel and cohesive strength would be reduced. The modulus was expected to decrease, but it was unknown how the eco-solvent and latex would compare in modulus reduction. This is likely caused by saturation of the film and adhesive with solvents from the inks. The eco-solvent inks contain a significant portion of glycol ether solvents and the latex inks contain a portion of 2-pyrillidone solvent.

Dot size and bleed images and measurements were taken using a Quality Engineering Associates PIAS-II handheld microscope and integrated software. The field of view for the high resolution mode was 3.2mm x 2.4mm. The count of ink dots per area, diameter, area and perimeter of the dots were reported. The bleed was measured by printing a line and measuring the width and raggedness of the line. The ideal print will have low raggedness, which indicates a clean line with low ink bleed.



Figure 3.10 Photograph of wide format printer with samples laminated to print roll

CHAPTER IV

RESULTS AND DISCUSSION

4.1 PVC-nanoclay cast film

4.1.1 Structure characterization

The structure of PVC-clay nanocomposite was first studied by use of WAXD. The Cloisite® 20 nanoclay powder was scanned first at a range of $2\theta = 0-30^\circ$. Next, the nanoclay powder was scanned in the range $2\theta = 0-10^\circ$ so that there was better resolution of the initial peak. The initial peak was at $2\theta = 2.78^\circ$, which corresponds to a d-spacing of 3.17 nm. The white PVC film with 3 phr Cloisite® 20 was scanned in the same range and no peaks were observed. The XRD plots are given in Figure 4.1. It was expected that the peak of the film should shift to lower angles indicating a change in the d-spacing thus intercalation of the polymer within the clay galleries.

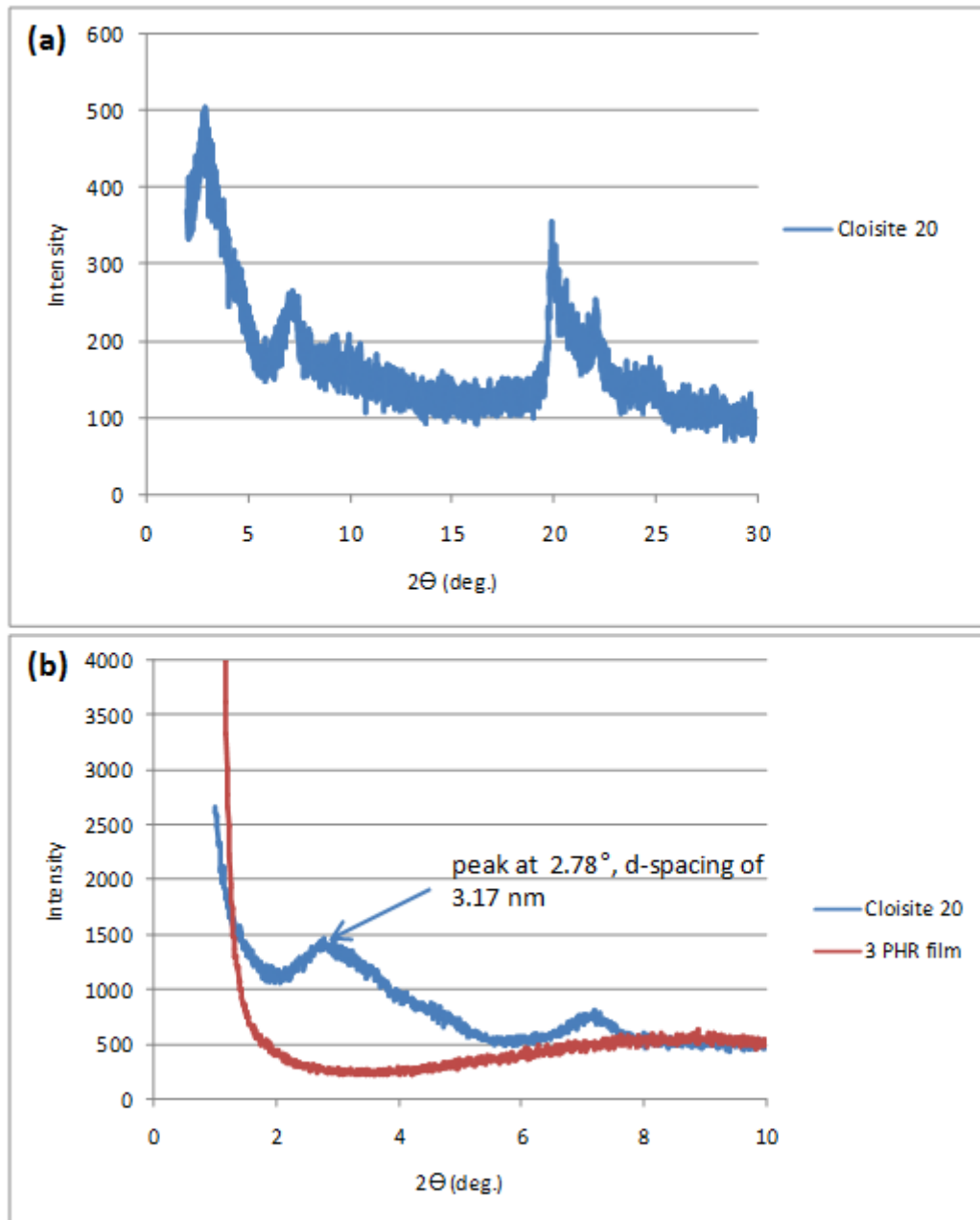


Figure 4.1 WAXD spectra of (a) Cloisite[®] 20 powder and (b) Cloisite[®] 20 powder and white PVC film with 3 phr Cloisite[®] 20

SEM top view images were taken at 2000x and 5000x magnification for the individual nanoclay powders and cross-section images were taken at 2000x magnification for the PVC-nanoclay films. The images are provided in Figures 4.2 and

4.3. The images of the powders showed the plate like layers of nanoclay stacked together in different sizes. There seemed to be a wide size distribution of the clay layer stacks. It was difficult to see the individual nanoclay layers from the cross-sectional view with SEM. For the white sample, the TiO₂ particles were very bright white and dominated the image. For the clear sample, the white areas that ran parallel to the surface appeared to be the stacks of nanoclay layers, but could not be confirmed from this imaging. An image of the TiO₂ particles was also taken and particle size measured at 200 nm. This image is provided in Figure 4.4.

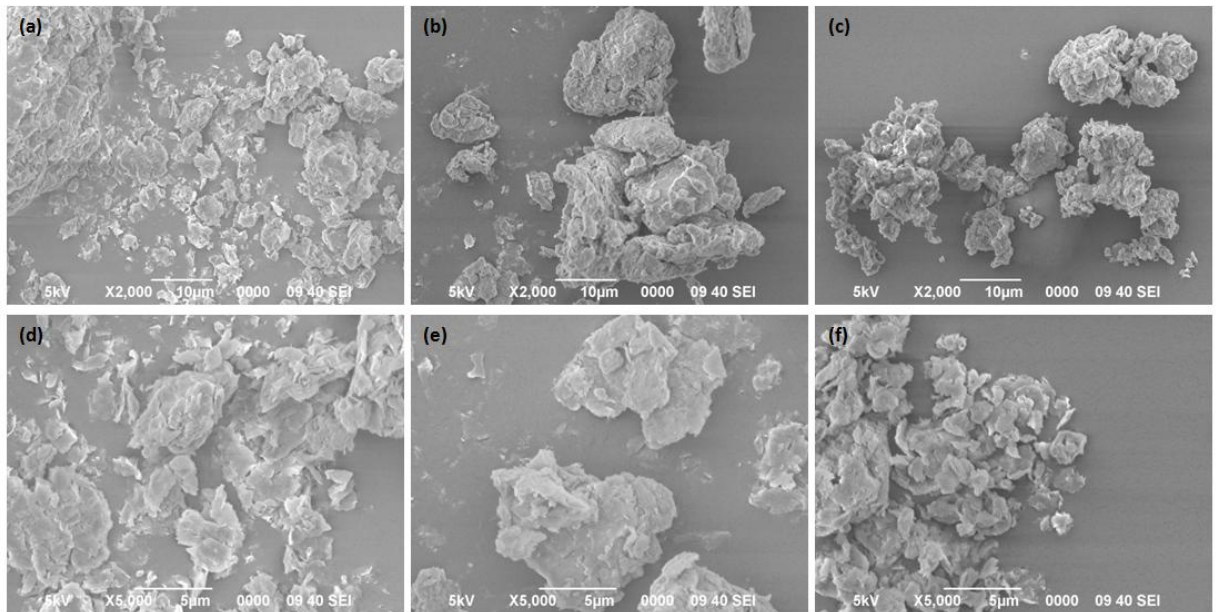


Figure 4.2 SEM top view images taken at 2000x and 5000x (a)(d) Cloisite® 10A (b)(e) Cloisite® Na+ (c)(f) Cloisite® 20

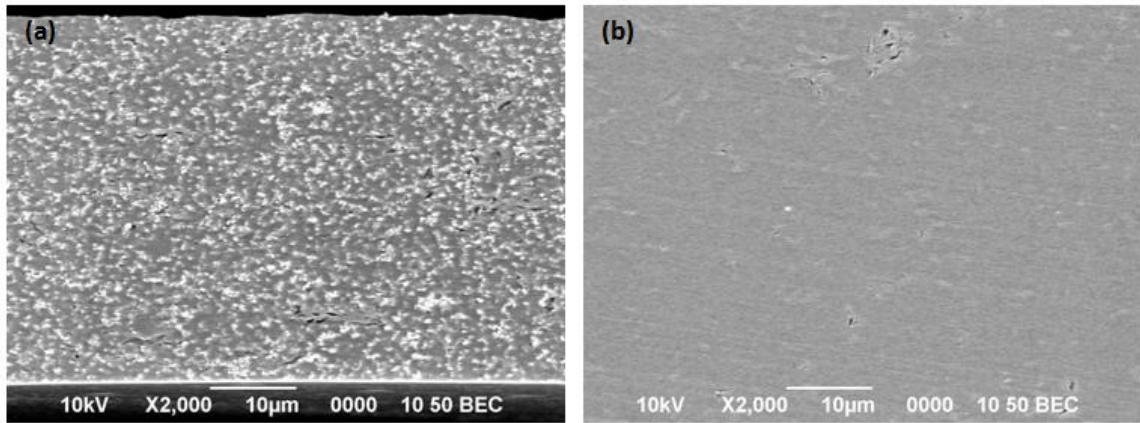


Figure 4.3 SEM cross-section images of (a) white PVC film with 5 phr Cloisite® 10A (b) clear film with 5 phr Cloisite® 10A

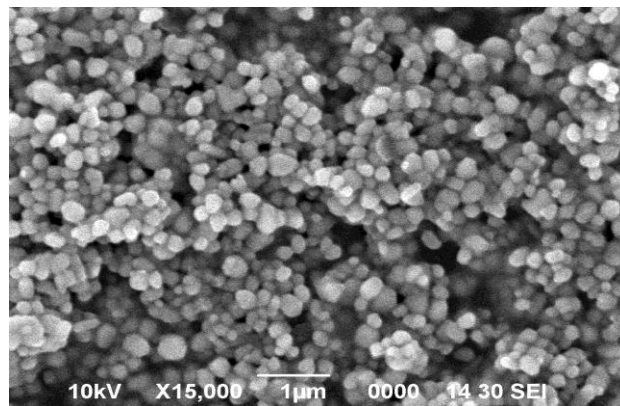


Figure 4.4 SEM top view image of TiO₂ particles at 15,000x

AFM was used to evaluate the surface topography of the white and clear PVC-nanoclay films. The white film with 5 phr Cloisite® 10A was compared with the 0 phr control film. These images are found in Figure 4.5. Both white films appeared to have a very uniform structure but some TiO₂ particles were observed at the surface. Nanoclay was not detected at the surface for the 5 phr film.

The clear film with 5 phr Cloisite® 10A was compared with the 0 phr control film. These images are found in Figure 4.6. The surface was observed to be mostly uniform with some spherical particles that were ~200 nm in size. Since no TiO_2 was present in the clear films, the particles were suspected to be the stabilizer, which had not been completely dispersed. The film with 5 phr Cloisite® 10A showed less of the particles than the 0 phr control. The 0.5 and 1 phr Cloisite® 10A films were also scanned for comparison. These images are found in Figure 4.6. The 0.5 and 1 phr clear films had similar particles as the 0 phr control film and images can be found in Figure 4.7.

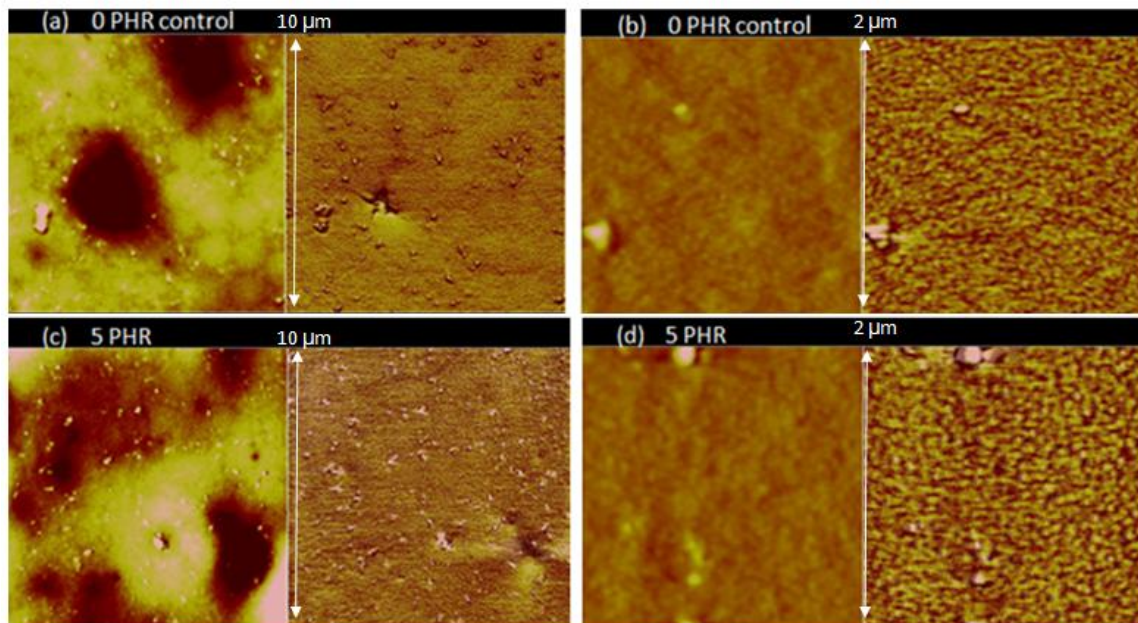


Figure 4.5 AFM images of white films (a) 0 phr 10 μm (b) 0 phr 2 μm (c) 5 phr 10 μm (d) 5 phr 2 μm

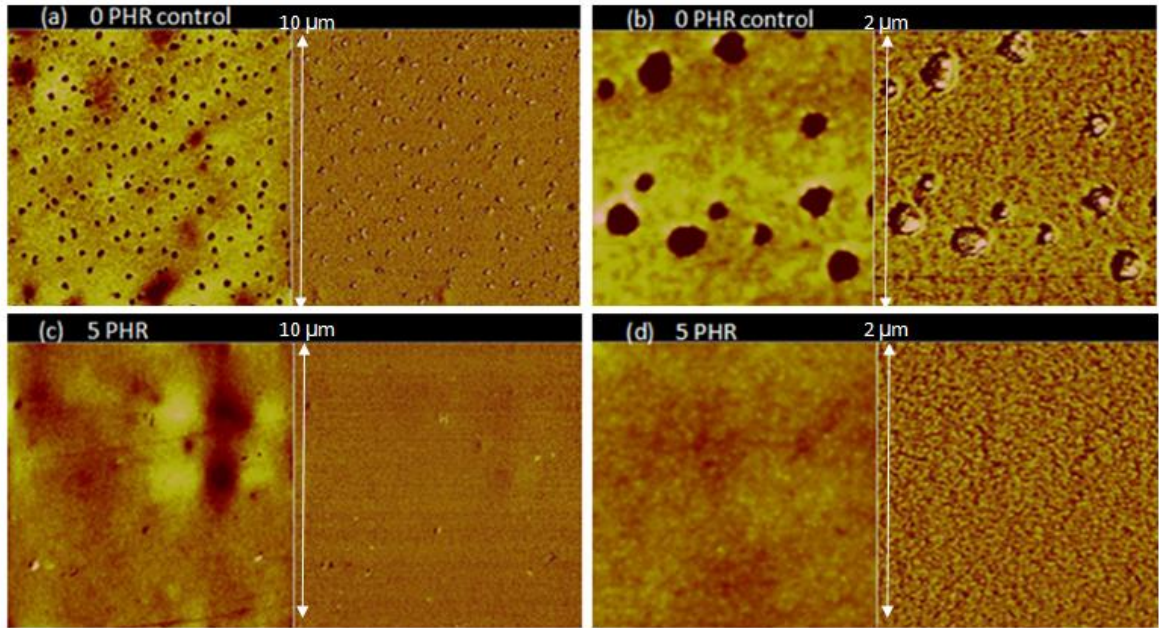


Figure 4.6 AFM images of clear films (a) 0 phr 10 μm (b) 0 phr 2 μm (c) 5 phr 10 μm (d) 5 phr 2 μm

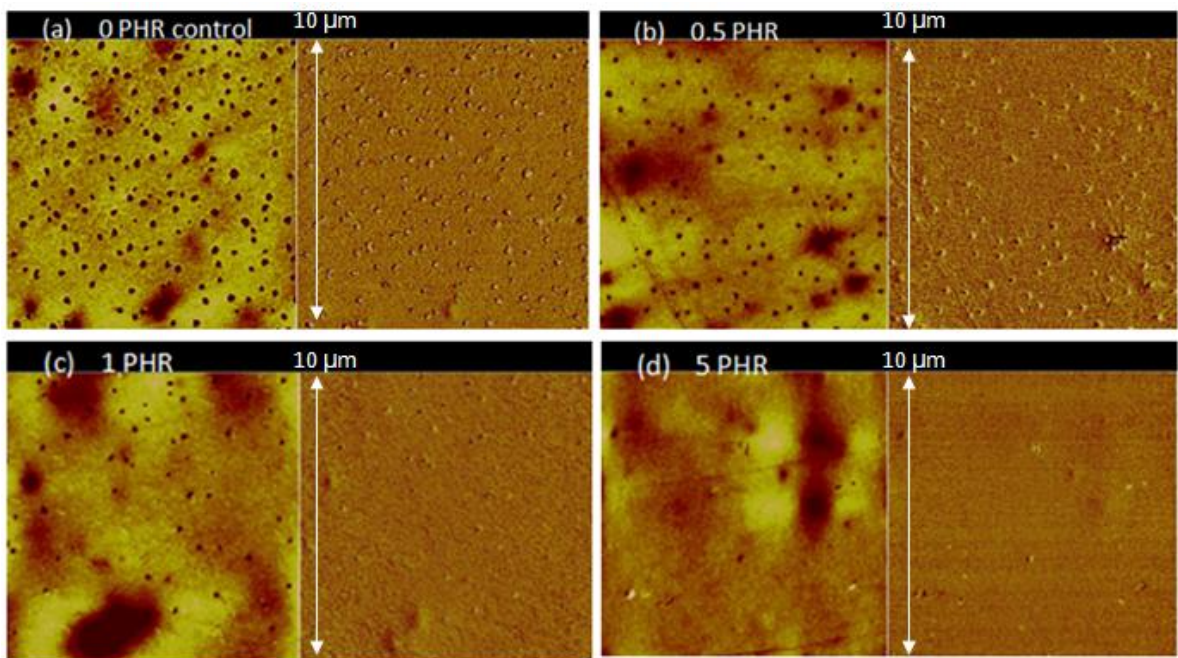


Figure 4.7 AFM images of clear films (a) 0 phr 10 μm (b) 0.5 phr 10 μm (c) 1 phr 10 μm (d) 5 phr 10 μm

TEM was used to characterize the structure and the scale of dispersion of the nanoclay in PVC. Both white and clear films were evaluated. The nanoclay loadings were 0.5 phr and 5 phr. These samples were chosen in order to compare the range of nanoclay levels in PVC that were prepared. The nanoclay was Cloisite® 20 and the film thickness was 50 µm. The images of the white film at 0.5 phr nanoclay loading are shown in Figure 4.8a in bright field mode and the two images in Figure 4.8b,c in dark field mode. The dark field mode is also known as high-angle annular dark-field imaging (HAADF). In the bright field mode, the individual clay layers were denser and crystalline and thus appeared darker in the image. Figure 4.8a indicates that nanoclay formed an intercalated structure within PVC. In the dark field mode, the crystalline nanoclay layers appeared brighter. The white particles appeared to be TiO₂.

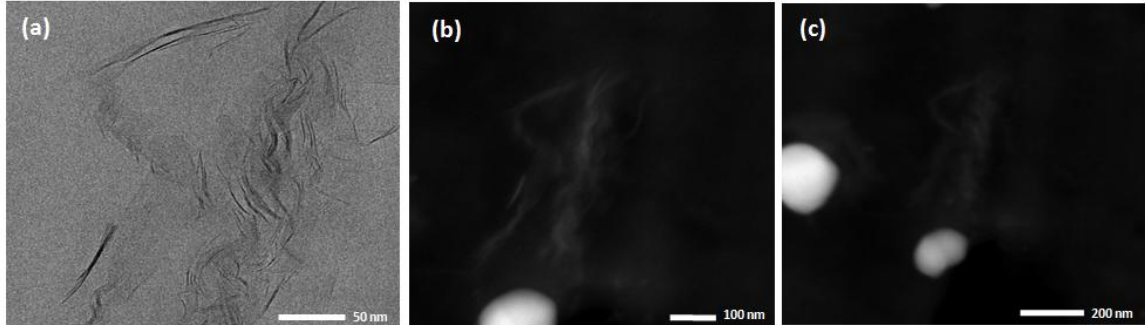


Figure 4.8 TEM images of print film (a) 0.5 PHR bright field mode (b,c) 0.5 PHR dark field mode

Energy dispersive X-ray spectroscopy (EDS) was used to identify the elemental components in different regions of the material. The area with clay layers showed peaks for Si, Al, and O on the EDS spectra in Figure 4.9. This was consistent with the

composition of MMT nanoclay which has the general structure $M_x(Al_{4-x}Mg_x)Si_8O_{20}(OH)_4$.

The other area was confirmed to be TiO_2 from the spectra in Figure 4.10.

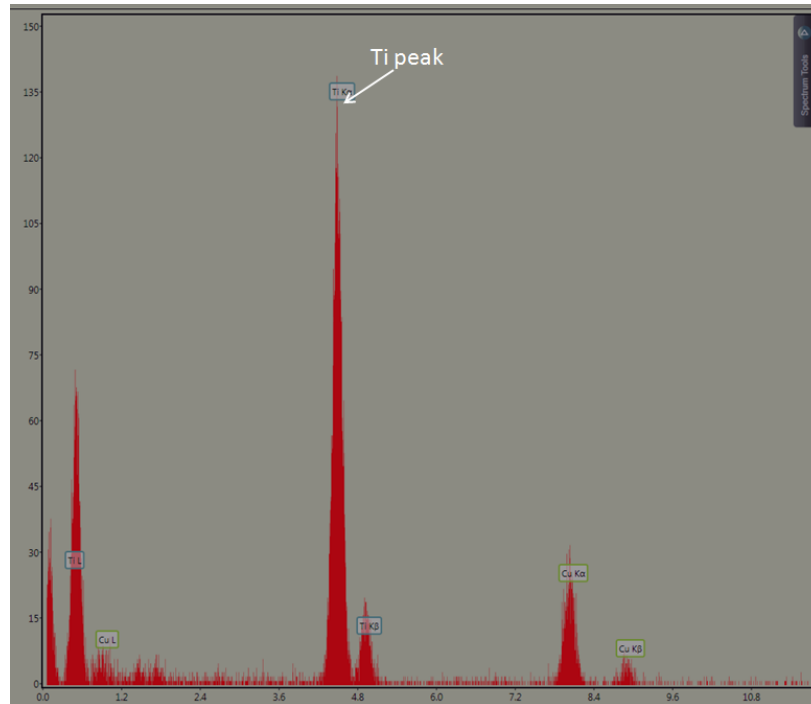


Figure 4.9 EDS Spectra of 0.5 phr white film confirming that the white particles in Figure 4.7b,c are TiO_2

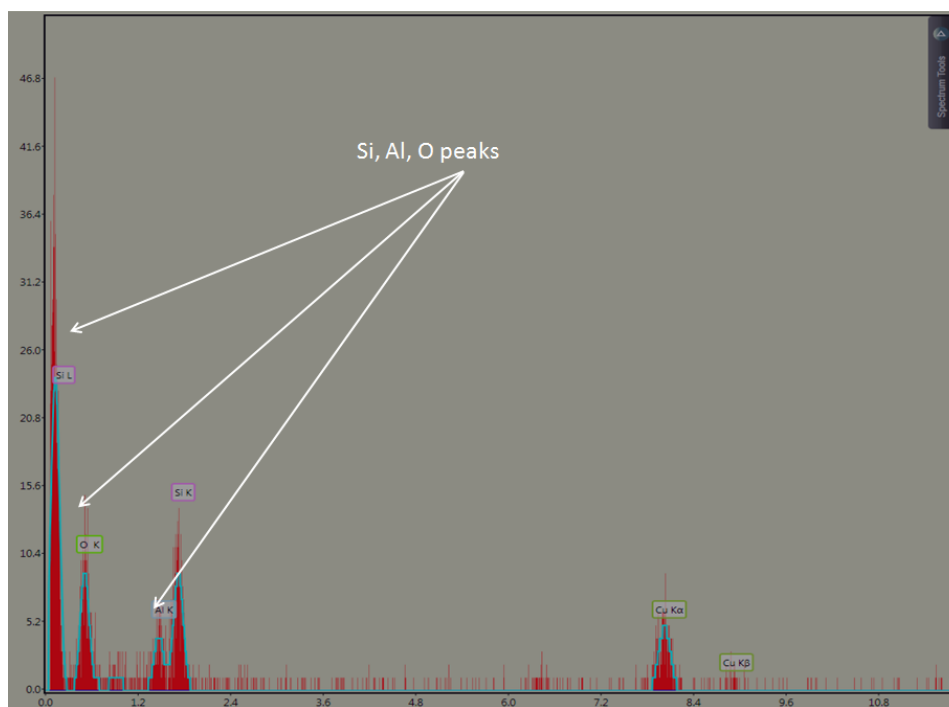


Figure 4.10 EDS spectra of 0.5 phr white film confirming that the white layers in Figure 4.7b,c are nanoclay

The images of the white film at 5 phr nanoclay loading are shown in Figure 4.11. Figures 4.11a,b,c were taken in bright field mode and Figures 4.11d,e in dark field mode. The dispersion of nanoclay layers did not appear to be as uniform as the 0.5 phr loaded sample. Certain areas appear to have higher density of nanoclay layers. The larger particles are TiO_2 , which appear darker in the bright field mode. The nanoclay layers appear to be grouped together and may not be intercalated as well as the previous sample. EDS confirmed that the white particles were TiO_2 and the layered structure was due to nanoclay.

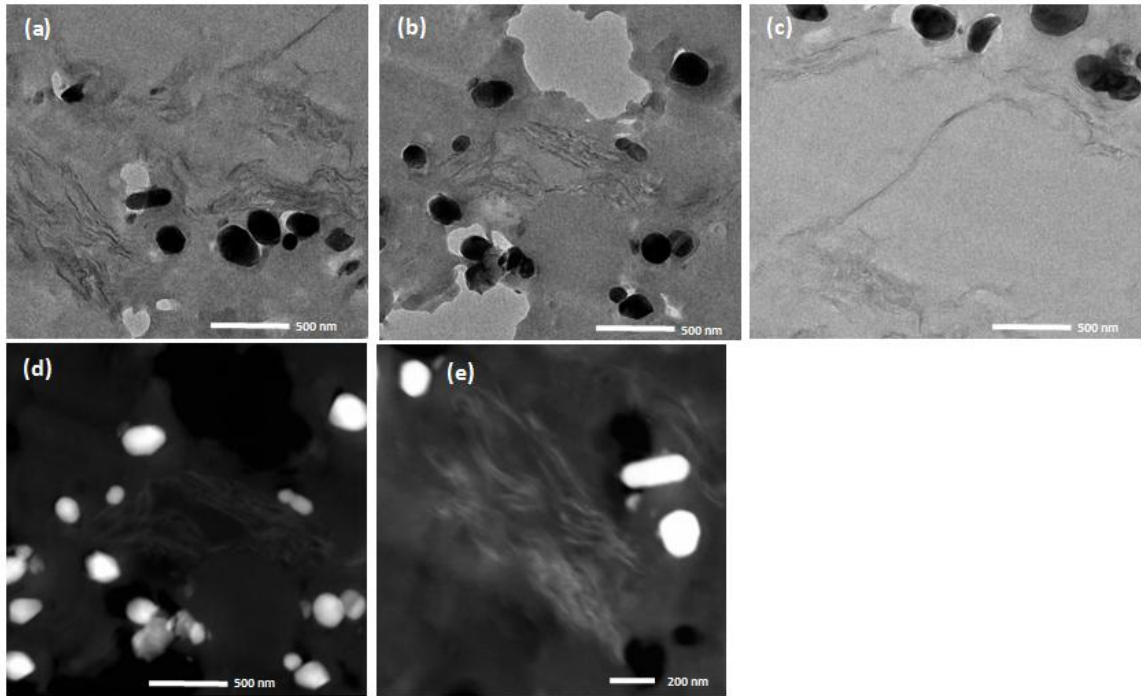


Figure 4.11 TEM images of white films (a,b,c) 5 phr bright field mode (d,e) 5 phr dark field mode

The clear films were scanned in dark field mode only because there was not much detection of the structure in bright field mode. The images of the clear film at 0.5 and 5 phr nanoclay loading are shown below in Figure 4.12. The figures show some spherulite structures that were not expected. These structures are denser and more crystalline than the PVC matrix. The structures may be stabilizer that was not fully dispersed. The clay layers appear to be intercalated. Figure 4.12f shows the nanoclay layers of the 5 phr sample. It was expected that the orientation of the clay layers within the film structure would be important for effective barrier properties. Based on the TEM results, the nanoclay does not appear to be oriented in a certain direction in the PVC film structure.

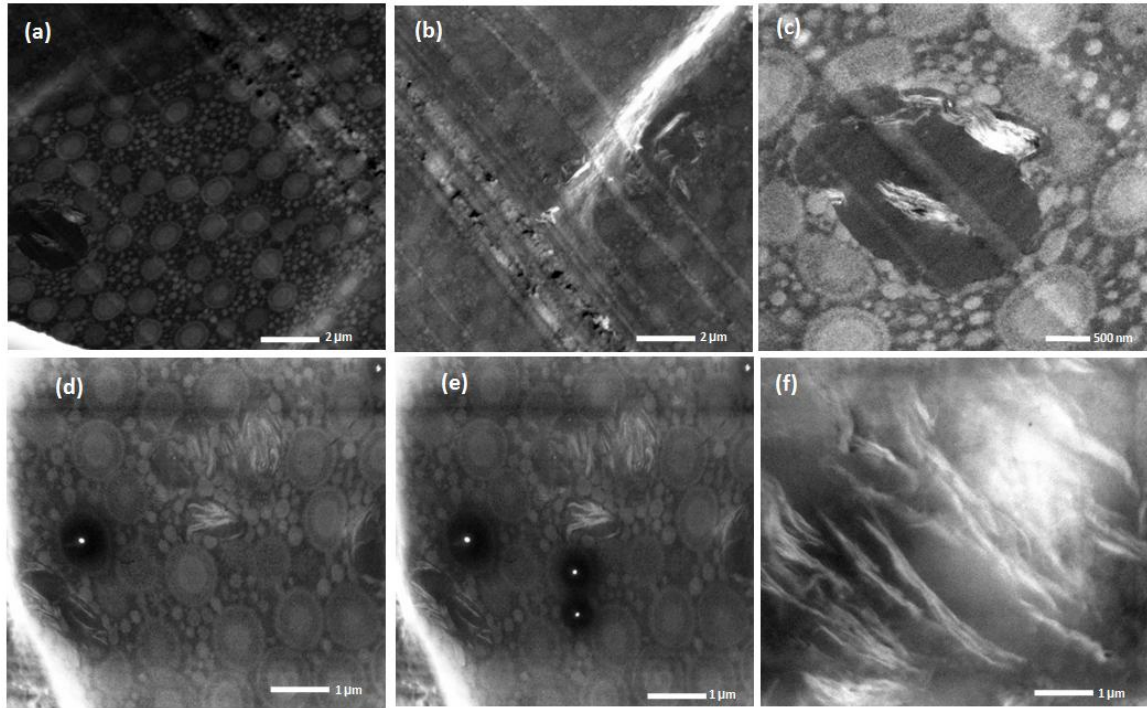


Figure 4.12 TEM images of clear films (a,b,c) 0.5 phr dark field mode (d,e,) 5 phr dark field mode

4.1.2 Thermal stability

After the thermal cycle in the Metrastat oven, the samples were removed and photographed. The images in Figure 4.13 show the difference in heat stability with loading of Cloisite® 10A in the PVC films. The top image shows the print film and the bottom image shows the clear film. The set of 5 strips on the left of each image are the film only and the strips on the right are the film with the adhesive and the liner. The print film showed some shift to darker purple color as the loading of nanoclay increased. The clear films showed a more significant shift in color as the loading of nanoclay was increased. The color shift started earlier for the clear samples and the 5 phr loading showed significant dark black discoloration. There was no significant difference in color

change when the adhesive and the liner were added to the structure. This indicated that the adhesive did not discolor and the interaction between the PVC and adhesive did not cause a color change. For the clear films, the 0.5 and 1 phr loadings showed similar discoloration as the 0 phr control.

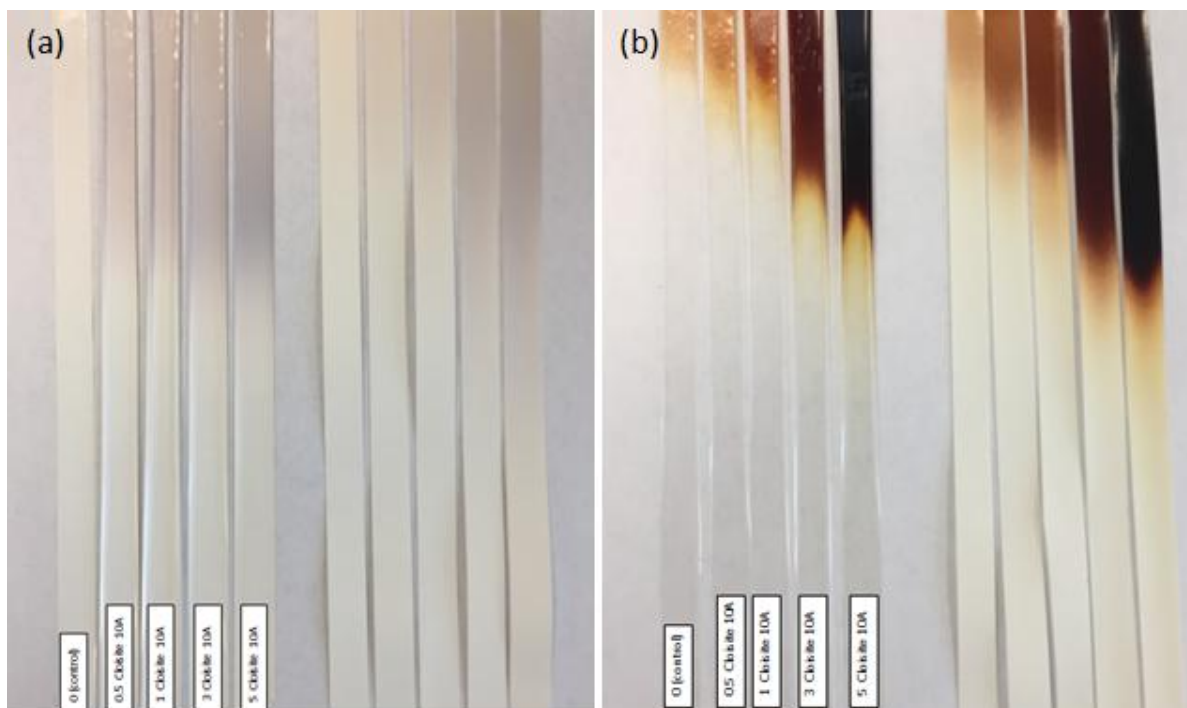


Figure 4.13 Photographs of the films after heating in Metrastat (a) white print films, film only on left, film, adhesive, and liner on right (b) clear films, film only left, film/adhesive/liner on right

Figure 4.14 shows the white films formulated with Cloisite® 10A, Cloisite® Na+ and Cloisite® 20. The three Cloisite® Na+ films all showed no discoloration, which was consistent with the control. The films made with Cloisite® 10A and Cloisite® 20 showed similar discoloration at all three loadings.



Figure 4.14 Photographs of the white films after heating in Metrastat

The next test was to look at the thermal stability of the nanoclay powder separately. No significant color change was observed after aging the nanoclay at 180°C. The nanoclay was aged for 2 minutes and 30 minutes. An image of the clay disk is found in Figure 4.15 and ΔE measurements in Figure 4.16. The fact that the nanoclay alone did not show any color change leads to an interaction between the PVC and nanoclay. This is due to the degradation of the organic modifier.



Figure 4.15 Photographs of nanoclay disks after thermal aging for 30 minutes at 180°C

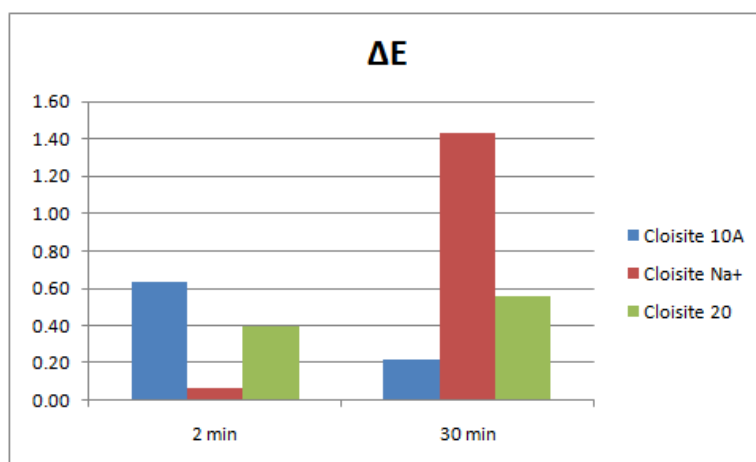


Figure 4.16 Color change of nanoclay disks after thermal aging for 2 minutes and 30 minutes at 180°C

The DSC thermograms for the white and clear films are shown in Figures 4.17 and 4.18 and the glass transition temperature (T_g) measurements are given in Table 4.1. The T_g of the print and clear film without nanoclay was 11.1°C and 18.2°C respectively. This was expected as the print film had a higher loading of plasticizer in the formulation. For the print film, the T_g decreased slightly with loading of nanoclay from 11.1°C to 8.8°C at 0 and 5 phr loading respectively. The T_g of clear film also decreased slightly as the nanoclay loading was increased. The values at 0 and 5 phr loading were 18.2°C and 16.8°C respectively.

Sample ID	Print film	Clear film
	T _g (°C)	T _g (°C)
0 (control)	11.1	18.2
0.5 PHR Cloisite 10A	9.2	16.6
1 PHR Cloisite 10A	9.7	8.9
3 PHR Cloisite 10A	5.7	12.4
5 PHR Cloisite 10A	8.8	16.8

Table 4.1 T_g results measured by DSC for white and clear films

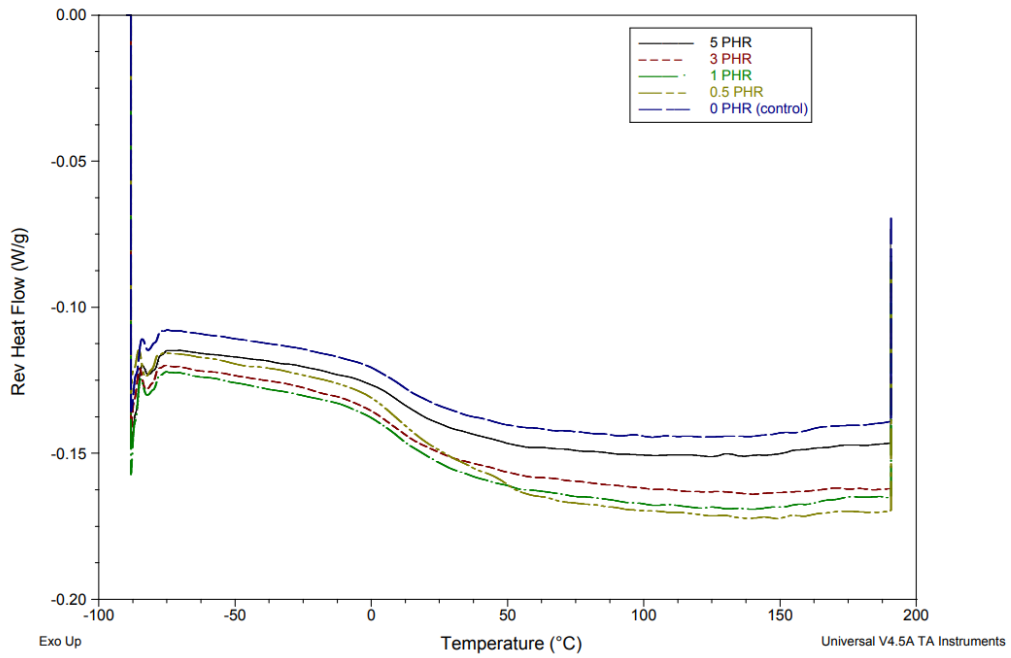


Figure 4.17 DSC thermogram for white PVC-clay nanocomposites with Cloisite 10A, 0-5 phr loading

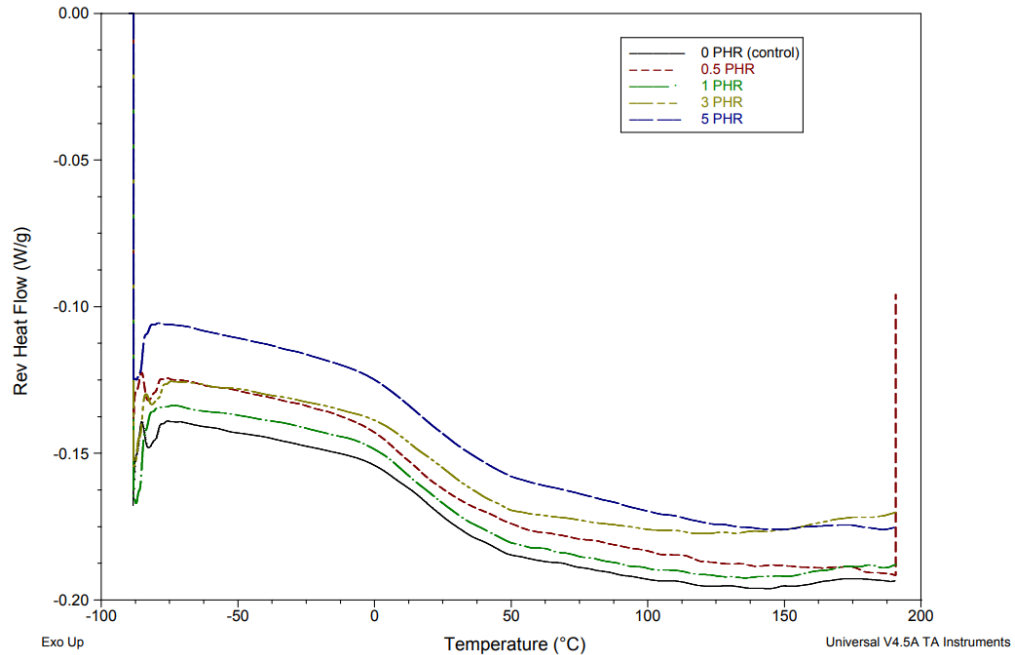


Figure 4.18 DSC thermogram for clear PVC-clay nanocomposites with Cloisite 10A, 0-5 phr loading

Previous researchers [44], [68] have shown an increase of T_g with nanoclay loading. Gong et al. [44] prepared PVC-nanoclay materials by in-situ polymerization and showed that the T_g increased from 85.3°C for virgin PVC to 87.6°C at 5% MMT loading. They suggested that when the polymer chains were intercalated between the nanoclay layers, they became less mobile which caused the T_g to increase. A different effect was seen for melt compounded materials reported by Pagacz and Pielichowski [68], where the PVC materials with MMT and OMMT showed a slight reduction in T_g . Their conclusion was that the nanoclay behaved as a plasticizer when PVC chains intercalated into the nanoclay layers.

4.1.3 Appearance and optical properties

In general, the color differences were low for all samples, and increased slightly as the nanoclay loading was increased. The individual L, a, b, values and ΔE are reported in Table 4.2. The highest value for ΔE was 3.44 for the print film at 5 phr nanoclay loading and 3.8 for the clear film at 5 phr nanoclay loading. The increase in b-value indicated that the color shifted slightly from blue to yellow.

		L*	a*	b*	ΔE
print film	0 clay	96.3	-1.4	2.0	-
	0.5 phr Cloisite® 10A	96.4	-1.4	1.8	0.2
	1 phr Cloisite® 10A	96.3	-1.5	1.9	0.1
	3 phr Cloisite® 10A	95.7	-1.3	4.4	2.4
	5 phr Cloisite® 10A	94.7	-0.8	5.0	3.4
clear film	0 clay	90.4	-1.6	1.9	-
	0.5 phr Cloisite® 10A	90.1	-1.7	2.3	0.5
	1 phr Cloisite® 10A	89.7	-2.0	3.6	1.9
	3 phr Cloisite® 10A	89.8	-1.9	3.4	1.6
	5 phr Cloisite® 10A	88.7	-2.3	5.2	3.8

Table 4.2 L*, a*, b* color values and ΔE color difference for white and clear films

The gloss values are reported in Table 4.3. Typically high gloss cast PVC films are required to have a gloss of ~90 gu measured at 60°. The gloss levels of the print and clear film were not affected by the addition of nanoclay.

		20°	60°	85°
print film	0 clay	51.3	88.1	95.0
	0.5 phr Cloisite® 10A	54.1	89.5	93.7
	1 phr Cloisite® 10A	55.4	90.0	94.9
	3 phr Cloisite® 10A	51.5	89.9	93.1
	5 phr Cloisite® 10A	54.5	92.1	93.1
clear film	0 clay	59.9	89.7	95.2
	0.5 phr Cloisite® 10A	56.2	90.0	95.5
	1 phr Cloisite® 10A	64.3	90.3	95.9
	3 phr Cloisite® 10A	60.6	89.7	95.8
	5 phr Cloisite® 10A	67.9	90.6	97.4

Table 4.3 Gloss values for white and clear films

The gloss level was known to be a function of surface roughness. For the cast PVC films, surface roughness was dictated by the surface roughness of the casting sheet. The roughness measurements are shown in Table 4.4. The roughness variables are calculated over a 1.5 mm x 1.5 mm measurement area where Sa is the arithmetical mean height, Sq is the root mean square height and Sz is the maximum height. The measurements indicated that the nanoclay did not disrupt the surface topography. All samples maintained the smooth surface of the PET cast sheet, which provides the high gloss level.

	Sa (nm)	Sq (nm)	Sz (um)
0 (control)	24.1 ± 1.7	51.0 ± 7.3	2.9 ± 0.5
1 PHR Cloisite 10A	24.2 ± 2.1	52.5 ± 9.9	4.3 ± 0.5
3 PHR Cloisite 10A	23.5 ± 0.8	52.1 ± 3.8	4.0 ± 0.6
5 PHR Cloisite 10A	22.7 ± 0.6	52.9 ± 5.7	3.7 ± 0.9
1 PHR Cloisite Na+	24.9 ± 1.9	59.1 ± 8.5	4.0 ± 0.6
3 PHR Cloisite Na+	24.1 ± 0.6	55.1 ± 8.6	4.9 ± 1.9
5 PHR Cloisite Na+	24.0 ± 1.5	51.3 ± 5.2	4.8 ± 1.2
1 PHR Cloisite 20	21.5 ± 0.4	41.7 ± 4.4	3.2 ± 0.4
3 PHR Cloisite 20	23.3 ± 1.6	51.6 ± 3.0	4.3 ± 1.2
5 PHR Cloisite 20	24.3 ± 0.6	58.0 ± 4.8	4.8 ± 1.0

Table 4.4 Surface roughness measurements for print film with different nanoclay types and loadings

The haze, clarity, and transmission of the clear films are shown in Figure 4.19.

The haze did not significantly increase at nanoclay loadings up to 3 phr. The clarity and transmission did not significantly change with nanoclay loading, indicating the nanoclay was effectively dispersed in the clear film. Figure 4.20 shows a comparison of haze values for the standard and two-step mixing processes. The results indicate that the mixing procedure did not affect the optical properties of the PVC films.

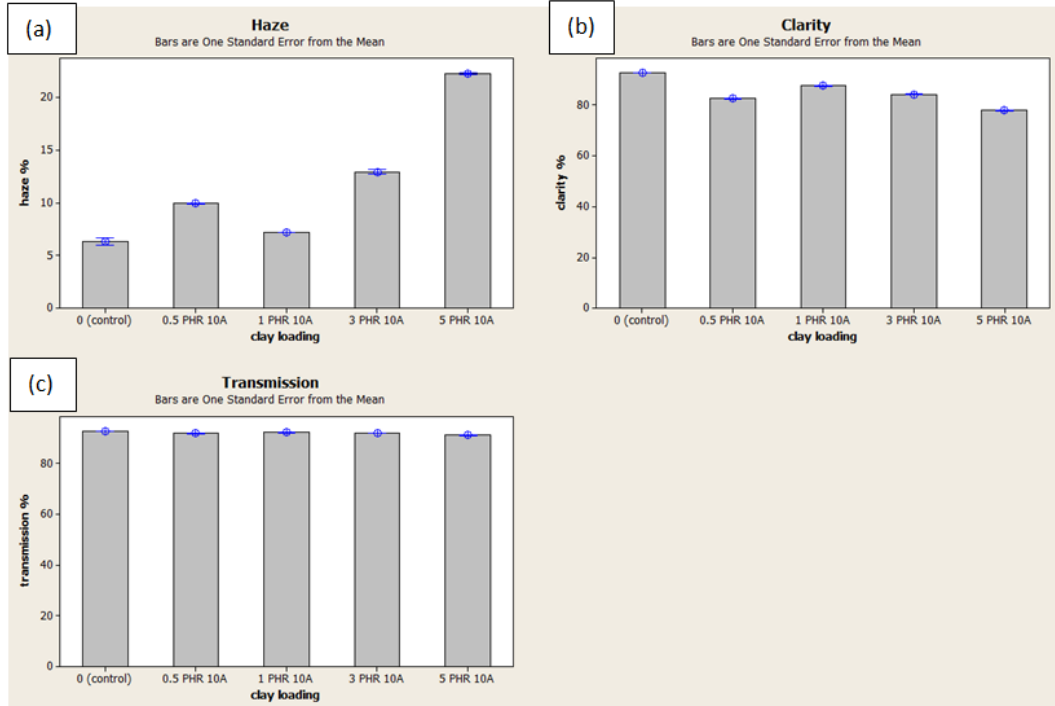


Figure 4.19 Impact of nanoclay loading on (a) Haze (b) Clarity (c) transmission of clear films

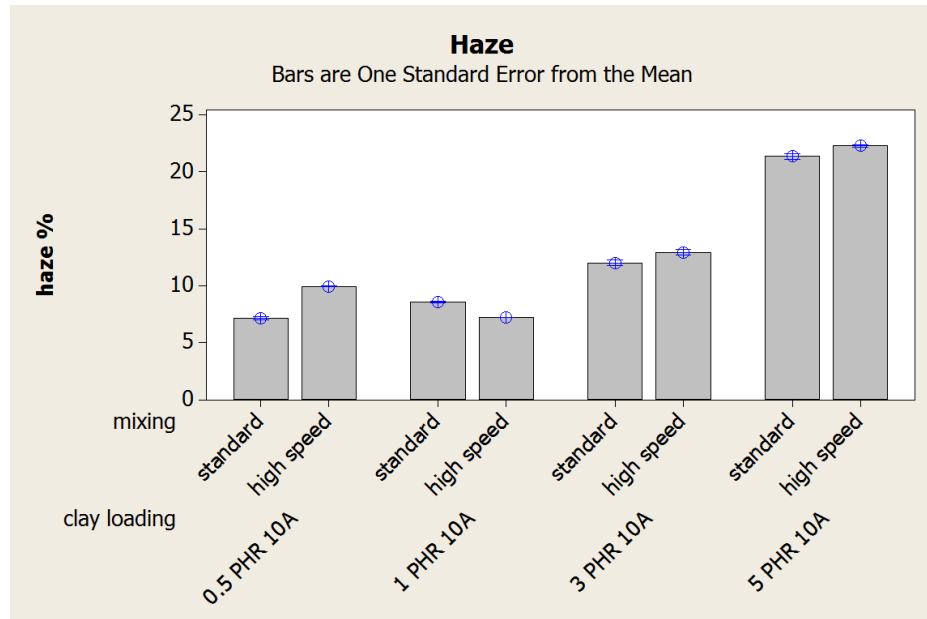


Figure 4.20 Impact of mixing procedure on haze of clear films

4.1.4 Mechanical properties

The first set of film samples were mixed using the dispersion blade mixing process described above. The Young's modulus and elongation at break are plotted in Figure 4.21. Young's modulus is given in Equation (5).

$$E = \frac{\sigma}{\epsilon} \quad (5)$$

E = Young's modulus (MPa)

σ = uniaxial stress (Pa)

ϵ = strain (dimensionless)

It was expected that the modulus would increase and the elongation at break would decrease with the addition of nanoclay. The nanoclay would act to stiffen the film as it reduced chain mobility. The data in Figure 4.21a indicated that the modulus of the white film did not change significantly with nanoclay loading for the three different grades of nanoclay. The white film did show a decrease in elongation at break of 44%, 27% and 61% at 5 phr loadings of Cloisite® 10A, Cloisite® Na+, and Cloisite® 20 respectively. The modulus of the clear film did change with the nanoclay loading, especially at 3 and 5 phr. The elongation at break showed a decrease of 23% and 29% at 5 phr loadings of Cloisite® 20 and Cloisite® 10A. The samples with Cloisite® Na+ were not tested due to poor dispersion. The impact of nanoclay may not be as significant for

these samples due to potentially poor dispersion versus the samples mixed at higher shear and speeds.

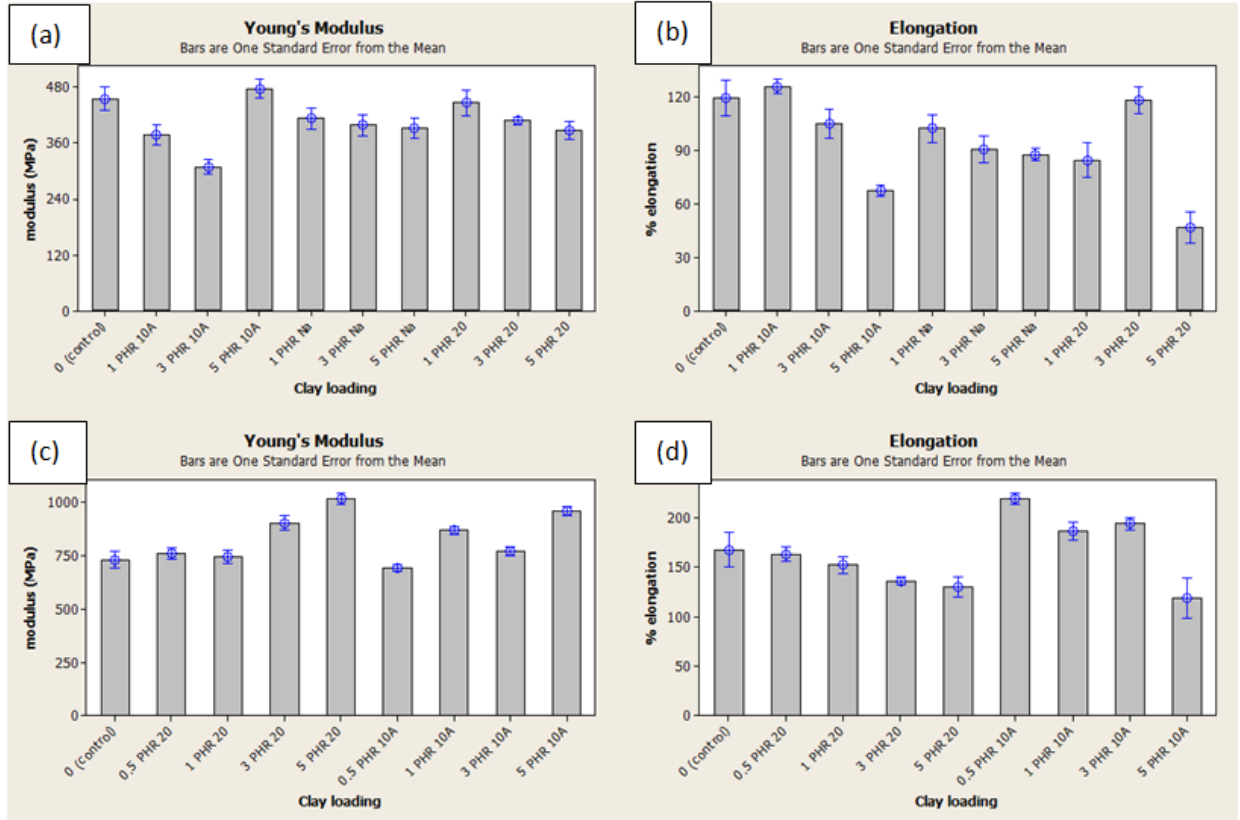


Figure 4.21 Young's modulus versus nanoclay loading for (a) white film (c) clear film and elongation at break versus nanoclay loading for (b) white film (d) clear film

The next sets of films were prepared with the high speed homogenizer to achieve better dispersion of nanoclay. The Young's modulus and elongation at break are plotted in Figure 4.22 and the stress-strain plot shown in Figure 4.23. The modulus of the 5 phr white sample increased by 10% and the elongation decreased by 51%. The clear film showed a more significant modulus increase of 63%, and 47% at 3 and 5 phr loadings. The elongation at break decreased by 14% and 25% at 3 and 5 phr loadings.

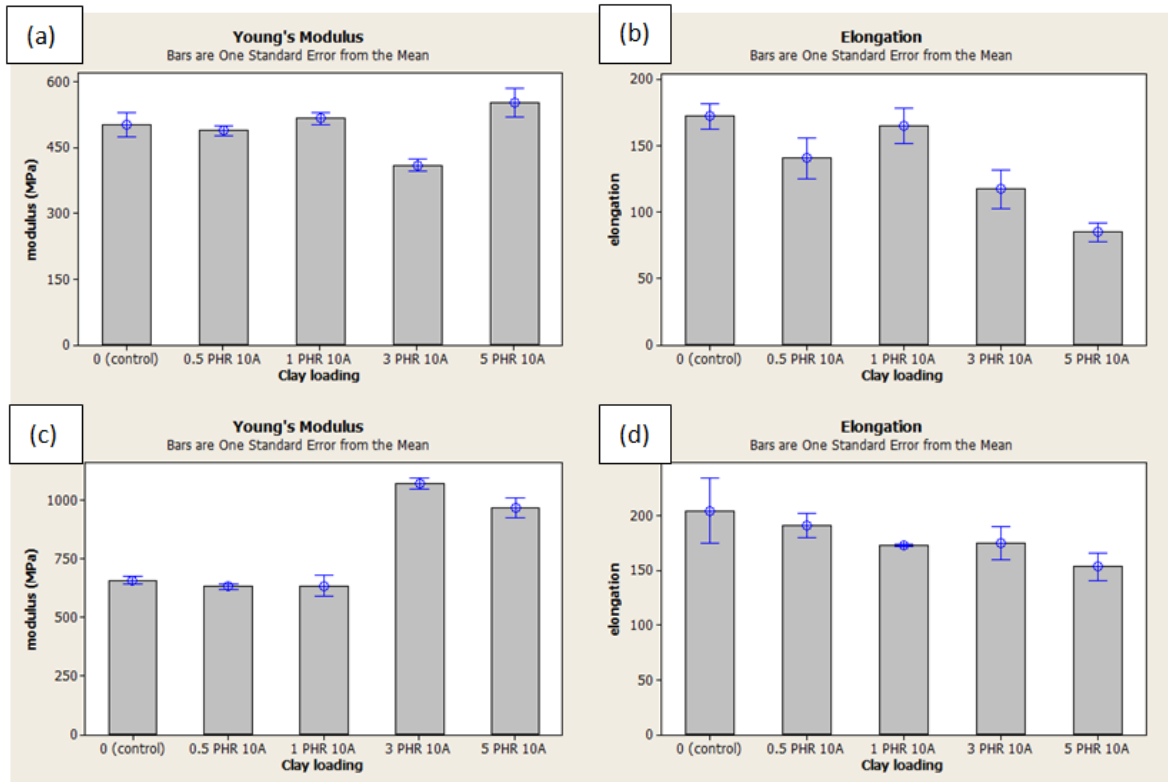


Figure 4.22 Young's modulus versus nanoclay loading for (a) white film (c) clear film and elongation at break versus nanoclay loading for (b) white film (d) clear film

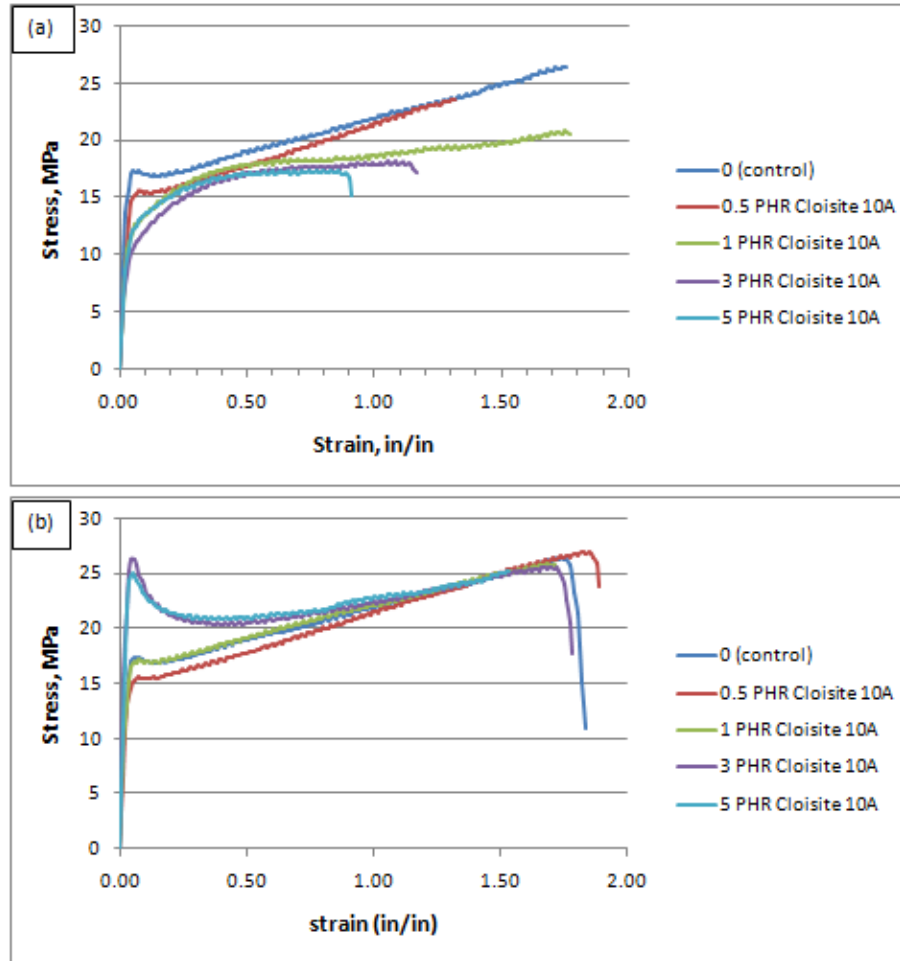


Figure 4.23 Stress-strain curves for (a) white films and (b) clear films mixed with high speed homogenizer

Next, the effect of mixing procedure on mechanical properties was evaluated.

This data is displayed in Figure 4.24. The white film showed an increase of modulus and elongation for all samples for the homogenizer mixing method, indicating that the nanoclay was more effectively dispersed in PVC. The clear film did not show significant differences between the mixing methods. The difference may be attributed to the interaction with TiO_2 in the white film, where higher shear was required to disperse the nanoclay in combination with TiO_2 particles.

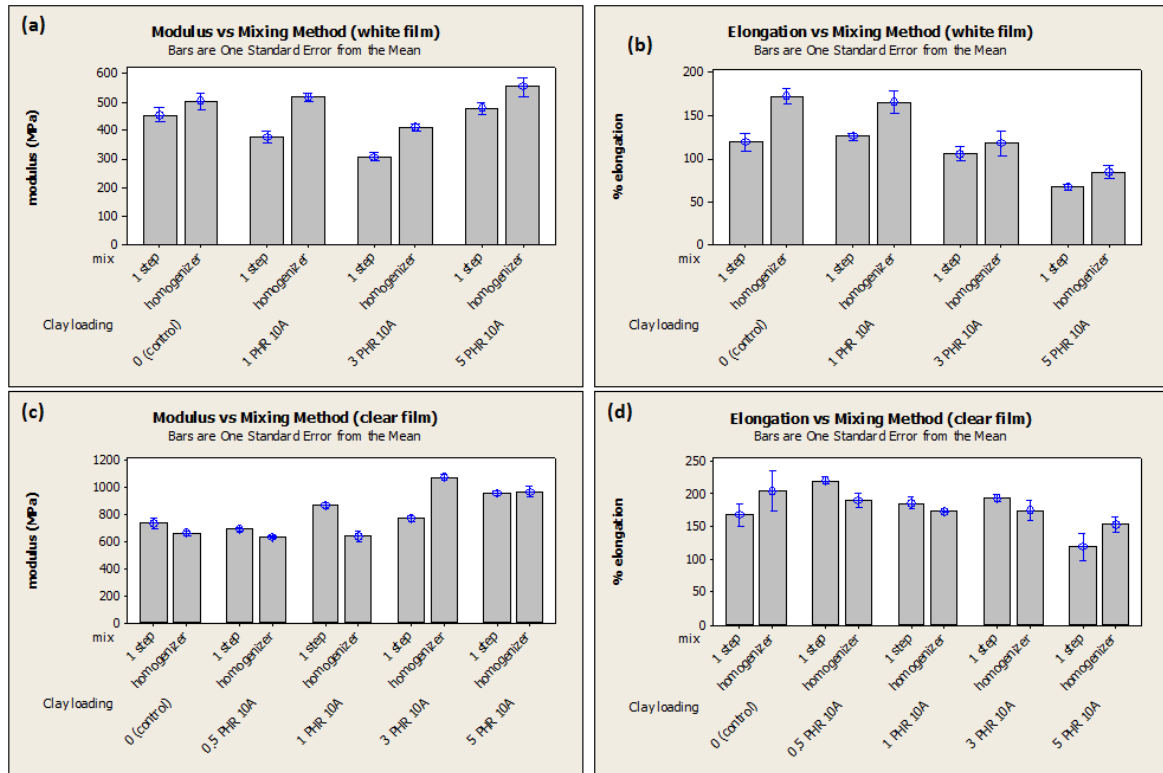


Figure 4.24 Effect of mixing method on elongation of the (b) white film and (d) clear film and modulus of the (a) white film and (c) clear film.

4.1.5 Durability and barrier properties

The durability was evaluated using the four accelerated weathering methods described in the materials and methods section page 64. The goal was to understand the impact of nanoclay on the film degradation. Polymers break down over time under outdoor exposure environments due to many factors including radiation from the sun. Radiation in the ultraviolet region has the capability to break chemical bonds. This is the case for PVC which was reported to have bond-dissociation energies of 73-92 Kcal/mole for the bonds in PVC molecules. [69] Goldman et al. [70] studied the effect of adding nanoclay to polybutylene terephthalate (PBT) on weathering performance. They

concluded that the filled material had better durability, which they attributed to the UV filtering of the nanoclay which altered its penetration depth in the material. They also found that UV radiation changed the crystallinity of the material, and proposed that smaller crystallite size provided improved durability.

The Super UV test was found to be the most severe for polymer degradation due to its high intensity UV radiation. It produced failures much quicker than the other methods. Typically a ΔE value of < 10 is deemed acceptable. Figure 4.25 and 4.26 show the color shift of the white films after the Super UV test. The ΔE was plotted versus exposure energy in units of megajoules (MJ). Figure 4.25 shows the ΔE of white films produced using the one step mixing process. The only samples that showed a significant color shift were the samples loaded with 5 phr of Cloisite[®] Na⁺ and Cloisite[®] 10A.

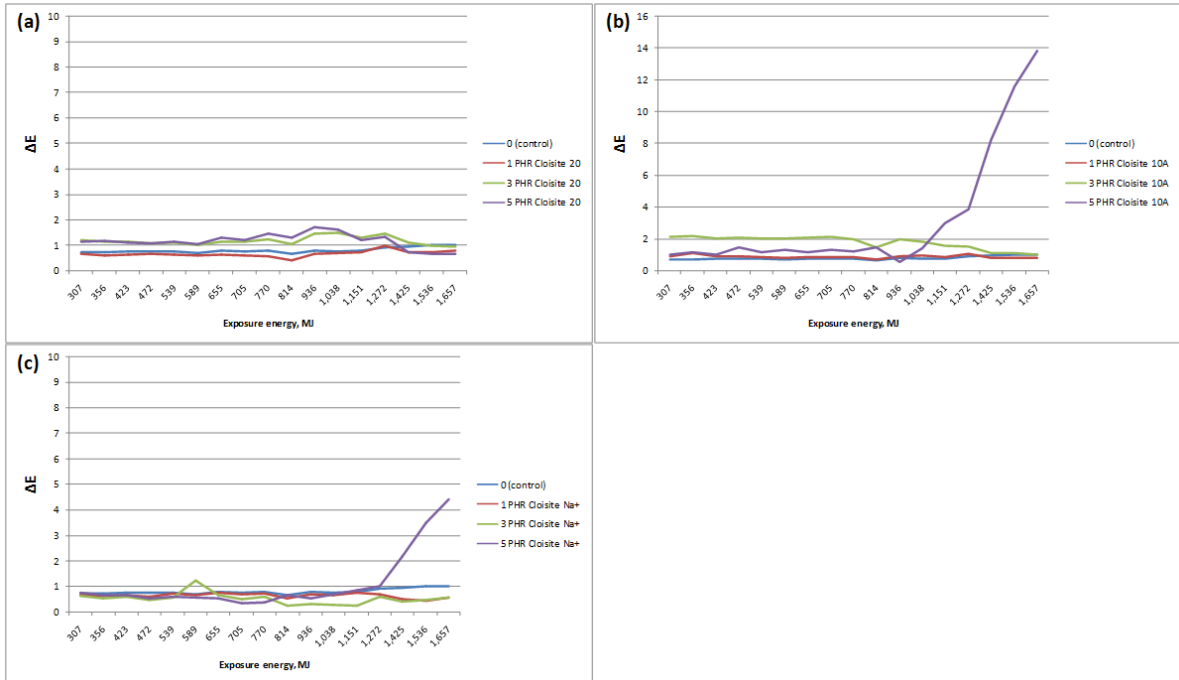


Figure 4.25 Color shifts of white films after Super UV test (a) white films with Cloisite[®] 20, (b) white films with Cloisite[®] 10A, and (c) white films with Cloisite[®] Na+.

Figure 4.26 shows the ΔE of white films produced using the high speed mixing method. In Figure 4.26a the only sample that showed a significant color shift was the sample loaded with 5 phr Cloisite[®] 10A. Figure 4.26b shows the white samples made with clear PVC laminated on top. It was anticipated that the samples with the clear PVC top layer would fail earlier. The clear PVC top layer may trap HCl and further accelerate the degradation process. All films with the clear PVC top layer show significant increase

in color shift, and the color shift increases with increasing loading of Cloisite® 10A.

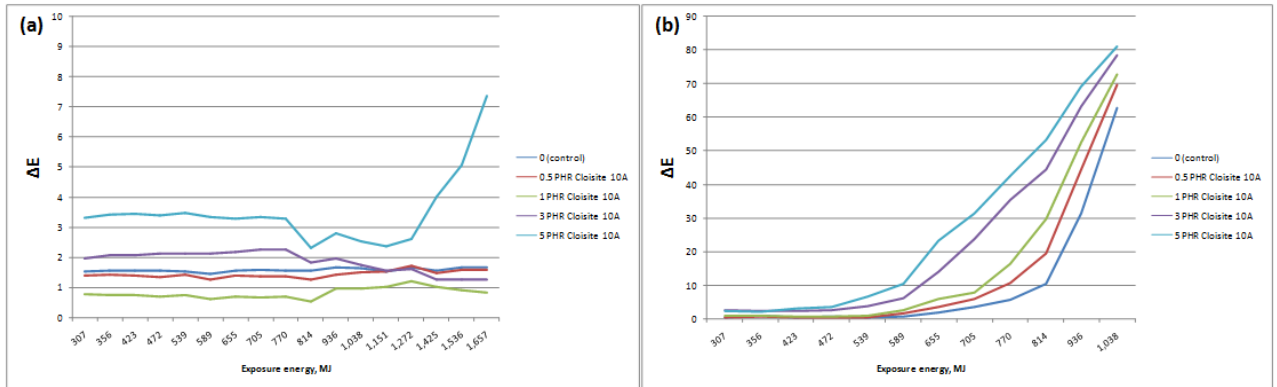


Figure 4.26 Color shifts of white films after Super UV test (a) white films with Cloisite® 10A and (b) white films with Cloisite® 10A plus clear PVC layer on top.

Figure 4.27 shows a comparison of the white film color shifts after the other three test methods. These samples were produced using the one step mixing process. In general, the color shift was very low for all samples. The samples with 3 and 5 phr Cloisite® 10A showed slightly higher color shift. Figure 4.28 shows the 60° gloss results of the same sample set. The QUV test method produced a more significant reduction in gloss compared to the other two methods. The sample with 5 phr Cloisite® 10A had a very large reduction in gloss. The 1 phr samples tracked closely to the control for the Xenon D7869 and D4956 test methods, but not as closely for the QUV method. The best performing sample in QUV was the sample loaded with 1 phr Cloisite® 20.

In summary, the Cloisite® Na+ and Cloisite® 20 showed a lower color shift than the Cloisite® 10A. The gloss retention was a strong function of nanoclay loading level, and should be kept at a lower level for better retention. This may be caused by the nanoclay acting as a matting agent as the polymer is degraded and it becomes exposed at the surface. This is typically observed with PVC films loaded with TiO₂. Accelerated

aging causes the PVC to break down and exposes the TiO₂ which forms a “chalky” surface and reduction in gloss level.

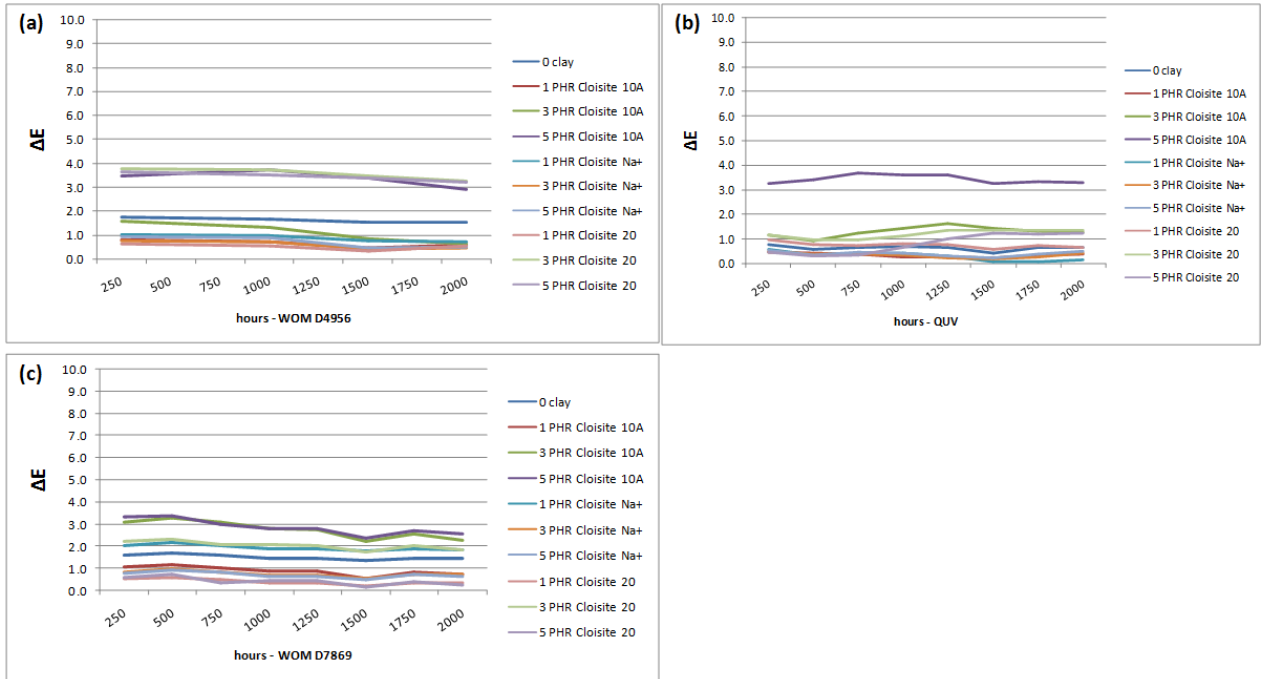


Figure 4.27 White film ΔE results (a) Xenon D4956, (b) QUV, and (c) Xenon D7869.

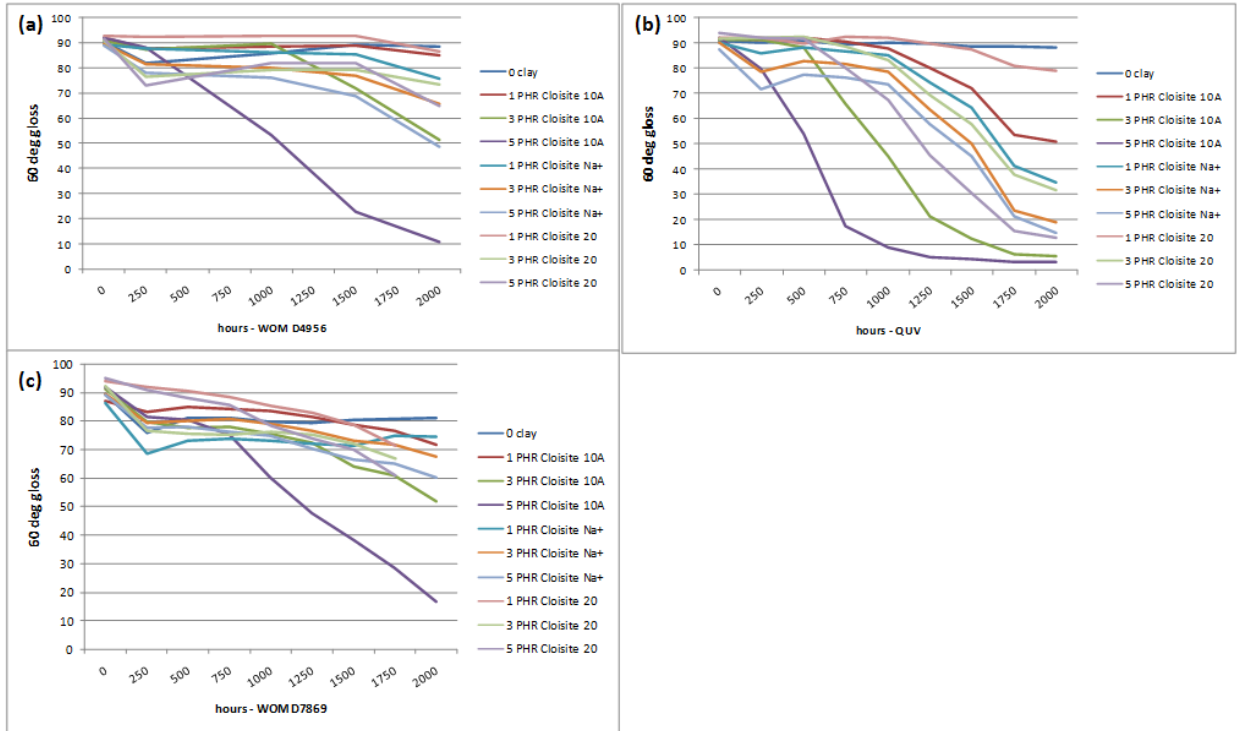


Figure 4.28 Gloss changes of white films (a) Xenon D4956, (b) QUV, and (c) Xenon D7869.

Figures 4.29 and 4.30 show the color shift of the clear films after the Super UV test. The samples loaded with Cloisite® Na+ showed acceptable results for color shift. The samples loaded with Cloisite® 10A and Cloisite® 20 showed acceptable results only for the 0.5 phr loading. The higher loadings show very significant color shift. Figure 4.31 shows the ΔE of clear films produced using the one step mixing process. All samples were acceptable except the samples loaded with Cloisite® 20 at 3 and 5 phr. The samples loaded with Cloisite® 20 and Cloisite® Na+ show the best performance.

Figure 4.30 shows the ΔE of the clear films producing using the high speed mixing method. The samples loaded at 3 and 5 phr Cloisite® 10A show the most

significant color shift. There was no a significant difference in color shift between the clear film and the clear film with white PVC film underneath.

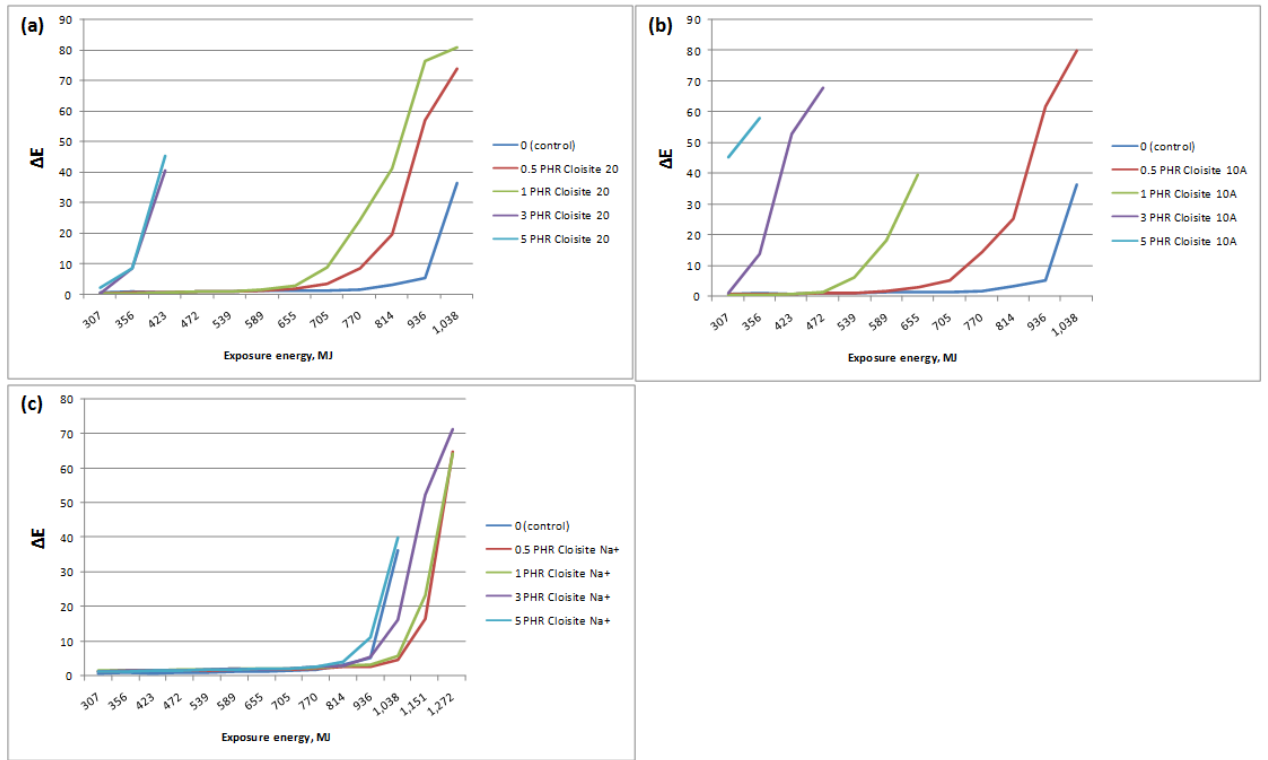


Figure 4.29 Color shift of clear films after Super UV test (a) clear films with Cloisite® 20 (b) clear films with Cloisite® 10A (c) clear films with Cloisite® Na+

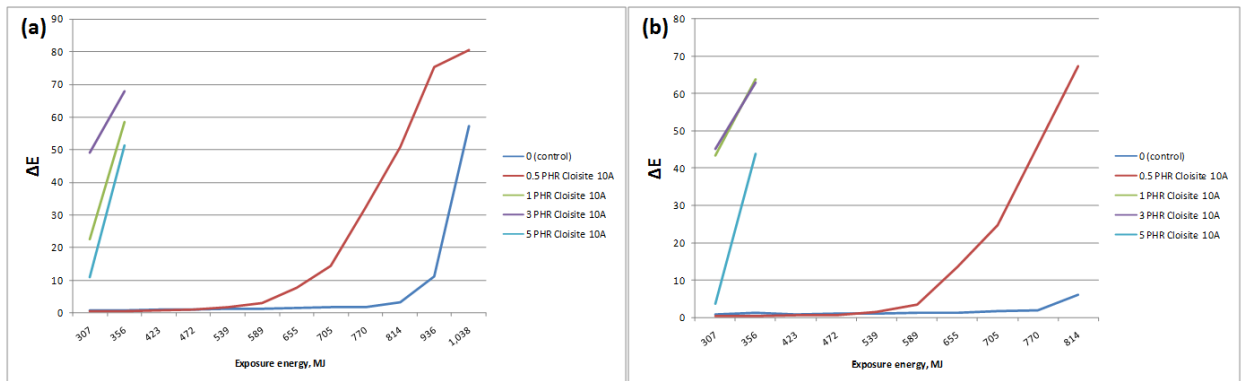


Figure 4.30 Color shift of clear films after Super UV test (a) clear films with Cloisite® 10A (b) clear films with Cloisite® 10A plus white PVC layer underneath

Figures 4.31 and 4.32 show a comparison of the clear film color and gloss shift after the other three test methods. These samples were produced using the one step mixing process. The QUV test method showed the highest ΔE . The highest ΔE was observed for the samples loaded with 3 and 5 phr Cloisite® 10A. Figure 4.32 shows the 60° gloss results of the same sample set. The sample loaded with 5 phr Cloisite® 10A showed the greatest reduction in gloss, followed by the sample loaded with 5 phr Cloisite® 20.

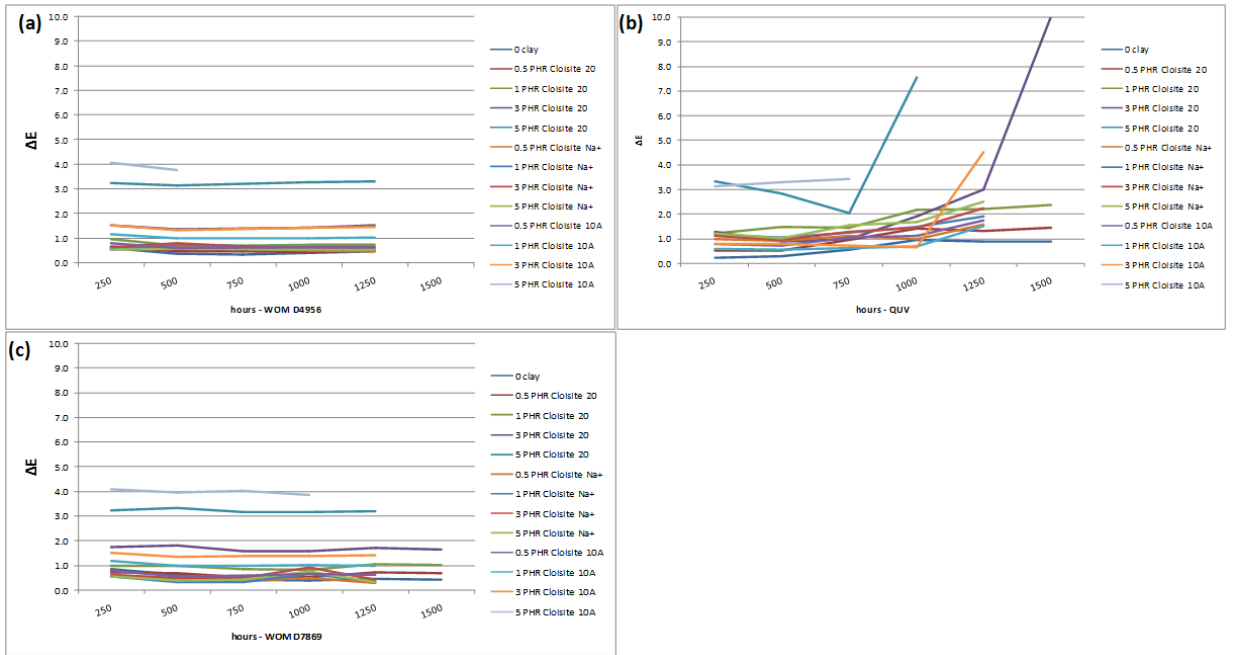


Figure 4.31 Color shift of clear films after accelerated weathering (a) Xenon D4956, (b) QUV, and (c) Xenon D7869.

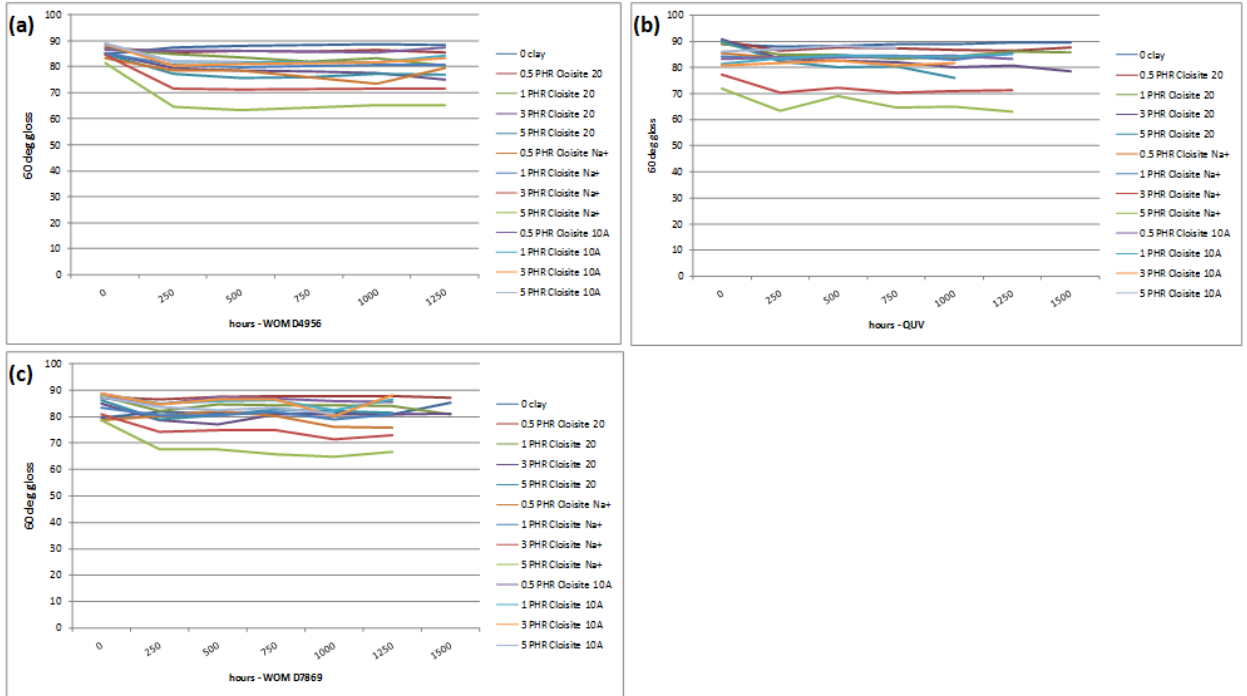


Figure 4.32 Gloss of clear films after accelerated weathering (a) Xenon D4956 (b) QUV (c) Xenon D7869.

The images in Figures 4.36-4.39 show the degradation of the clear films. The images in Figures 4.36-4.38 were taken after 1250 hours running the Xenon D7869 test. As indicated by Figure 4.38, the Cloisite® 10A samples showed the worst performance. The 5 phr sample was completely brown after 1250 hours and 3 phr sample started to show brown spotting. The samples at 3 and 5 phr of Cloisite® 20 showed some brown spotting but not as severe as the materials containing Cloisite® 10A. The Cloisite® Na+ samples were pristine and did not show signs of degradation at any loading. Figure 4.39 shows the samples after the QUV test. The samples with 5 phr Cloisite® 10A and Cloisite® 20 were completely brown, while the other samples did not change their color.

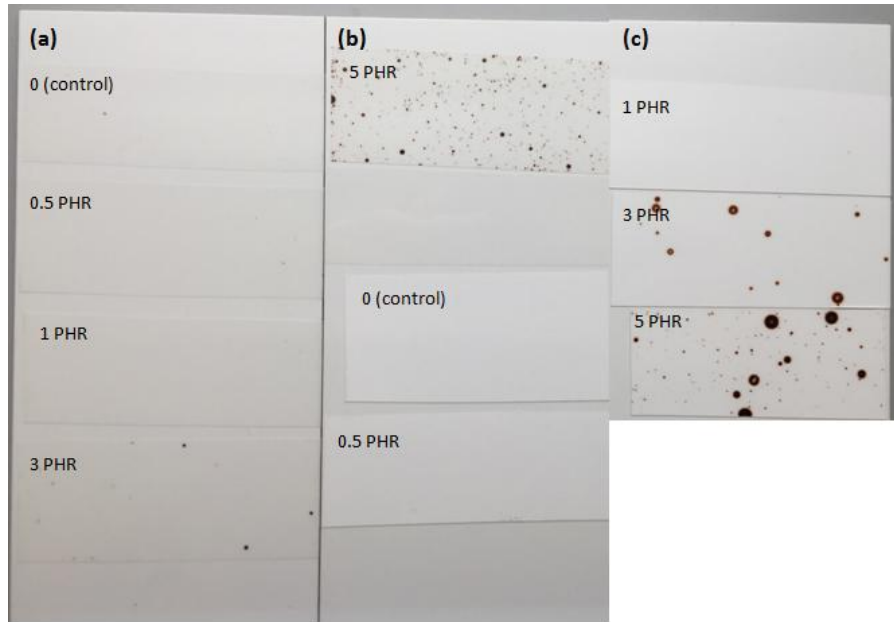


Figure 4.33 Photograph of clear films after 1250 hours D7869 test (a) clear films with Cloisite® 20 (b) top is clear film with Cloisite® 20 bottom 2 films are clear films with Cloisite® 20 plus white PVC layer underneath (c) clear films with Cloisite® 20 plus white PVC layer underneath.

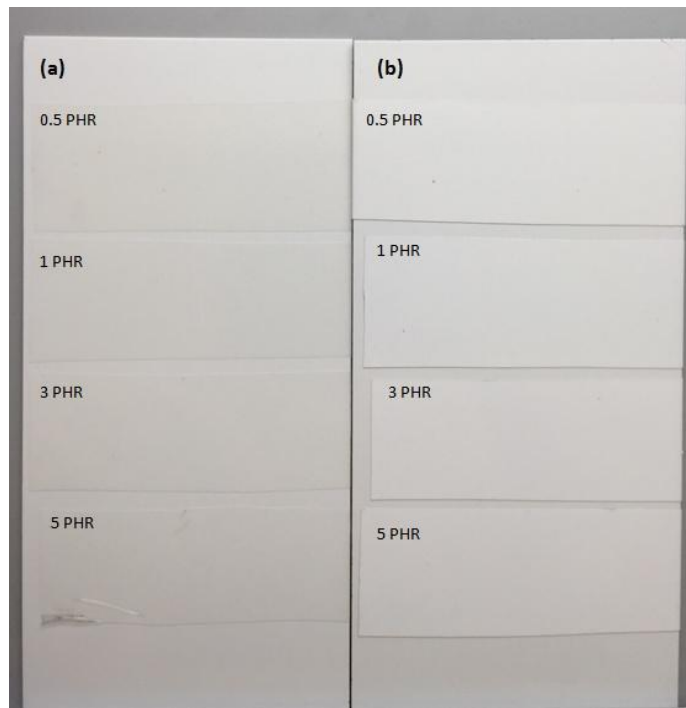


Figure 4.34 Photograph of clear films after 1250 hours D7869 test (a) clear films with Cloisite® Na+ (b) clear films with Cloisite® Na+ plus white PVC layer underneath.

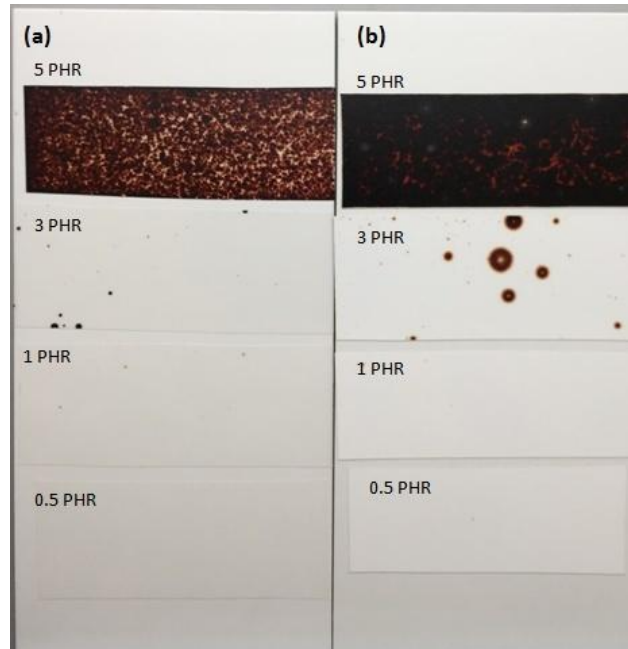


Figure 4.35 Photograph of clear films after 1250 hours D7869 test (a) clear films with Cloisite® 10A (b) clear films with Cloisite® 10A plus white PVC layer underneath.

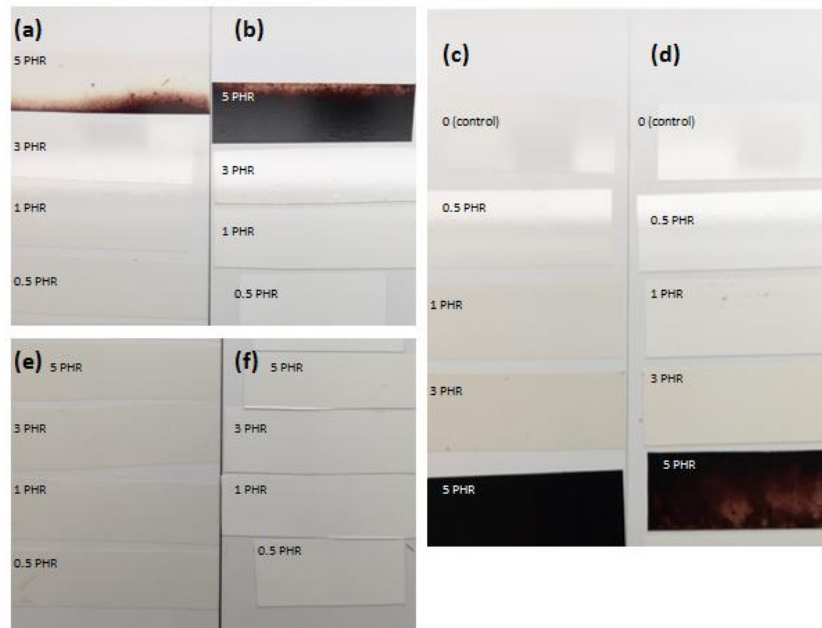


Figure 4.36 Photograph of clear films after 1000 hours QUV test (a) clear films with Cloisite® 10A (b) clear films with Cloisite® 10A plus white PVC film underneath (c) clear films with Cloisite® 20 (d) clear films with Cloisite® 20 plus white PVC film underneath (e) clear films with Cloisite® Na+ (f) clear films with Cloisite® Na+ plus white PVC film underneath.

The first set of samples tested for WVTR and OTR were the samples mixed with the dispersion blade only. The results are reported in Table 4.5. For the white films, the 5 phr samples were compared with the 0 phr control samples. The 5 phr Cloisite® 10A sample showed the highest reduction in WVTR of 63% and 60% for the 23°C and 38°C conditions respectively. The OTR results did not show as significant of a reduction, in fact, two of the samples showed an increase in transmission for the 38°C condition.

For the clear films, the 0.5, 1, 3, and 5 phr Cloisite® 20 samples were compared with the 0 phr control. The highest reduction in WVTR was observed for the 5 PHR sample which measured 35% and 43% at the 23°C and 38°C conditions respectively. The 1 PHR sample showed the greatest reduction for OTR at 26% and 48% for the 23°C and 38°C conditions respectively. Although the samples with nanoclay did show reduction in WVTR and OTR, there was no clear trend between nanoclay level and transmission level. It was also noted that some variation in thickness was observed for this set of samples which contributed to the variation in transmission levels. Previous data shown in Figure 4.37 demonstrated the effect of PVC film thickness on transmission level for clear films of 30.5 µm and 50 µm. When the PSA layer was added to the film, the transmission level was further reduced.

The transmission results for the films produced using the homogenization mixing procedure are shown in Table 4.6. For the WVTR test, all of the samples loaded with Cloisite® 10A showed a reduction in transmission. The highest reduction was 66% for the 5 phr sample at the 38°C-100%RH condition. For the OTR test, only the clear films

showed a reduction in transmission levels. The highest reduction was 49% for the samples loaded with 5 phr Cloisite® 10A at the 23°C-0%RH and 38°C-90%RH conditions.

(a)	Sample	thickness µm	WVTR 23°C, 100% RH		WVTR 38°C, 100% RH	
			g / (m ² - day)	% change	g / (m ² - day)	% change
			white film	0 clay	34	60
	5 PHR Cloisite 10A	56	22	-63%	81	-60%
	5 PHR Cloisite Na+	42	35	-42%	130	-35%
	5 PHR Cloisite 20	47	30	-50%	114	-43%
clear film	0 clay	53	23	-	87	-
	0.5 PHR Cloisite 20	60	16	-30%	58	-33%
	1 PHR Cloisite 20	63	24	4%	-	-
	3 PHR Cloisite 20	51	21	-9%	75	-14%
	5 PHR Cloisite 20	61	15	-35%	55	-43%

(b)	Sample	thickness µm	OTR 23°C, 0% RH		OTR 38°C, 90% RH	
			cc / (m ² - day)	% change	cc / (m ² - day)	% change
			white film	0 clay	34	473
	5 PHR Cloisite 10A	56	310	-34%	950	-14%
	5 PHR Cloisite Na+	42	440	-7%	1454	31%
	5 PHR Cloisite 20	47	510	8%	1505	36%
clear film	0 clay	53	360	-	1205	-
	0.5 PHR Cloisite 20	60	351	-3%	818	-32%
	1 PHR Cloisite 20	63	266	-26%	810	-48%
	3 PHR Cloisite 20	51	324	-10%	1030	-22%
	5 PHR Cloisite 20	61	299	-17%	924	-27%

Table 4.5 White and clear film transmission results (a) WVTR and (b) OTR.

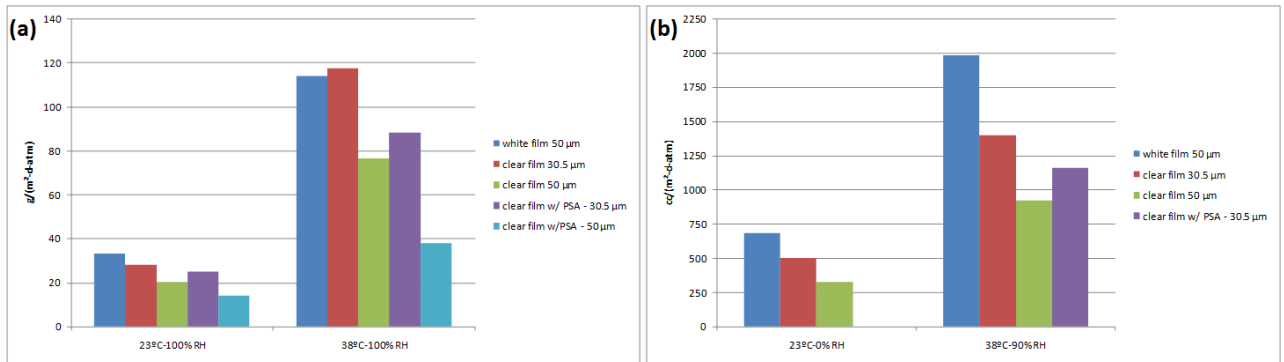


Figure 4.37 Effect of PVC film thickness and addition of PSA on (a) WVTR and (b) OTR.

(a)	Sample	thickness μm	WVTR		WVTR	
			23°C, 100% RH		38°C, 100% RH	
			$\text{g} / (\text{m}^2 \cdot \text{day})$	% change	$\text{g} / (\text{m}^2 \cdot \text{day})$	% change
white film	0 clay	41	49	-	290	-
	0.5 PHR 10A	43	37	-24%	180	-38%
	1 PHR 10A	45	36	-27%	130	-55%
	3 PHR 10A	46	34	-31%	126	-57%
	5 PHR 10A	46	30	-39%	100	-66%
clear film	0 clay	43	24	-	86	-
	0.5 PHR 10A	46	29	21%	-	-
	1 PHR 10A	47	23	-4%	83	-3%
	3 PHR 10A	47	18	-25%	66	-23%
	5 PHR 10A	43	19	-21%	70	-19%

(b)	Sample	thickness μm	OTR		OTR	
			23°C, 0% RH		38°C, 90% RH	
			$\text{cc} / (\text{m}^2 \cdot \text{day})$	% change	$\text{cc} / (\text{m}^2 \cdot \text{day})$	% change
white film	0 clay	44	400	-	1300	-
	0.5 PHR 10A	43	440	10%	1410	8%
	1 PHR 10A	45	440	10%	1330	2%
	3 PHR 10A	46	470	18%	1415	9%
	5 PHR 10A	43	420	5%	1300	0%
clear film	0 clay	48	600	-	1970	-
	0.5 PHR 10A	43	400	-33%	1240	-37%
	1 PHR 10A	47	470	-22%	1370	-30%
	3 PHR 10A	46	320	-47%	1040	-47%
	5 PHR 10A	47	307	-49%	1000	-49%

Table 4.6 White and clear film transmission results for samples mixed with high speed homogenizer (a) WVTR and (b) OTR.

4.1.6 Printing and surface analysis

The initial contact angle was measured for the white film samples. The surface energy was calculated from the contact angle values and displayed in Table 4.7. It is apparent from the data that the type or loading of nanoclay did not have an effect on the initial contact angle values. The surface energy for all samples was found to be ~50 dyne/cm.

Sample ID		Fluid	Contact Angle (deg)		Surface Energy (dyne/cm)			
			Avg	Std Dev	Avg	Std Dev	Disperse	Polar
0 PHR	control	Water	77.8	1.3	49.8	1.0	46.9	2.9
		Diiodomethane	22.9	1.7				
1 PHR	Cloisite 10A	Water	75.7	0.6	50.7	0.4	47.2	3.5
		Diiodomethane	21.8	0.5				
3 PHR		Water	75.9	1.8	50.1	1.4	46.6	3.5
		Diiodomethane	23.6	2.3				
5 PHR		Water	74.6	1.2	50.9	0.7	47.0	3.9
		Diiodomethane	22.4	0.9				
1 PHR	Cloisite Na+	Water	77.6	1.0	50.2	0.5	47.3	2.9
		Diiodomethane	21.7	0.7				
3 PHR		Water	75.9	1.7	51.1	0.7	47.8	3.3
		Diiodomethane	20.0	0.5				
5 PHR		Water	76.0	1.6	50.6	0.7	47.2	3.4
		Diiodomethane	21.9	0.5				
1 PHR	Cloisite 20	Water	74.3	1.2	51.4	0.7	47.5	3.9
		Diiodomethane	21.1	0.9				
3 PHR		Water	74.2	1.0	51.4	0.5	47.5	3.9
		Diiodomethane	20.9	0.6				
5 PHR		Water	73.9	0.5	51.2	0.5	47.1	4.1
		Diiodomethane	22.3	1.0				

Table 4.7 Initial contact angle measurements of white films.

The nanocontact angle was measured for the white films and the chart of contact angle as a function of time is reported in Figure 4.38. Figure 4.38a shows the initial results, and Figure 4.38b shows the results after aging the films for one week at 80°C. All initial samples showed a similar trend. This indicates that the nanoclay did not affect the initial print surface. The contact angle of the films after aging show a slightly shifted curve for the 3 and 5 phr Cloisite® 10A.

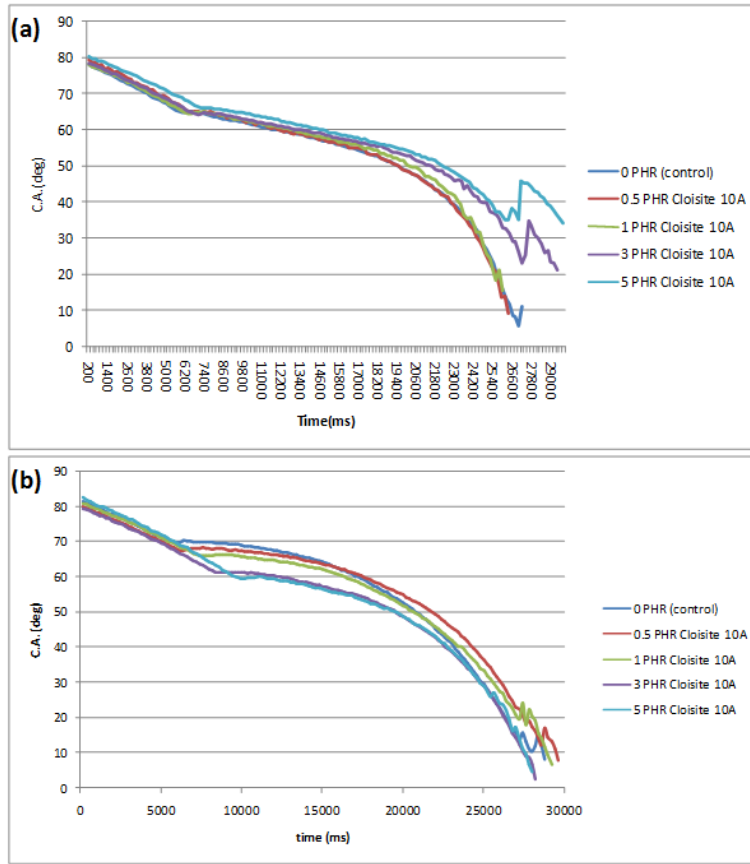


Figure 4.38 Nanocontact angle of water drop over time (a) initial and (b) films aged 1 wk at 80°C.

The print performance was evaluated by laminating the film to a 1.5 meter roll and printing on a Roland eco-solvent printer and an HP latex printer. It was expected that a difference in absorption of the ink droplet on the film would alter the characteristic shape and bleed of the ink droplet. A template image file was used in order to measure dot size and ink bleed. Table 4.8 shows the ink dot characteristics on the white films loaded with Cloisite® 10A nanoclay. Table 4.8a shows the results with latex ink and Table 4.8b shows the results with eco-solvent ink. There was no significant difference in the ink dot characteristic sizes or count for samples loaded with

nanoclay compared to the control. Images of the ink dots are shown in Figure 4.39 for the eco-solvent ink and Figure 4.40 for the latex ink.

(a)	Cloisite® 10A loading	Count	Diameter (µm)	Area (µm ²)	Perimeter (µm)
	0 PHR	48	59.9	3090.7	211
	0.5 PHR	39	69.2	3940	255.6
	1 PHR	52	57.9	2904.2	210.5
	3 PHR	42	63.7	3415.3	227.8
	5 PHR	41	58.9	4037.6	253.5

(b)	Cloisite® 10A loading	Count	Diameter (µm)	Area (µm ²)	Perimeter (µm)
	0 PHR	36	98.3	7587.9	316.4
	0.5 PHR	36	81.1	5188.4	260.6
	1 PHR	38	98.9	7678.8	321
	3 PHR	36	91.2	6557.5	326.8
	5 PHR	33	90.2	6397.2	288.3

Table 4.8 Dot size measurements for PVC films printed with (a) latex ink (b) eco-solvent ink

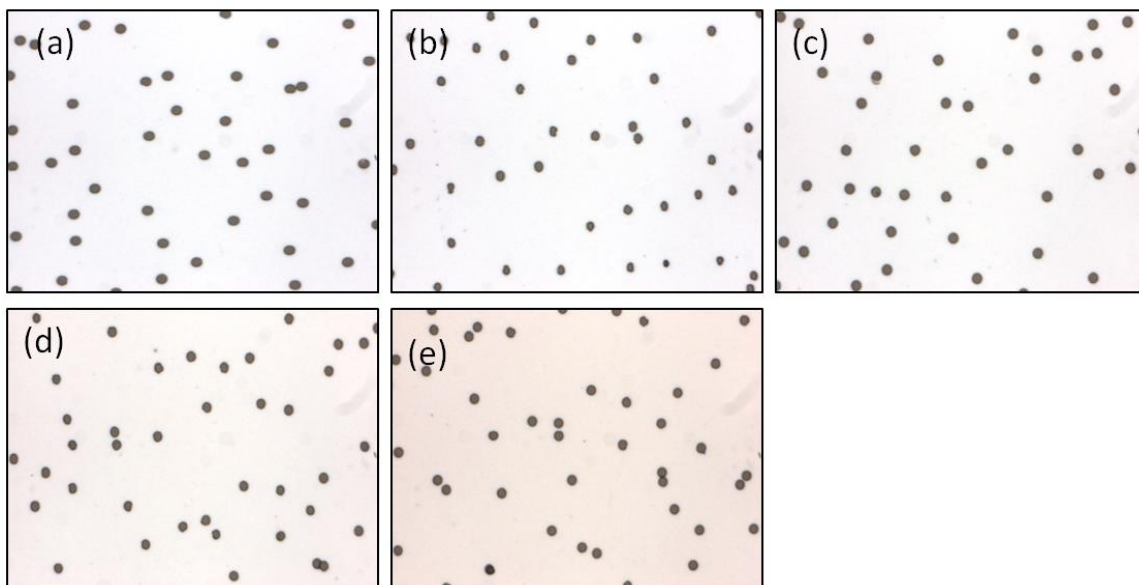


Figure 4.39 Images of ink dots printed with eco-solvent ink onto PVC film with different loadings of Cloisite® 10A (a) 0 PHR (b) 0.5 PHR (c) 1 PHR (d) 3 PHR (e) 5 PHR

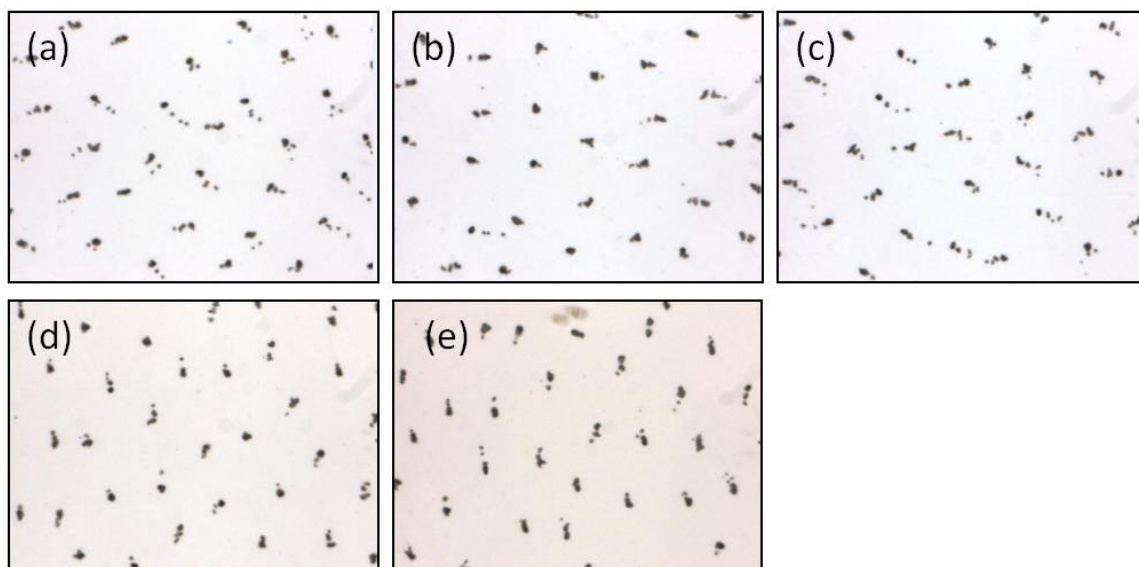


Figure 4.40 Images of ink dots printed with latex ink onto PVC film with different loadings of Cloisite® 10A (a) 0 PHR (b) 0.5 PHR (c) 1 PHR (d) 3 PHR (e) 5 PHR

Table 4.9 shows the results of the ink bleed evaluation. Table 4.9a shows the results for latex ink and Table 4.9b shows the results for eco-solvent ink. There was no

significant change in ink bleed for the samples loaded with Cloisite® 10A nanoclay compared to the control sample. Images of the printed bleed samples are shown in Figure 4.41 for the eco-solvent ink and Figure 4.42 for the latex ink.

		White		Yellow		Magenta	
(a)	Cloisite® 10A loading	Lead r (µm)	Width (µm)	Lead r (µm)	Width (µm)	Lead r (µm)	Width (µm)
	0 PHR	10.6	1084.4	7.3	1087.2	9.4	1083.0
	0.5 PHR	9.9	1087.5	10.3	1079.9	8.6	1087.5
	1 PHR	13.7	1088.1	13.8	1086.2	12.6	1078.6
	3 PHR	18.7	1098.0	15.1	1100.1	15.7	1093.0
	5 PHR	15.5	1091.8	12.0	1090.9	14.1	1088.5
	<hr/>						
		White		Yellow		Magenta	
(b)	Cloisite® 10A loading	Lead r (µm)	Width (µm)	Lead r (µm)	Width (µm)	Lead r (µm)	Width (µm)
	0 PHR	6.9	1051.4	41.8	1707.8	29.3	1879.1
	0.5 PHR	11.4	1037.2	44.4	1774.5	64.2	1650.0
	1 PHR	5.1	1062.3	34.4	1802.9	34.1	1936.1
	3 PHR	6.6	1064.5	51.0	1609.9	28.3	1866.3
	5 PHR	8.1	1069.6	43.5	1638.1	36.8	1848.2

Table 4.9 Bleed measurements for PVC films printed with (a) latex inks (b) eco solvent inks

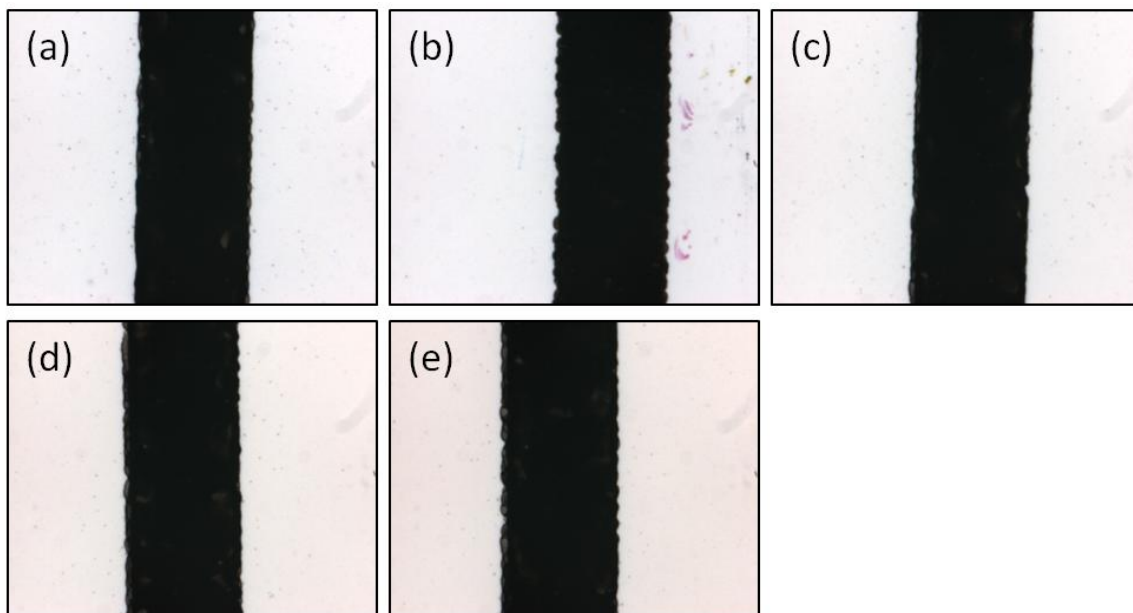


Figure 4.41 Images of black ink for bleed measurement with eco-solvent ink onto PVC film with different loadings of Cloisite® 10A (a) 0 PHR (b) 0.5 PHR (c) 1 PHR (d) 3 PHR (e) 5 PHR

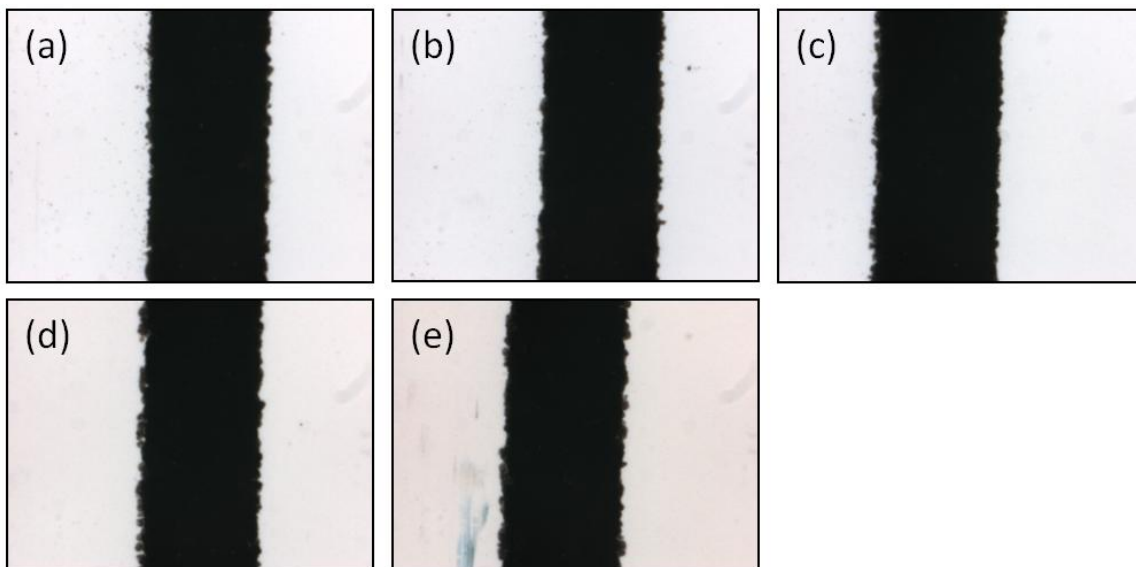


Figure 4.42 Images of black ink for bleed measurement with latex ink onto PVC film with different loadings of Cloisite® 10A (a) 0 PHR (b) 0.5 phr (c) 1 phr (d) 3 phr (e) 5 phr

The images of the ink dots printed with eco-solvent ink on film that was aged are shown in Figure 4.43 and the ink dot measurements are shown in Table 4.10. There was

no significant change in the ink dot size after aging for the samples loaded with nanoclay compared to the control sample. The bleed measurements are shown in Table 4.11. There was an increase in values of lead raggedness (lead r) and width for the samples loaded with nanoclay compared to the control. This indicates a change at the surface which causes the ink to wet the surface differently.

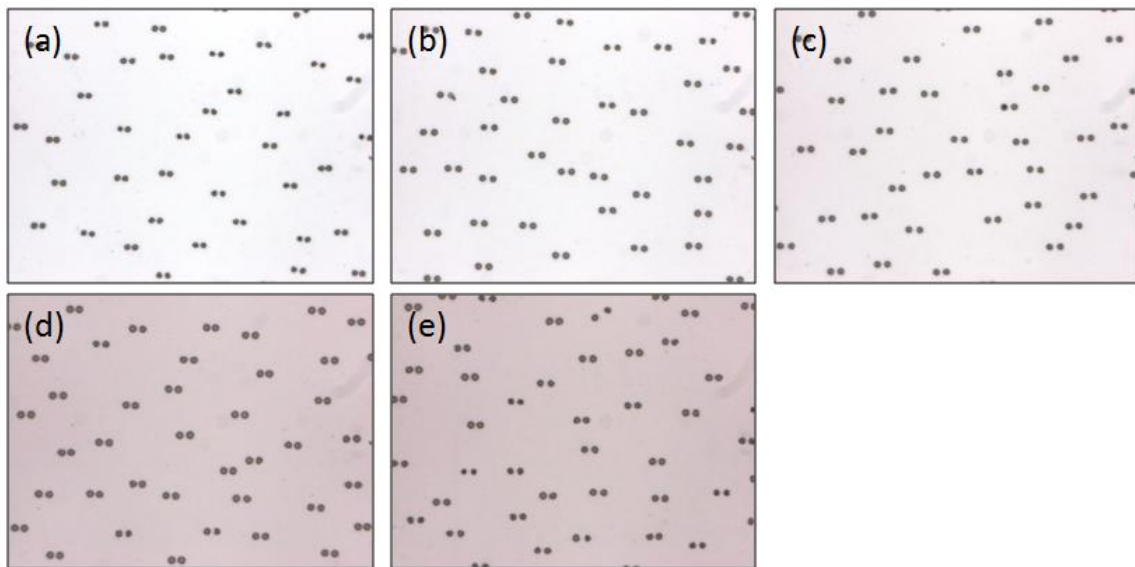


Figure 4.43 Images of ink dots printed with eco-solvent ink onto PVC film with different loadings of Cloisite® 10A after aging for 1 wk 80°C (a) 0 phr (b) 0.5 phr (c) 1 phr (d) 3 phr (e) 5 phr

Cloisite® 10A loading	Count	Diameter (µm)	Area (µm ²)	Perimeter (µm)
0 PHR	71	54.8	2403.2	174.8
0.5 PHR	80	60.2	2851.6	187.5
1 PHR	76	60	2825.2	184
3 PHR	79	67.8	3614.5	213.6
5 PHR	72	61.8	3012.6	192.9

Table 4.10 Dot size measurements for PVC films printed with eco-solvent ink

Cloisite 10A loading	Cyan		Yellow		Magenta	
	Lead r (µm)	Width (µm)	Lead r (µm)	Width (µm)	Lead r (µm)	Width (µm)
0 PHR	22.2	1116.4	14.4	1043.4	22.0	1171.0
0.5 PHR	81.7	1517.7	12.1	988.0	24.0	1336.4
1 PHR	79.7	1468.2	15.8	1005.4	35.7	1304.2
3 PHR	-	1503.0	17.0	1106.5	30.4	1420.6
5 PHR	40.6	1694.9	27.9	1505.8	46.9	1384.8

Table 4.11 Bleed measurements for PVC films printed with eco solvent inks

4.2 Coating on calendered PVC film

4.2.1 Thermal stability

Thermal stability was evaluated visually after thermally aging the samples at 180°C. This test provides a relative comparison of how different PVC materials will perform over their service life, but it should be supplemented with accelerated weathering testing. The images of samples are shown in Figure 4.44. There was some color change noted for the samples with 3 and 5 phr nanoclay, but the color change for the coatings was not as significant as the PVC films with nanoclay. The images in Figure

4.44a show the full construction with PVC film, coating, and adhesive and liner and the images in Figure 4.44b show the coating on PET. The nanoclay coating on PET did not show color change even at high clay loading. This indicates that there may be some interactions between PVC and nanoclay even when the nanoclay is in contact with the coating.

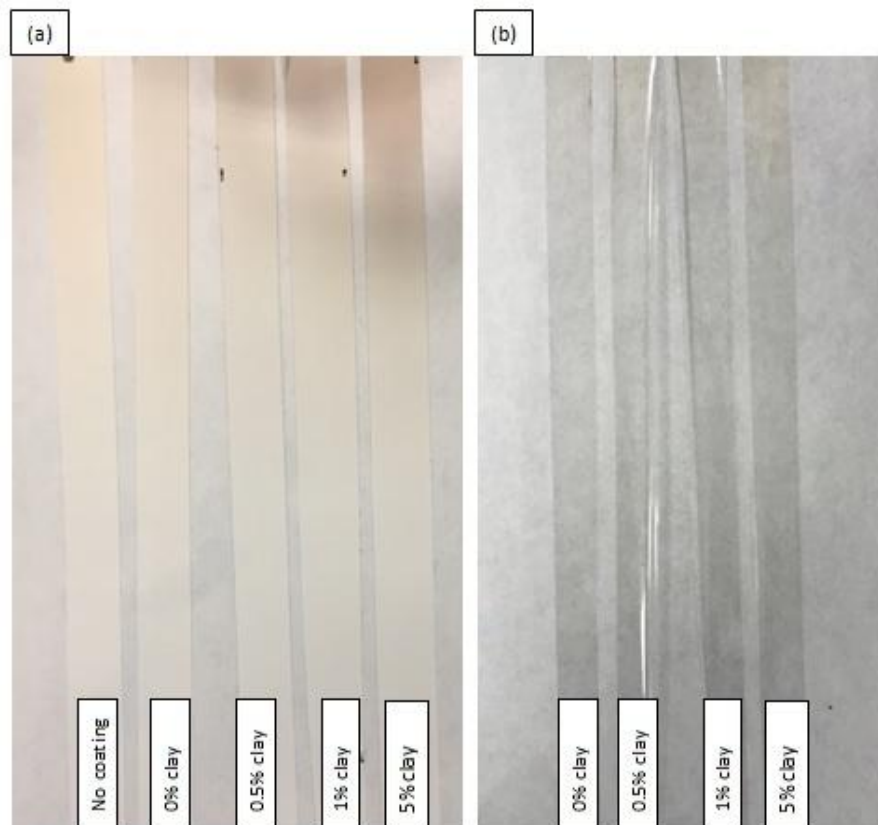


Figure 4.44 Photographs of films after Metrastat thermal aging at 180°C (a) shows full construction film, coating, adhesive, and liner, (b) coating on PET.

4.2.2 Appearance and optical properties

The haze, clarity, and transmission of the clear coating are shown in Figure 4.45.

The haze did not significantly increase for the samples with 0.5% and 1% nanoclay. The

clarity decreased with addition of nanoclay but was similar for all nanoclay levels. This indicates that at low levels the nanoclay may be added onto the backside of clear PVC films without significantly disrupting the optical properties.

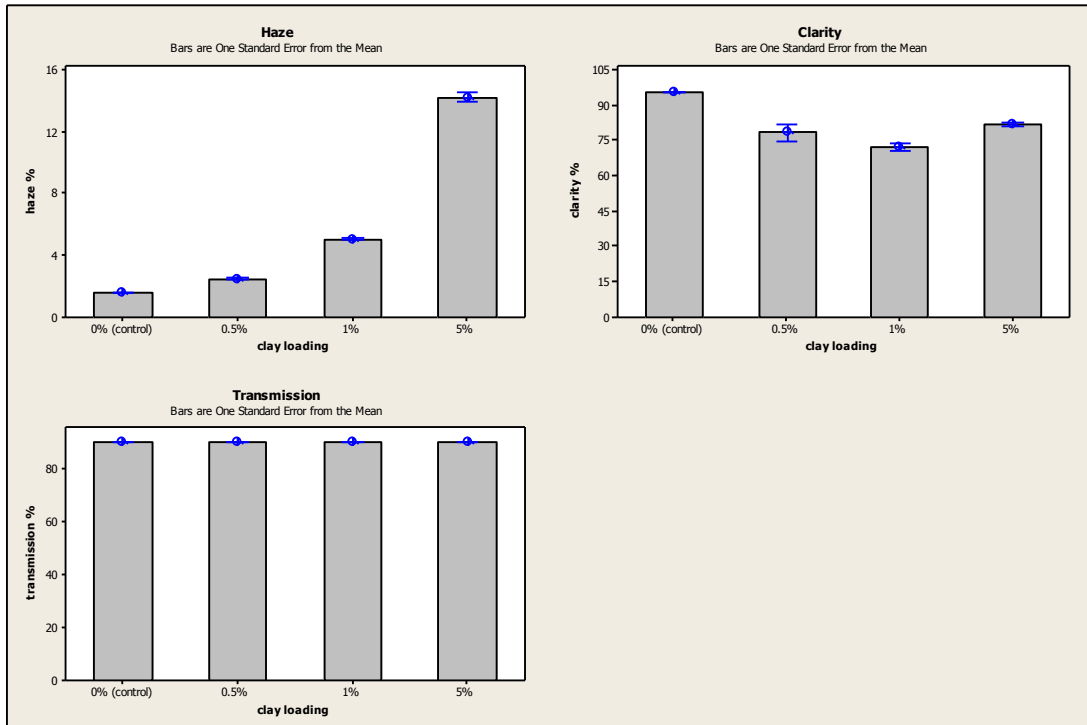


Figure 4.45 Effect of nanoclay level on haze, clarity and transmission.

4.2.3 Mechanical properties

The mechanical properties were measured as a function of aging time. The goal was to understand if plasticizer was migrating to the interfaces with air and the adhesive which would cause a change to the materials stress-strain curve. It is expected that the modulus would increase as a consequence. Also, the elongation at break would decrease and the tensile strength would increase. The measurements were taken at 0, 3, 7, and 21 days after aging at 60°C and 80°C. First, the control sample without any

coating was evaluated with and without adhesive to understand the effect of both components. The elongation, modulus, and tensile strength are plotted in Figure 4.47 and the stress-strain plot is shown in Figure 4.46. The elongation decreased significantly over time for the samples with the adhesive, while the samples with film only did not show a significant change. This suggests that the adhesive adds a driving force for the plasticizer to migrate to the interface. The initial modulus for the sample with adhesive was lower than that of the film only because the film with the adhesive is a combination of the modulus of the film and the adhesive. Note that the adhesive has a very low value of modulus compared to the film.

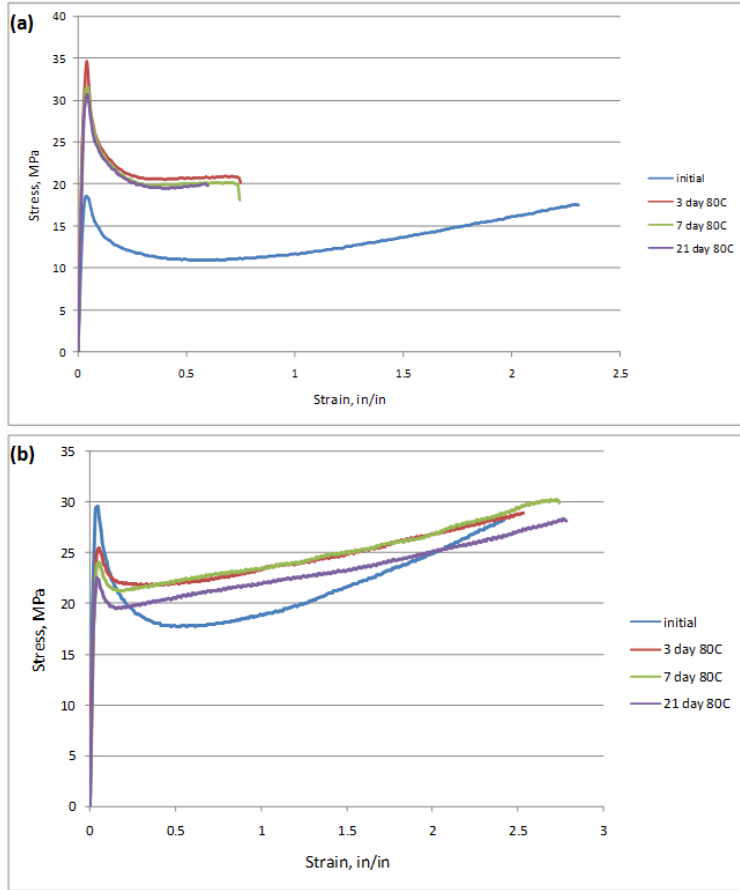


Figure 4.46 Stress-strain curve for calendered PVC film after aging (a) film with PSA and (b) film only.

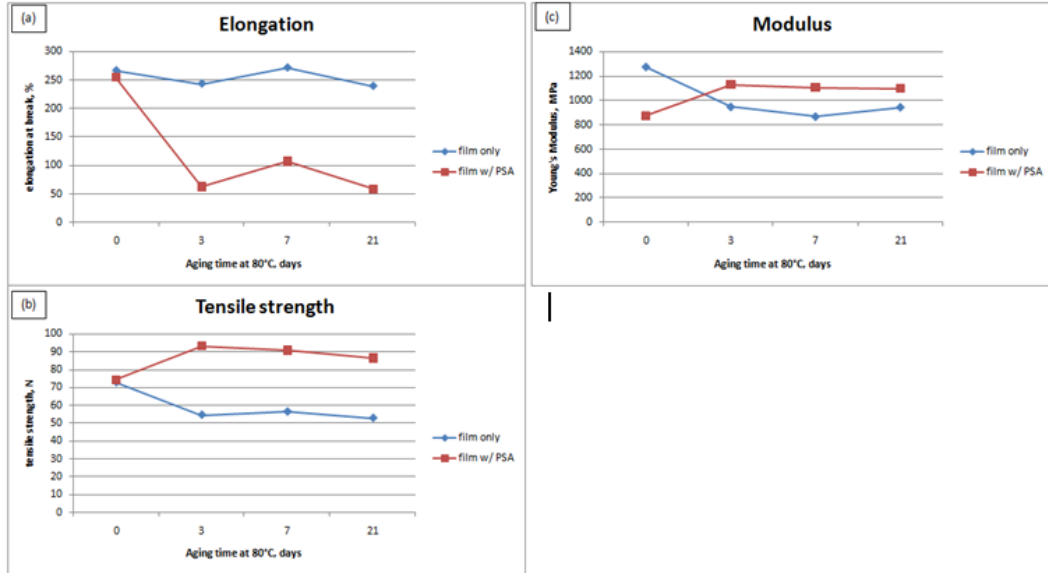


Figure 4.47 Effect of aging on (a) elongation at break, (b) tensile strength, and (c) Young's modulus.

Next, the mechanical properties of the nanoclay coated films were evaluated.

The values of elongation, modulus, and tensile strength were plotted as a function of aging time in Figure 4.48. It is seen that the elongation decreased for all samples. The modulus and tensile strength increased for all samples. This indicates that there was no trend between nanoclay loading and mechanical properties.

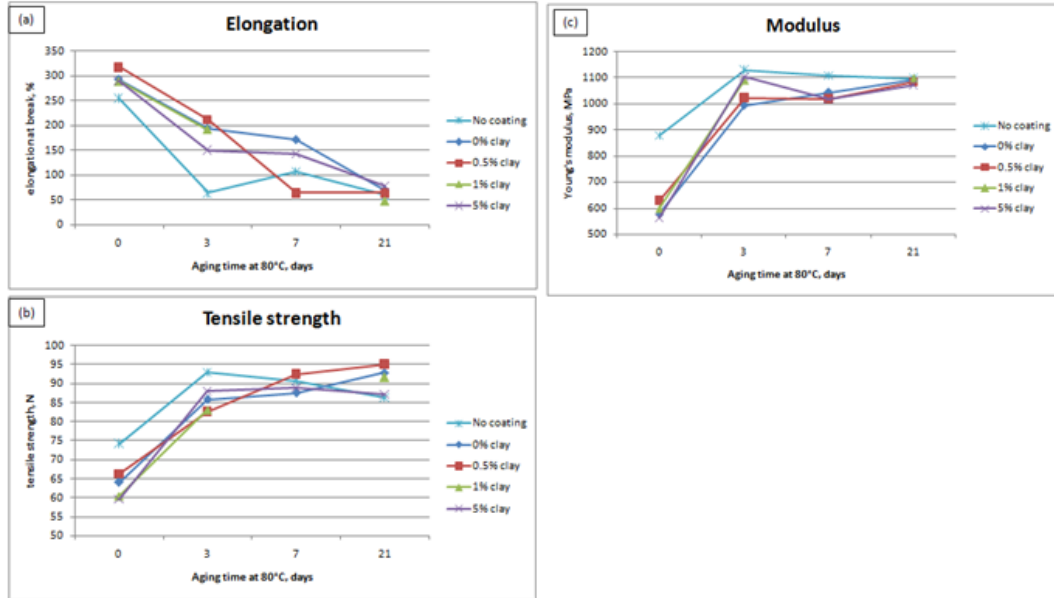


Figure 4.48 Effect of aging on (a) elongation at break, (b) tensile strength, and (c) Young's modulus.

Lastly, the mechanical properties were measured after printing the films with eco-solvent ink. The modulus, elongation at break, and tensile strength were plotted in Figure 4.49. It is found that the modulus decreased about 60-70% after printing. There was no trend between nanoclay loading and modulus after printing. There was no significant change in elongation for any samples and the tensile strength decreased ~20% for all samples. This indicates that after printing the material become softer and more flexible due to the solvent in the ink penetrating the film.

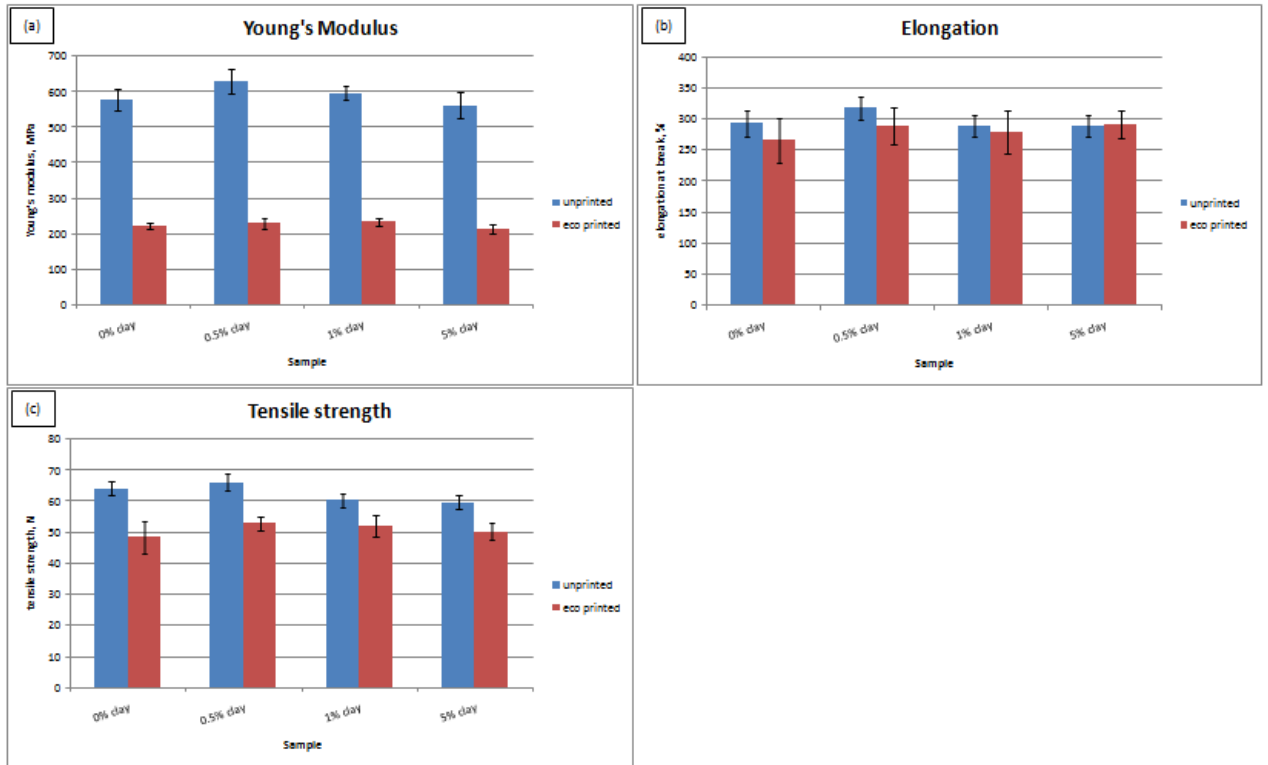


Figure 4.49 Effect of eco-solvent printing on (a) Young's modulus, (b) elongation at break, and (c) tensile strength.

4.2.4 Durability and barrier properties

The ΔE results for the Super UV test are plotted in Figure 4.50. The nanoclay coated films showed minimal change in ΔE at all loading and performed better than the control sample that did not have any coating. All coated samples had a ΔE of < 2 after 1,515 MJ of exposure. This indicates that the nanoclay coating did not accelerate degradation to the PVC. The uncoated film did show a high ΔE of >10 after 1,515 MJ of exposure. The performance of these films should be confirmed by reviewing data from the other weathering tests in combination with the Super UV results once the data is available.

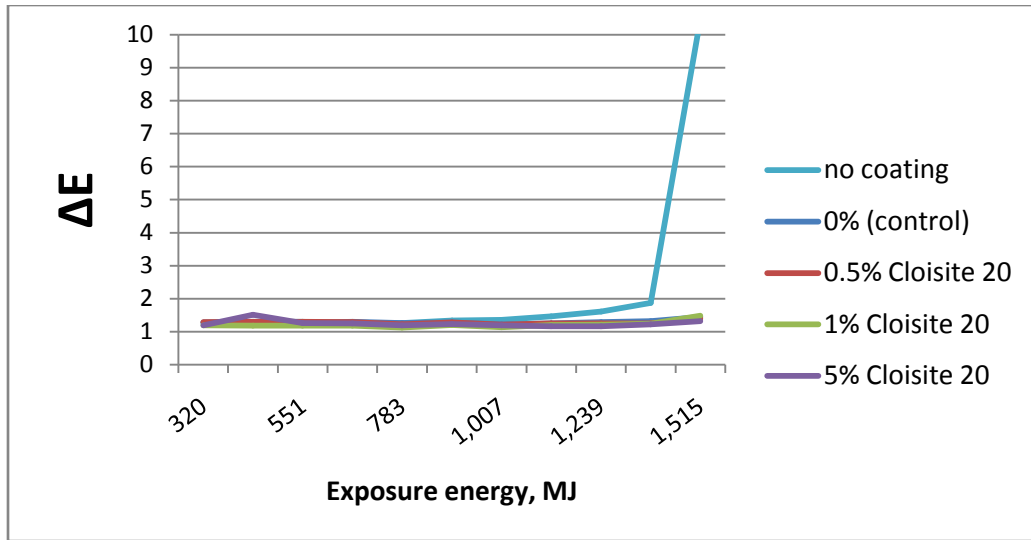


Figure 4.50 Super UV results for PVC films with nanoclay coating.

The result of WVTR and OTR testing of the nanoclay coated films are shown in Table 4.12. For the WVTR test, there was no clear trend between nanoclay loading and transmission level. It appeared that certain coated films showed a reduction in WVTR. The highest reduction was 25% for the 0.5% Cloisite® 20 sample at the 38°C-100%RH condition. For the OTR test, all coated samples showed a reduction in OTR but there was no trend with nanoclay loading, as shown in Table 4.10b. The 0.5% Cloisite® 20 sample is recommended as it has the minimal loading of nanoclay that still provides an improvement to OTR.

(a)	thickness	WVTR		WVTR	
		23°C, 100% RH		38°C, 100% RH	
Sample	μm	$\text{g} / (\text{m}^2 \cdot \text{day})$	% change	$\text{g} / (\text{m}^2 \cdot \text{day})$	% change
no coating	76	16	-	55	-
0% (control)	81	20	25%	67	22%
0.5% Cloisite 20	81	16	0%	41	-25%
1% Cloisite 20	81	15	-6%	51	-7%
5% Cloisite 20	81	16	0%	43	-22%

(b)	thickness	OTR		OTR	
		23°C, 0% RH		38°C, 90% RH	
Sample	μm	$\text{cc} / (\text{m}^2 \cdot \text{day})$	% change	$\text{cc} / (\text{m}^2 \cdot \text{day})$	% change
no coating	76	660	-	1500	-
0% (control)	81	427	-35%	1260	-16%
0.5% Cloisite 20	81	380	-42%	1210	-19%
1% Cloisite 20	81	410	-38%	1290	-14%
5% Cloisite 20	81	450	-32%	1280	-15%

Table 4.12 Transmission results for nanoclay coating on PVC film (a) WVTR and (b) OTR.

The plasticizer migration test was completed for the control sample that did not have the nanoclay coating. The film samples were left in the test for 33 days at 80°C. The weight loss results are shown in Table 4.13. There was no significant change in weight percentage over this time period, and there was a high degree of variation amongst the measurements. It was decided that this test was unreliable and the other samples were not run.

	% wt loss	
	mean	sd
2 day	0.57	0.33
10 day	1.11	0.44
19 day	1.53	0.47
33 day	2.00	0.73

Table 4.13 Weight loss measurements of calendered PVC without nanoclay coating.

4.2.5 Adhesive properties

Based on the historical data, it was expected that the peel strength and tack would be reduced as the plasticizer migration from the PVC films increased. These results were confirmed with the control sample that did not have any backside coating as shown in Figure 4.51. The results of peel adhesion and tack tests were plotted versus aging time at 60°C and 80°C. After aging for 21 days at 80°C, the peel adhesion and tack were reduced by ~90%. The 60°C aging condition showed less severe results but the peel adhesion and tack were still reduced by ~40%.

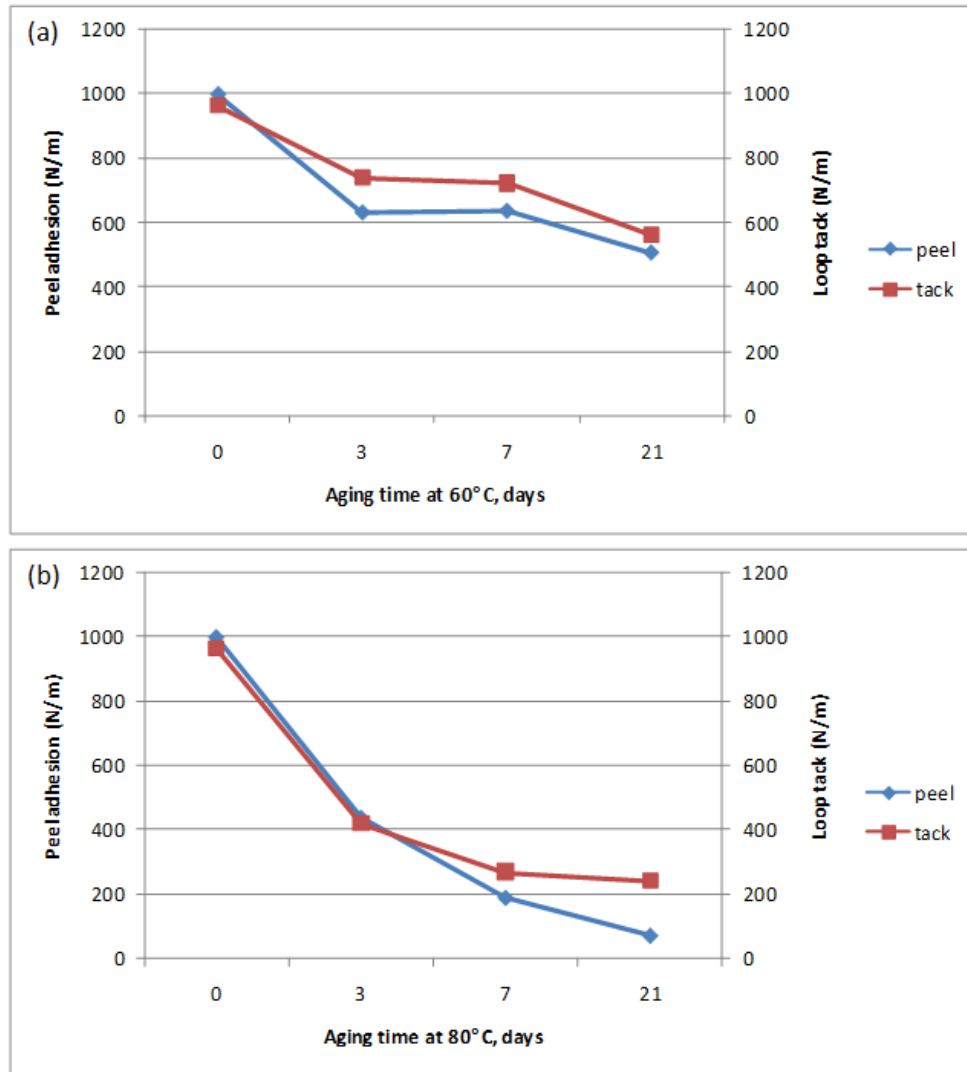


Figure 4.51 Effect of aging at (a) 60°C and (b) 80°C on peel adhesion and tack of PSA.

The bar chart in Figure 4.53 shows a comparison of the uncoated samples, and the samples coated with polyamide-nanoclay coating as a function of peel adhesion over time. It is seen that the coated samples had significant improvement to retention of adhesive properties. There were no significant differences in the nanoclay loading in the coatings. Another chart in Figure 4.54 shows the tack for the same samples over a period of time. It is seen that the reduction in tack is more significant when aging at

80°C compared to 60°C. The coated samples showed lower reduction in tack compared to the uncoated sample. There was no trend between nanoclay loading and reduction in tack.

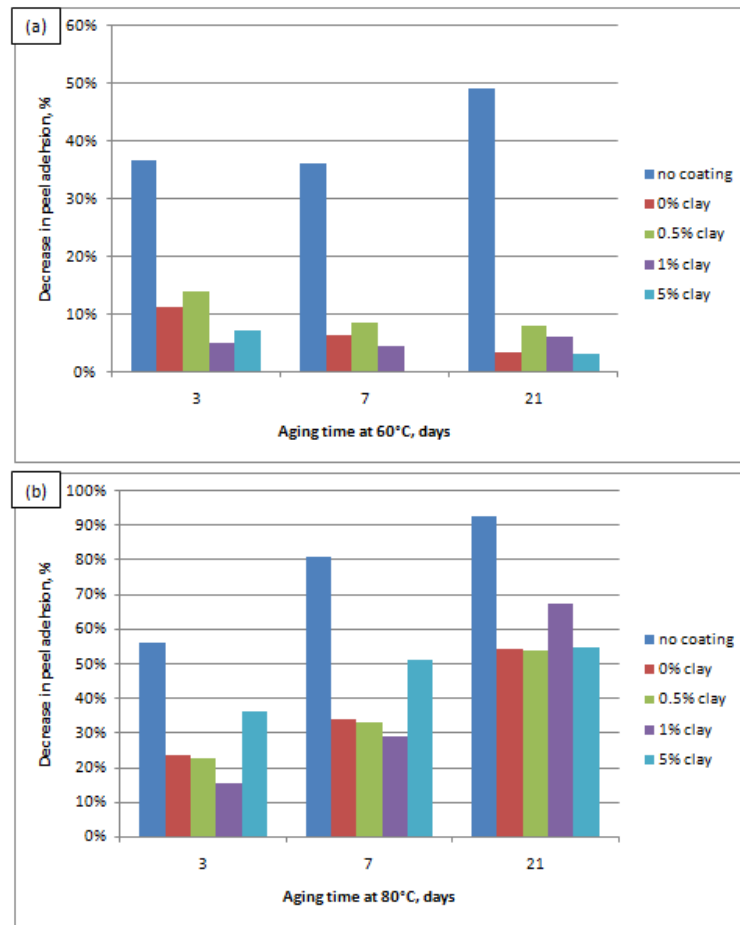


Figure 4.52 Effect of thermal aging on peel adhesion of nanoclay coated films (a) 60°C and (b) 80°C.

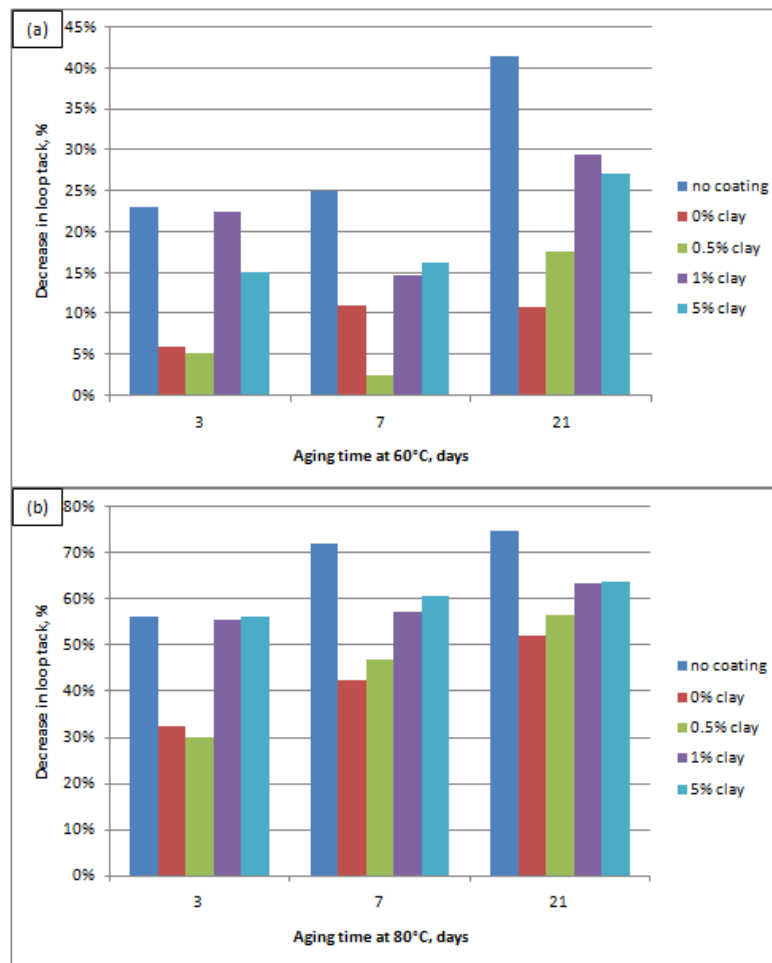


Figure 4.53 Effect of thermal aging on tack of nanoclay coated films at (a) 60°C and (b) 80°C.

4.2.6 Surface analysis

The contact angles of the calendered PVC samples were measured before and after thermal aging at 80°C for one week. It was expected that the contact angle would shift over time as the plasticizer and other components migrate to the surface. The results are shown in Table 4.14. The two samples measured were the control film

without coating, and the film with coating that contained 0% clay. For the control sample that was uncoated and coated sample that did not contain nanoclay, there was no significant change in surface energy after aging for either sample.

Sample ID	condition	Fluid	Contact Angle (deg)		Surface Energy (dyne/cm)			
			Avg	Std Dev	Avg	Std Dev	Disperse	Polar
0% clay (control)	initial	Water	78.7	1.8	41.8	1.5	37.4	4.4
		Diiodomethane	44.3	1.6				
0% clay (control)	1 wk 80C	Water	77.6	0.8	45.8	0.9	41.9	3.9
		Diiodomethane	35.2	1.3				
No coating	initial	Water	77.7	1.8	44.0	1.7	39.8	4.2
		Diiodomethane	39.6	2.0				
No coating	1 wk 80C	Water	79.7	1.3	42.2	3.7	38.4	3.8
		Diiodomethane	42.5	5.7				

Table 4.14 Contact angle measurements comparing initial versus aged results

CHAPTER V

CONCLUSIONS

Intercalated PVC-clay nanocomposite films were produced using organosol formulations and casting process. The nanoclay could be efficiently dispersed into plasticizer and solvent using a high speed homogenizer, and then dispersed into the PVC matrix. This is evident from the TEM imaging analysis which shows PVC chains intercalated between nanoclay galleries.

The PVC films loaded with nanoclay did show some variation in thermal stability and durability based on the type of nanoclay. The samples loaded with Cloisite Na⁺ nanoclay showed the greatest performance for thermal stability and durability similar to the unfilled control. The samples loaded with Cloisite[®] 10A and Cloisite[®] 20 showed reduced thermal stability and durability at higher loadings. The samples loaded with Cloisite[®] 20 performed better than those with Cloisite[®] 10A. This may be caused by degradation of the organic modifier used to modify the MMT clay. The print surface of the films was not significantly altered with addition of nanoclay, as indicated by the contact angle and ink drop measurements.

The polyamide-nanoclay coating on calendered PVC shows positive results for barrier properties, although no correlation was found between the extent of barrier properties and nanoclay level. The coating approach would allow for barrier properties without impacting the stability and durability of the PVC film which was observed for

the nanoclay in PVC film approach. The coated PVC film shows positive results for thermal stability and durability, indicating that the nanoclay coating did not initiate or accelerated degradation. The nanoclay did not change the interaction of the film with eco-solvent ink, which is apparent from the mechanical property testing.

The effect of coating thickness should be evaluated in the future, as a higher coat weight may further improve barrier properties. The rheology profile of nanoclay filled coatings should also be evaluated to understand how effectively the material can be coated onto the PVC film.

REFERENCES

- [1] M. Alexandre and P. Dubois, "Polymer-layered silicate nanocomposites : preparation , properties and uses of a new class of materials," *Mater. Sci. Eng. R Reports*, vol. R28, no. 1–2, pp. 1–63, 2000.
- [2] A. Leszczy, J. Njuguna, K. Pielichowski, and J. R. Banerjee, "Polymer / montmorillonite nanocomposites with improved thermal properties Part I . Factors influencing thermal stability and mechanisms of thermal stability improvement," vol. 453, pp. 75–96, 2007.
- [3] A. Leszczy, J. Njuguna, K. Pielichowski, and J. R. Banerjee, "Polymer / montmorillonite nanocomposites with improved thermal properties Part II . Thermal stability of montmorillonite nanocomposites based on different polymeric matrixes," *Thermochim. Acta*, vol. 454, no. 1, pp. 1–22, 2007.
- [4] S. S. Ray and M. Okamoto, "Polymer / layered silicate nanocomposites : a review from preparation to processing," *Prog. Polym. Sci.*, vol. 28, no. 11, pp. 1539–1641, 2003.
- [5] C. E. Wilkes, J. W. Summers, and C. Daniels, "PVC Handbook," in *PVC Handbook*, 2005, pp. 173, 176–190.
- [6] C. E. Wilkes, J. W. Summers, and C. Daniels, "PVC Handbook," in *PVC Handbook*, Munich, Germany: Carl Hanser Verlag, 2005, pp. 174–175.
- [7] B. T. D. Stark, H. Choi, and P. W. Diebel, "The influence of molecular weight on plasticizer retention," *Geotech. Spec. Publ.*, vol. 23, p. 6370/1-6370/15, 2005.
- [8] D. MESSADI, J.-M. VERGNAUD, and M. HIVERT, "A New Approach to the Study of Plasticizer Migration From PVC into Methanol," *J. Appl. Polym. Sci.*, vol. 26, no. 2, pp. 667–677, 1981.
- [9] J. Pagacz and K. Pielichowski, "Preparation and Characterization of PVC / Montmorillonite Nanocomposites — A Review," *J. Vinyl Addit. Technol.*, vol. 15, no. 2, pp. 61–76, 2009.

- [10] M. S. Nazir, M. H. M. Kassim, L. Mohapatra, M. A. Gilani, M. R. Raza, and K. Majeed, "Characteristic Properties of Nanoclays and Characterization of Nanoparticulates and Nanocomposites," pp. 35–56, 2016.
- [11] J. Ren, Y. Huang, Y. Liu, and X. Tang, "Preparation , characterization and properties of poly (vinyl chloride)/ compatibilizer / organophilic-montmorillonite nanocomposites by melt intercalation," *Polym. Test.*, vol. 24, no. 3, pp. 316–323, 2005.
- [12] D. Benderly, F. Osorio, and W. Ijdo, "PVC Nanocomposites—Nanoclay Chemistry and Performance," *J. Vinyl Addit. Technol.*, vol. 14, no. 4, pp. 155–162, 2008.
- [13] C. E. Wilkes, J. W. Summers, and C. Daniels, "PVC Handbook," in *PVC Handbook*, 2005, pp. 95–101.
- [14] D. Wang, D. Parlow, Q. Yao, and C. A. Wilkie, "PVC-Clay Nanocomposites: Preparation, Thermal and Mechanical Properties," *J. Vinyl Addit. Technol.*, vol. 7, no. 4, pp. 203–213, 2001.
- [15] K. Stoeffler, P. G. Lafleur, and J. Denault, "Thermal decomposition of various alkyl onium organoclays : Effect on polyethylene terephthalate nanocomposites ' properties," *Polym. Degrad. Stab.*, vol. 93, no. 7, pp. 1332–1350, 2008.
- [16] H. Petersen, I. Jakubowicz, J. Enebro, and N. Yarahmadi, "Organic modification of montmorillonite for application in plasticized PVC nanocomposites," *Appl. Clay Sci.*, vol. 107, pp. 78–84, 2015.
- [17] C. Liu *et al.*, "Thermal Degradation Behaviors of Poly (vinyl chloride)/ Halloysite Nanotubes Nanocomposites," *Int. J. Polym. Mater. Polym. Biomater.*, vol. 62, no. 3, pp. 128–132, 2013.
- [18] C. Liu, Y. Luo, Z. Jia, S. Li, B. Guo, and D. Jia, "Structure and Properties of Poly (vinyl chloride)/ Halloysite Nanotubes Nanocomposites," *J. Macromol. Sci. Part B Phys.*, vol. 51, no. 5, pp. 968–981, 2012.
- [19] C. Liu, Y. Luo, Z. Jia, S. Li, D. Huang, and D. Jia, "Particle Configuration and Properties of Poly (vinyl chloride)/ Halloysite Nanotubes Nanocomposites via In Situ Suspension Polymerization," *Polym. Compos.*, vol. 35, no. 5, pp. 856–863, 2014.
- [20] M. Hasan and M. Lee, "Enhancement of the thermo-mechanical properties and efficiency of mixing technique in the preparation of graphene / PVC nanocomposites compared to carbon nanotubes / PVC," *Prog. Nat. Sci. Mater. Int.*, vol. 24, no. 6, pp. 579–587, 2014.

- [21] G. Broza, K. Piszczek, K. Schulte, and T. Sterzynski, "Nanocomposites of poly(vinyl chloride) with carbon nanotubes (CNT)," *Compos. Sci. Technol.*, vol. 67, no. 5, pp. 890–894, 2007.
- [22] H. Akhina *et al.*, "Plasticized PVC Graphene Nanocomposites : Morphology , Mechanical , and Dynamic Mechanical Properties," vol. 58, no. S1, pp. E104–E113, 2018.
- [23] D. Pierleoni *et al.*, "Graphene-based coatings on polymer films for gas barrier applications," *Carbon N. Y.*, vol. 96, pp. 503–512, 2016.
- [24] N. Ahmad, A. Kausar, and B. Muhammad, "An investigation on 4-aminobenzoic acid modified polyvinyl chloride / graphene oxide and PVC / graphene oxide based nanocomposite membranes," vol. 32, pp. 419–448, 2016.
- [25] G. M. Joshi and K. Deshmukh, "Optimized Quality Factor of Graphene Oxide-Reinforced PVC Nanocomposite," vol. 43, no. 4, pp. 1161–1166, 2014.
- [26] K. Deshmukh, S. M. Khatake, and G. M. Joshi, "Surface properties of graphene oxide reinforced polyvinyl chloride nanocomposites," vol. 20, no. 11, pp. 1–11, 2013.
- [27] O. Breuer and U. Sundararaj, "Big Returns From Small Fibers : A Review of Polymer / Carbon Nanotube Composites," *Polym. Compos.*, vol. 25, no. 6, pp. 630–645, 2004.
- [28] A. Gholami, M. Hajian, F. Rafiemanzelat, and A. R. Zanjanijam, "Plasticized poly (vinyl chloride) composites : Influence of different nanofillers as antimigration agents," vol. 42559, pp. 1–9, 2015.
- [29] D. Wang and C. A. Wilkie, "Preparation of PVC-Clay Nanocomposites by Solution Blending," *J. Vinyl Addit. Technol.*, vol. 8, no. 4, pp. 238–245, 2002.
- [30] A. Kalendova, J. Zykova, L. Kovarova, M. Slouf, and J. F. Gerard, "The Effect of processing on the PVC / Clay Nanocomposites Structure," in *AIP Conference Proceedings*, 2010, vol. 1255, pp. 181–183.
- [31] L. M. Matuana, "Rigid PVC /(Layered Silicate) Nanocomposites Produced Through a Novel Melt-Blending Approach," 2009.
- [32] S. Bohn, P. S. Balzer, and D. Becker, "Role of Plasticizer and Dispersion Methods on the Properties of Poly (vinyl chloride) and Clay Nanocomposites," *J. Vinyl Addit. Technol.*, vol. 24, no. S1, pp. E172–E176, 2018.

- [33] N. G. Shimpi and S. Mishra, "Influence of surface modification of montmorillonite on properties of PVC nanocomposites," *J. Compos. Mater.*, vol. 45, no. 23, pp. 2447–2453, 2011.
- [34] Maria Eugenia Romero-Guzma ´n, A. Romo-Urbe, E. Ovalle-García, R. Olayo, and C. A. Cruz-Ramos, "Microstructure and dynamic mechanical analysis of extruded layered silicate PVC nanocomposites," *Polym. Adv. Technol.*, vol. 17, no. April, pp. 395–418, 2006.
- [35] B. Yalcin and M. Cakmak, "The role of plasticizer on the exfoliation and dispersion and fracture behavior of clay particles in PVC matrix: A comprehensive morphological study," *Polymer (Guildf)*., vol. 45, no. 19, pp. 6623–6638, 2004.
- [36] D. L. Vanderhart, A. Asano, and J. W. Gilman, "Solid-State NMR Investigation of Paramagnetic Nylon-6 Clay Nanocomposites . 2 . Measurement of Clay Dispersion , Crystal Stratification , and Stability of," *Chem. Mater.*, vol. 13, no. 10, pp. 3796–3809, 2001.
- [37] C. H. Davis *et al.*, "Effects of Melt-Processing Conditions on the Quality of Poly (ethylene terephthalate) Montmorillonite Clay," *J. Polym. Sci. Part B Polym. Phys.*, vol. 40, no. 23, pp. 2661–2666, 2002.
- [38] W. Xie *et al.*, "Thermal Stability of Quaternary Phosphonium Modified Montmorillonites," *Chem. Mater.*, vol. 14, no. 11, pp. 4837–4845, 2002.
- [39] W. Xie, Z. Gao, W. Pan, D. Hunter, A. Singh, and R. Vaia, "Thermal Degradation Chemistry of Alkyl Quaternary Ammonium Montmorillonite," *Chem. Mater.*, vol. 13, no. 9, pp. 2979–2990, 2001.
- [40] X. Zheng and M. Gilbert, "Structure and Properties of Poly(vinyl chloride)/ Montmorillonite Composites Produced From Plasticsols," *J. Vinyl Addit. Technol.*, vol. 22, no. 2, pp. 140–145, 2016.
- [41] X. Zheng and M. Gilbert, "Effects of Processing on the Structure of PVC/Montmorillonite Composites. I. Melt and Solution Processes," *J. Vinyl Addit. Technol.*, vol. 17, no. 4, pp. 231–238, 2011.
- [42] L. Madaleno, J. Schjødt-Thomsen, and J. C. Pinto, "Morphology , thermal and mechanical properties of PVC / MMT nanocomposites prepared by solution blending and solution blending + melt compounding," *Compos. Sci. Technol.*, vol. 70, no. 5, pp. 804–814, 2010.

- [43] H. Haiyan, P. Mingwang, L. Xiucuo, S. Xudong, and Z. Liucheng, "Preparation and characterization of poly (vinyl chloride)/ organoclay nanocomposites by in situ intercalation," *Polym. Int.*, vol. 53, no. 2, pp. 225–231, 2004.
- [44] F. Gong, M. Feng, C. Zhao, S. Zhang, and M. Yang, "Thermal properties of poly (vinyl chloride)/ montmorillonite nanocomposites," *Polym. Degrad. Stab.*, vol. 84, no. 2, pp. 289–294, 2004.
- [45] F. Gong, M. Feng, C. Zhao, S. Zhang, and M. Y. Ā, "Particle configuration and mechanical properties of poly (vinyl chloride)/ montmorillonite nanocomposites via in situ suspension polymerization," vol. 23, pp. 847–853, 2004.
- [46] G. Chen, K. Yao, and J. Zhao, "Montmorillonite clay/poly(methyl methacrylate) hybrid resin and its barrier property to the plasticizer within poly(vinyl chloride) composite," *J. Appl. Polym. Sci.*, vol. 73, no. 3, pp. 425–430, 1999.
- [47] C. Giannini, M. Ladisa, D. Altamura, D. Siliqi, T. Sibillano, and L. De Caro, "X-ray Diffraction: A Powerful Technique for the Multiple-Length-Scale Structural Analysis of Nanomaterials," *Crystals*, vol. 6, no. 8, p. 87, 2016.
- [48] J. Pagacz, M. Chrzanowski, I. Krucinska, and K. Pielichowski, "Thermal aging and accelerated weathering of PVC/MMT nanocomposites: Structural and morphological studies," *J. Appl. Polym. Sci.*, vol. 132, no. 24, p. 42090/1-42090/12, 2015.
- [49] H. Ishida, S. Campbell, and J. Blackwell, "General approach to nanocomposite preparation," *Chem. Mater.*, vol. 12, no. 5, pp. 1260–1267, 2000.
- [50] C. Chen, C. Teng, and C. Yang, "Preparation and Characterization of Rigid Poly (vinyl chloride)/MMT Nanocomposites," *J. Polym. Sci. Part B Polym. Phys.*, vol. 43, no. 12, pp. 1465–1474, 2005.
- [51] A. Berzinis, O. Guise, T. Hoeks, V. Ramakrishnan, and R. Kamalakaran, "Quantification of nanoclay dispersion and exfoliation in polymer composites," *Annu. Tech. Conf. - ANTEC, Conf. Proc.*, vol. 2, pp. 851–857, 2010.
- [52] S.-I. Hong, H.-H. Lee, and J.-W. Rhim, "Effects of clay type and content on mechanical, water barrier and antimicrobial properties of agar-based nanocomposite films," *11th Int. Congr. Eng. Food*, vol. 86, no. 2, pp. 691–699, 2011.
- [53] K. Alena, M. Dagmar, G. J. Francois, and S. Miroslav, "Polymer/clay nanocomposites and their gas barrier properties," *Polym. Compos.*, vol. 34, no. 9, pp. 1418–1424, 2013.

- [54] H. Petersen, I. Jakubowicz, J. Enebro, and N. Yarahmadi, "Development of nanocomposites based on organically modified montmorillonite and plasticized PVC with improved barrier properties," *J. Appl. Polym. Sci.*, vol. 133, no. 3, 2016.
- [55] C. Wan, X. Qiao, Y. Zhang, and Y. Zhang, "Effect of different clay treatment on morphology and mechanical properties of PVC-clay nanocomposites," *Polym. Test.*, vol. 22, no. 4, pp. 453–461, 2003.
- [56] D. Dharaiya and S. C. Jana, "Thermal decomposition of alkyl ammonium ions and its effects on surface polarity of organically treated nanoclay," *Polymer (Guildf.)*, vol. 46, no. 23, pp. 10139–10147, 2005.
- [57] E. Esmizadeh, M. Moghri, M. R. Saeb, M. M. Nia, and N. Nobakht, "Application of Taguchi Approach in Describing the Mechanical Properties and Thermal Decomposition Behavior of Poly (vinyl chloride)/Clay Nanocomposites : Highlighting the Role of Organic Modifier," *J. Vinyl Addit. Technol.*, vol. 22, no. 3, pp. 182–190, 2016.
- [58] D. Wang, D. Parlow, Q. Yao, and C. A. Wilkie, "Melt Blending Preparation of PVC-Sodium Clay Nanocomposites," *J. Vinyl Addit. Technol.*, vol. 8, no. 2, pp. 139–150, 2002.
- [59] T. Peprnicek, J. Duchet, L. Kovarova, J. Malac, J. F. Gerard, and J. Simonik, "Poly (vinyl chloride)/clay nanocomposites : X-ray diffraction , thermal and rheological behaviour," *Polym. Degrad. Stab.*, vol. 91, no. 8, pp. 1855–1860, 2006.
- [60] X. Zheng and M. Gilbert, "An Investigation into the Thermal Stability of PVC / Montmorillonite Composites," *J. Vinyl Addit. Technol.*, vol. 17, no. 2, pp. 77–84, 2011.
- [61] C. Wan, Y. Zhang, and Y. Zhang, "Effect of alkyl quaternary ammonium on processing discoloration of melt-intercalated PVC-montmorillonite composites," *Polym. Test.*, vol. 23, no. 3, pp. 299–306, 2004.
- [62] T. Ren, J. Yang, Y. Huang, J. Ren, and Y. Liu, "Preparation, Characterization, and Properties of Poly(vinyl chloride)/Organophilic-Montmorillonite Nanocomposites," *Polym. Compos.*, vol. 27, no. 1, pp. 55–64, 2006.
- [63] J. Du, D. Wang, C. A. Wilkie, and J. Wang, "An XPS investigation of thermal degradation and charring on poly (vinyl chloride)–clay nanocomposites," *Polym. Degrad. Stab.*, vol. 79, no. 2, pp. 319–324, 2002.

- [64] S. V Levchik and E. D. Weil, "Review Overview of the recent literature on flame retardancy and smoke suppression in PVC," *Polym. Adv. Technol.*, vol. 16, no. 10, pp. 707–716, 2005.
- [65] J. W. Gilman, "Flammability and thermal stability studies of polymer layered-silicate (clay) nanocomposites," *Appl. Clay Sci.*, vol. 15, no. 1–2, pp. 31–49, 1999.
- [66] P. Kroushl, "Resin Selection for PVC Applications," in *Handbook of Vinyl Formulating*, 2nd ed., R. F. Grossman, Ed. Hoboken, N. J.: John Wiley & Sons, Inc., 2008, pp. 13–56.
- [67] D. Satas, "Acrylic Adhesives," in *Handbook of Pressure Sensitive Adhesive Technology*, 1989, pp. 429–430.
- [68] J. Pagacz and K. Pielichowski, "PVC/MMT nanocomposites," *J. Therm. Anal. Calorim.*, vol. 111, no. 2, pp. 1571–1575, 2013.
- [69] J. W. Summers and E. B. Rabinovitch, "Weatherability of Vinyl and Other Plastics," in *Weathering of Plastics: Testing to Mirror Real Life Performance*, G. Wypych, Ed. Brookfield, Conn.: SPE, 1999, pp. 61–68.
- [70] A. Y. Goldman, J. A. Montes, A. Barajas, G. Beall, and D. D. Eisenhour, "Effect of Aging on Mineral-Filled Nanocomposites," in *Weathering of Plastics: Testing to Mirror Real Life Performance*, G. Wypych, Ed. 1999, pp. 195–208.